3D Geomodeling for Europe

Project number: GeoE.171.005

Deliverable 6.1

Report on the harmonization procedure of the western Pyrenees using geological, gravimetric, petrophysical and seismic data.

Authors and affiliation:

Rosibeth Toro, Esther Izquierdo-Llavall, Antonio M. Casas, Félix M. Rubio, Conxi Ayala, Juliana Martín León, Pilar Clariana, Ruth Soto, Pablo Santolaria, Javier Navas, Carmen Rey-Moral, Emilio L. Pueyo (and the WP6 Team).
[IGME][UZ]

E-mail of lead author:
unaim@igme.es

Version: 30-10-2021

This report is part of a project that has received funding by the European Union's Horizon 2020 research and innovation program under grant agreement number 731166.

Deliverable Data	
Deliverable number	D6.1
Dissemination level	Public
Deliverable name	Report on the harmonization procedure of the western Pyrenees using geological, gravimetric, petrophysical and seismic data

Work package **Lead WP/Deliverable beneficiary**	WP6, Optimizing reconstructions of the subsurface to reduce structural uncertainty in 3D models IGME	
Deliverable status		
Submitted (Author(s))	29/10/2021	Emilio L. Pueyo, ….
Verified (WP leader)	29/10//2021	Emilio L. Pueyo
Approved (Coordinator)	30/10//2021	Stefan Knopf

Contributors by tasks (3DGeoEU WP6 Team)

Database harvesting: Juliana Martín León, Javier Navas, Carlos Peropadre, Pilar Clariana, Fernando Bohoyo, Félix Rubio

Structure; Rosibeth Toro, Esther Izquierdo-Llavall, Antonio Casas

Seismic interpretation: Rosibeth Toro, Esther Izquierdo-Llavall, Antonio Casas, Pablo Santolaria

Gravimetry; Félix M. Rubio; Agustín González, Jose Mª Llorente, Arturo García, Emilio L. Pueyo, Carmen Rey, Conxi Ayala, Pablo Calvín, Carlos Marín

Mountain Gravimetry: Alejandro Montañés, Lope Ezquerro, Pablo Santolaria, Esther Izquierdo

Petrophysics; Emilio L. Pueyo, Pilar Clariana, Ruth Soto, Cristina Pérez Bielsa, Jon Jiménez, Oscar Pueyo Anchuela, Belén Oliva-Urcia, Ana Gimeno, Elena Fernández de Arévalo

2D and 3D modeling: Rosibeth Toro, Antonio M. Casas, Conxi Ayala, Esther Izquierdo-Llavall, Emilio L. Pueyo.

Deliverable leader: Emilio L. Pueyo

Cited as: Toro, R.; Izquierdo-Llavall, E.; Casas, A.M.; Rubio, F.M.; Ayala, C.; Martín-León, J.; Clariana, P.; Soto, R.; Santolaria, P.; Navas, J.; Rey-Moral, C.; Pueyo, E.L. and the 3DGeoEU WP6 Team. (2021). Deliverable 6.1. Harmonization procedure of the western Pyrenees using geological, gravimetric, petrophysical, and seismic data. GEOERA 3DGEO-EU, 3D Geomodeling for Europe, project number GeoE.171.005. Report, 90 p

Abstract for stakeholders

Beyond cross border harmonization (usually with a lack of data in the boundary region), harmonization in the absence of sufficient subsurface information is also a challenge for the exploration and the evaluation of energetic resources and gas reservoirs all around Europe. The oil industry has boosted the seismic exploration, however, a number of reasons have precluded the acquisition of these key data in several regions; shallow or highly subsiding basins, mountainous terrains (very costly), areas with step dips (technically impossible), as well as border conflicts.

In the case of the southwestern Pyrenees the problem is not the seismic coverage itself (relatively good because of the finding of a gas reservoir in the 70's), but the access to information. Access to the seismic and borehole information is precluded due to privatization of former public companies in the 90's (current government databases are very incomplete) as well as ongoing exploration permits that imply a temporal embargo to relevant information. For all these reasons, only 6% of the digital information (*.sgy files) were available for the 3D reconstruction of our case study, being the rest image scans of seismic sections with different levels of processing. In total, less than 50% of the information was available being part of them of very low quality without the possibility of reprocessing. This situation may easily happen in other EU regions that will have to be evaluated in the frame of the transition of the energy system (Green Agenda), as in the southwestern Pyrenees, where a potential deep geothermal reservoirs have been already evaluated in the region with good prospects.

Therefore, and aiming to harmonize a reliable 3D reconstruction of the subsurface in this case study, we have tackled the building of a reliable 3D model by applying gravimetric exploration and joint modeling (Geology, Gravimetry and Petrophysics) as fully described in the Optimized Reconstruction Workflow proposed in D6.4

More than 3,100 new gravimetric stations were acquired in the study area (mostly in the main target area, about 2000 km^2 in surface) and were joined to previous datasets. The final Bouguer anomaly is based on more than 8,500 gravimetric evenly distributed stations. Besides we have acquired and harmonized petrophysical data in more than 300 localities (> 800 density determinations). About two thousand seismic reflectors (stratigraphic horizons and faults) were identified from 142 seismic sections- They allow building a new 3D model of the southwestern Pyrenees as well as build three new balanced sections to support the subsurface interpretation.

The evaluation of residual anomalies of the Bouguer gravimetric map display a good degree of correlation with the basement topography in those areas supported by seismic exploration. The basement rocks display the highest density in the evaluated formations, and thus, the maximum contrast comparing to any other rocks of the cover units. Therefore, gravimetric modeling (forward and inverse methods) are an excellent approach to harmonize the subsurface information in this region.

The results derived from the application of our modelling workflow are very promising and open a new research line for building larger and more reliable 3D models in the region and will allow, for example, the evaluation of potential deep geothermal reservoirs. The situation (poor seismic coverage) and the 3D modeling workflow (integrating geological, gravimetric and petrophysical data) described in this report can be easily applied to other European regions.

INDEX

1 INTRODUCTION, MOTIVATION AND GOALS

The Western Pyrenees is a key portion to understand the 4D evolution of the mountain chain. At a cortical level, the net subduction of the Iberian plate underneath the European one along the ECORS profile (Muñoz, 1992) changes its style in the Western sectors, ECORS-Arzacq (Teixell, 1998) and in the Cantabrian part (ESCIN and MARCONI profiles, Pedreira et al., 2003 and 2015 and references therein) and shows an indentation of the European lower crust (and the Cantabrian margin) within the Iberian plate (see recent reviewed modelling at Pedrera et al., 2017 and García-Senz et al., 2020). Focusing on the upper crustal levels of the western isthmic termination, a significant change is remarkable with respect to the outcrop of the basement rocks; the Axial zone (backbone of the chain) shows a moderate plunge westwards and vanishes in the Western Pyrenees. Only isolated spots of these rocks outcrop to the West of the Axial Zone termination in limited portions (Basque massifs) right before the Cantabrian margin (Choukroune and Seguret, 1973; Barnolas et al., 2008). Hence, this region comprises a genuine non-coaxial and non-cylindrical style of deformation with significant lacks of information:

1) The oil exploration (seismic and well data) performed mostly during the 1960s and 1970s (see compilation by Lanaja, 1987) were concentrated to the west around Pamplona city and, especially, in the Serrablo gas field to the east, while the central and northern portions were explored to a much more limited extend.
2) Apart from this heterogeneity, only a reduced portion of this information is publically available (even for IGME).
3) Limited potential-fields geophysical data (gravimetry and magnetics) (Ayala et al., 2016 and cited references) comparing to other regions of the country (partially due to the difficult access in the Pyrenean region).
4) There exists an uncertainty related to the role of main faults. The North Pyrenean fault displays a complex geometry and may have played a key role in the articulation of the basement and cover relationships which is not fully understood (e.g. García-Senz et al., 2020).
5) Limited balanced and restored sections (Schellart, 2002; Larrasoaña et al., 2003; Pueyo-Anchuela 2003) in the Navarra portion, in comparison with the better known central-eastern one (Labaume et al., 1985; Teixell , 1996; Izquierdo-Llavall et al., 2013) or other portions of the Pyrenees (Muñoz, 2019).
6) Lack of precise control of the deformation ages in the Navarra area due to the absence of paleothermometers and/or barometric indicators in comparison to the eastern area (Cantarelli et al., 2013; Izquierdo-Llavall et al., 2013; Bosch et al., 2016; Labaume et al., 2016).
7) This lack of kinematic data also precludes the characterization of the diachrony of the deformation, fully characterized in the southern sector (External Sierras) by abundant syntectonic deposits (Millán et al., 2000).
8) Evidence of natural and induced seismicity (Souriau et al., 2014; Casas, 2005; Sansegundo, 2014) without clear relationships with basement faults.

This scarcity of relevant information is a major drawback for the harmonization of a geological model in the region and precludes building consistent 3D models for interesting subsurface structures identified as CO2 storages (Pueyo et al., 2010 and 2012; García-Lobón et al., 2011) or as deep geothermal reservoirs (Lamarca-Irisarri, 2012). Beyond cross border harmonization, part of these problems (lack of data, or access to them) are often found in other European regions and represents one of the main obstacles if we aim to build a unified 3D geological model for Europe (one of the midterm goals of EuroGeoSurveys and of the GeoERA project)

The WP6 of the 3DGeoEU project, among other goals, focuses on potential field geophysics (gravimetry and magnetics) as a quick, cost-effective and efficient method for 3D modeling, especially useful for the harmonization of cross-borders regions or regions with scarce and heterogeneous subsurface information. Therefore, the main goal of this report is **to build a consistent 3D model for the Western Pyrenees** integrating geological, geophysical and petrophysical information. Additionally, we also consider some secondary goals:

A) Interpreting all available reflection seismic information and building serial balanced cross sections together with available geological surface information (1:50.000).

B) Acquiring a vast net of new gravimetric data to improve the homogeneity and resolution of this data.

C) Obtaining (new), recovering (from previous studies) and harmonizing the ample petrophysical data of the target formations.

D) Integrating all newly obtained information in a consistent 3D model together with previous cartographies, well logs, structural and stratigraphic data, cross sections, etc.

E) Performing a joint 3D forward and inversion modelling of this datasets to improve the knowledge of the subsurface and reduce its uncertainty.

2 GEOLOGICAL SETTING

2.1 Introduction

The Pyrenean range constitutes a doubly vergent WNW-ESE chain resulted from the North-South convergence between the Iberian and Eurasian plates between the Late Cretaceous and the earliest Miocene (e.g. Choukroune and ECORS Team, 1989; Muñoz, 1992). It can be followed onshore from the Gulf of Lion to the Galicia margin, with a total length of about 1000 km, integrated in the Alpine Chain system (e.g. Muñoz, 1992, 2019) (Fig. 1). The Pyrenean range has been classically divided into the Pyrenees s.s. and the Cantabrian Mountains to the East and West, respectively (e.g. Vera et al., 2004) (Fig. 1). The Pyrenees s.s. represent a collisional orogen formed by the limited subduction of the continental Iberian lithospheric mantle and lower crust underneath the Eurasian plate (e.g. Muñoz, 1992; Beaumont et al., 1999).

The Pyrenees s.s. are traditionally divided into the following zones (Mattauer, 1968) (Fig. 2): the North Pyrenean Zone, the Axial Zone and the South Pyrenean Zone. The Axial Zone represents the core of the chain and it consists of an antiformal stack of basement rocks separating the northern from the southern Pyrenees, which are overthrusted above the Aquitaine and Ebro foreland basins, respectively (e.g. Muñoz, 1992) (Fig. 2). The North Pyrenean Zone is characterized by north vergent folds and thrusts and a thick Mesozoic series (e.g. Choukroune and Séguret, 1973), whereas the South Pyrenean Zone is characterized by thick Cenozoic synorogenic successions affected by a wide south vergent fold-and-thrust belt (e.g. Teixell, 1998). The western part of the Pyrenees are strongly asymmetric, formed by a narrow north-verging retrowedge including the inverted Mauléon basin and the Aquitaine foreland basin and the wide south-verging prowedge including the western termination of the Axial Zone, the South Pyrenean piggyback basin so called Jaca basin and the Ebro foreland basin (e.g. Teixell, 1998) (Fig. 2).

The present-day structural architecture of the Pyrenean range is the result of a complex tectonic evolution, being the Pyrenean compression (Late Cretaceous-earliest Miocene) the latest main tectonic event (e.g. Muñoz, 1992). Paleozoic basement rocks were already deformed during the Variscan Orogeny (Middle-Late Carboniferous) (e.g. Poblet, 1991; García-Sansegundo, 1996). Localized extension and pull-apart basins took place between the Late Carboniferous to Early Triassic, followed by a generalized Mesozoic extension associated with the opening of the North Atlantic and Bay of Biscay and formation of rift basins (e.g. Le Pichon and Sibuet, 1971; García-Senz, 2002).

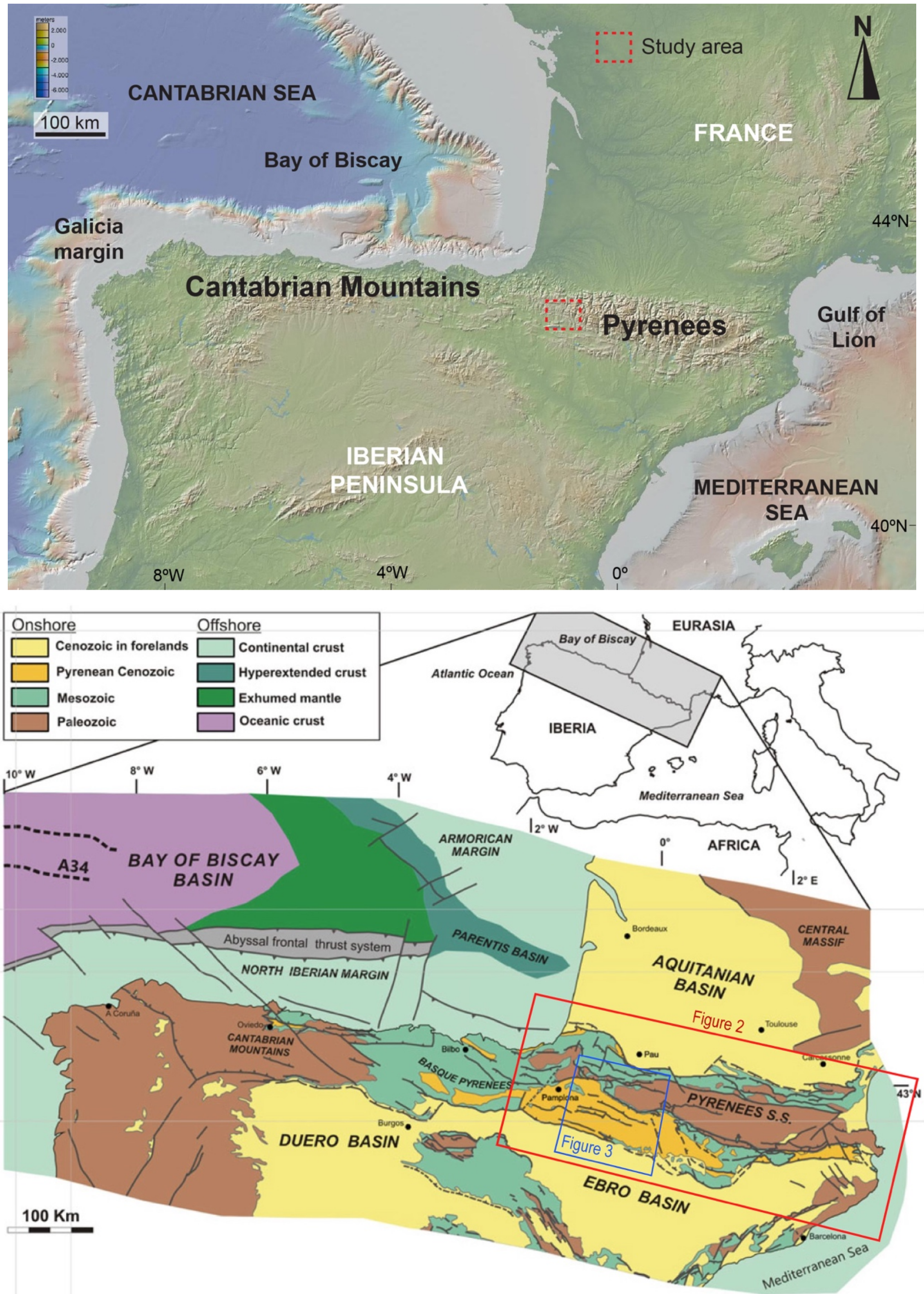

Figure 1. Location of the Pyrenean range in the context of the northern Iberian Peninsula and Southern France. Top; sketch from GeoMapApp, (http://www.geomapapp.org). The study area is shown in red dashed line. Bottom; simplified geodynamic context and main geological units (from Carola et al., 2013 and Muñoz, 2019).

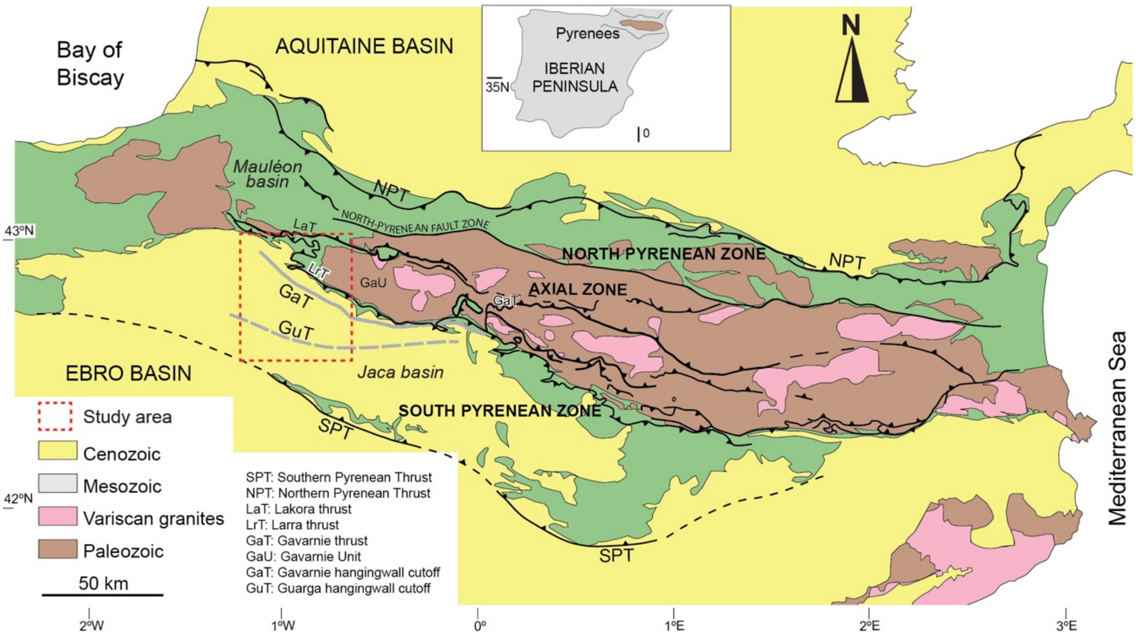

Figure 2. Geologic and tectonic sketch map of the Pyrenees showing the study area. Grey lines (GaT and GuT) represent the projections of the hanging wall cutoff of the Gavarnie and Guarga thrusts onto the horizontal plane. Modified from Soto et al. (2006).

2.2 Stratigraphy

The rocks outcropping in the area of the GeoEra Project span a wide age range from the Late Paleozoic (Devonian) to Early Cenozoic (Oligocene-Miocene). The Devonian, Carboniferous and Permian rocks form the Western Axial Zone of the Pyrenees (Fig. 3) and they are overlain by Upper Cretaceous to Lower Eocene carbonate sequences that form the Pyrenean Internal Sierras (Fig. 3). Towards the south, the South Pyrenean basin is mainly filled by thick sequences of Upper Paleocene – Eocene turbidites (Fig. 3) and in the southern end of the study area, in the foreland Ebro basin, Upper Eocene - Miocene continental rocks outcrop (Fig. 3). The main lithostratigraphic features of the Paleozoic, Mesozoic and Cenozoic rocks that crop out in the study area are briefly described below:

<u>Paleozoic</u>

The Paleozoic of the studied area comprises Devonian, Carboniferous and Permian rocks. In the study area, the Devonian rocks are characterized by two types of successions, one characterized by detrital and carbonate rocks deposited in shallow platforms located mainly in the South of the Axial Zone (Ternet et al. 2008) (Fig 3) and other mainly siliciclastic interpreted as deposits of turbidites which are located in the northern-central sector of the Axial Zone (Ternet et al. 2008) (Fig 3). The Carboniferous rocks have been divided into a lower part (pre-orogenic Carboniferous succession) formed by condensed carbonate sequences and cherts and an upper part (synorogenic Carboniferous succession) that consists of terrigenous turbiditic deposits (Colmenero et al. 2002). The lower part of the Carboniferous is normally showing an angular unconformity with the Devonian successions. The westernmost Late Carboniferous-Early

Permian granites (Panticosa-Cauterets and Eaux Chaudes; Gleizes et all., 1998 and Izquierdo-Llavall et al., 2012) outcrop just to the East of the study area. The Permian rocks post-date the Variscan Orogeny (Late Carboniferous), and mainly consist of conglomerates, sandstone and shales deposited in small isolated continental basins (Rodríguez-Méndez et al. 2019).

Mesozoic

The Mesozoic rocks correspond mainly to Upper Cretaceous carbonate sequences that outcrop in the Internal Sierras domain (Fig. 3) and can reach ~1450 m of thickness (e.g. Izquierdo-Llaval et al. 2015). Three units can be distinguished: (i) The Cañones limestones Formation (Fournier, 1905) characterized by Cenomanian to Santonian sequences of carbonate shelves; (ii) The Zuriza marls and limestone Formation (Teixell, 1992) of Campanian to Maastrichtian age that was deposited in deeper environments, and (iii) The Marboré sandstones Formation (Souquet, 1967) formed by Maastrichtian bioclastic sandstones, marly limestone and marls deposited in middle platform environments (Zuriza marls Fm.). To the south of the study area, in the External Sierras of the southern-western Pyrenees, very thinned Mesozoic rocks also outcrop delineating the Southern Pyrenean front. They consist of Middle-Upper Triassic evaporites which are unconformably overlain by Upper Cretaceous (Santonian-Maastrichtian) limestone and sandstone (Puigdefàbregas and Soler, 1973) (Fig. 3). Keuper evaporitic facies do not outcrop in the study area (not shown in Fig. 3), but they are present in the Roncal-1 and Sanvicente-1 boreholes, and they role as detachment units it is well-known (Calvín et al., 2018 and references therein)

Cenozoic

The Cenozoic sedimentation in this sector of the Pyrenees is characterized by syn-orogenic sedimentation which began in the Late Santonian and continued until the Early Miocene (e.g. Puigdefàbregas, 1975). The earliest Cenozoic materials outcropping in the study area are located in the Internal Sierras domain. They are represented by Paleocene to Lower Eocene carbonate sequences formed by limestones, marls and dolomites (e.g. Izquierdo-Llavall et al. 2015 and references therein). The Early and Middle Eocene is represented by thick sequences of siliciclastic turbidites (Hecho Group) up to ~4000 m-thick (Payros et al., 1999) with interbedded carbonated megaturbidites (up to 200 m-thick) whose sedimentation was highly controlled by tectonic activity (e.g. Teixell, 1992; Barnolas and Teixell, 1994). During the Middle-Late Eocene, the sedimentation changed to shallower facies dominated by marls (the Arro-Fiscal and Larrés marls and the Arguis – Pamplona marls, with the interbedded Sabiñanigo sandstone) deposited in the distal part of a deltaic system (Puigdefàbregas, 1975). During the Upper Bartonian, two progradations represented by deltaic facies occurred (Belsúe-Atarés Formation) (Barnolas et al. 1992). From Late Eocene and during the overfilled stage of the South Pyrenean basin (Late Priabonian - Rupelian), fluvial sediments represented by conglomerates, sandstones and mudstones were deposited (Campodarbe Formation) (Puigdefàbregas, 1975; Barnolas and Teixell, 1994; Montes, 2002). The last Cenozoic unit in the study area corresponds to the Uncastillo Formation, Late Oligocene - Early Miocene in age. This unit shows an angular conformity and also paraconformity with the underlying Campodarbe Formation and consists of sandstones, mudstones and conglomerates. The sedimentation of this unit represents the latest stage of the filling of the Ebro basin as the southern Pyrenean foreland basin (Arenas and Pardo, 1996; Oliva-Urcia et al., 2019).

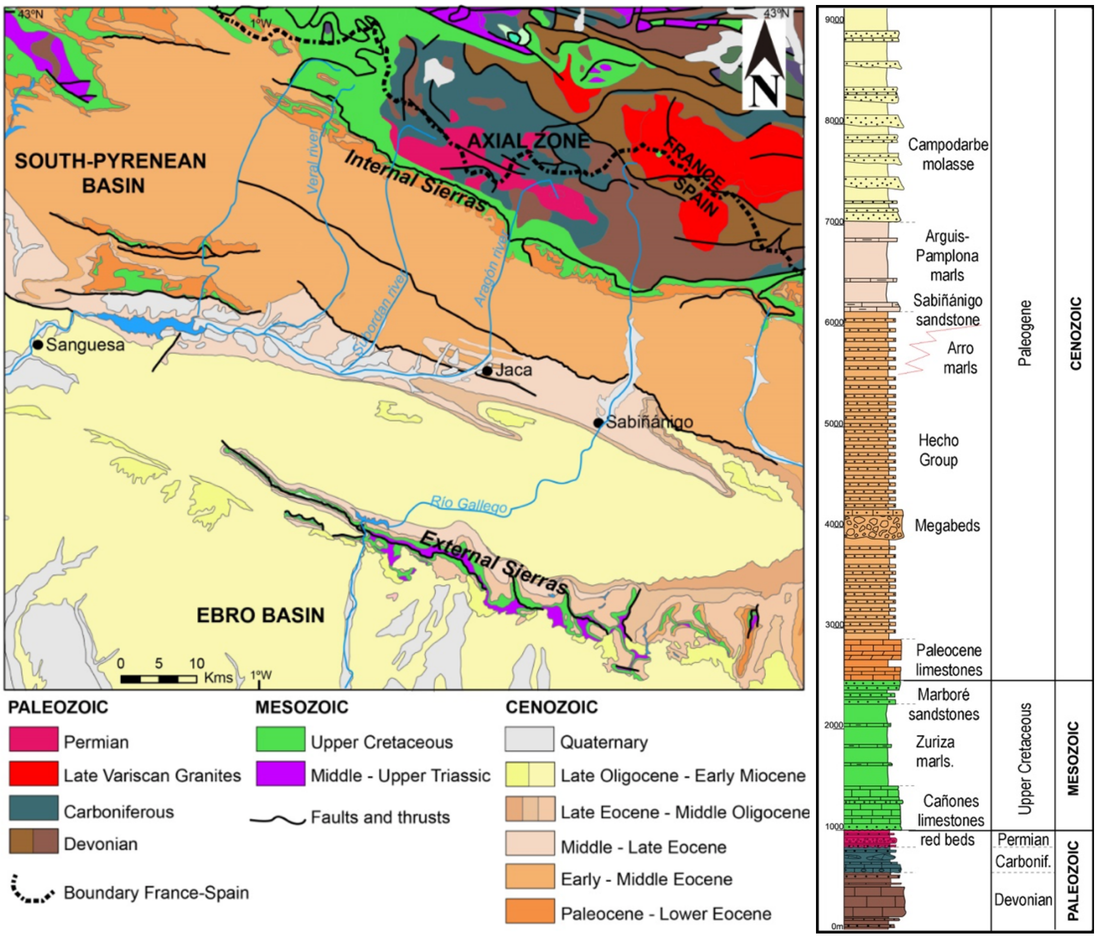

Figure 3. Geological map of the study area showing the lithostratigraphic units described in the text. Modified from the 1:400000 Geological map of the Pyrenees (Barnolas et al., 2008; Ternet et al. 2008).

2.3 Structure

The study area is located at the western termination of the Axial Zone and the central Jaca basin (Fig. 2, 3). The Axial Zone is a south-verging fold and thrust system that involves Paleozoic units unconformably overlain by Mesozoic and Cenozoic sequences to the North and to the South. In the study area, this thrust system displays a shallow westwards plunge that makes the Paleozoic units of the Axial Zone disappear to the West where Upper Cretaceous units crop widely out. Further to the West, Paleozoic outcrops are found again in the Oroz-Betelu anticline and the Basque Massifs (Fig. 2). Basement thrust sheets in the western Axial Zone form a south-verging imbricated thrust system affecting the upper crust (Cámara and Klimowitz 1985; Teixell 1996, 1998; Labaume et al. 2016; Labaume and Teixell, 2018). They merge downwards into a North-directed thrust ramp that detaches into the upper-lower crust transition and emerges at surface at the North Pyrenean Frontal Thrust (Teixell, 1996, Teixell et al., 2016; Fig. 4).

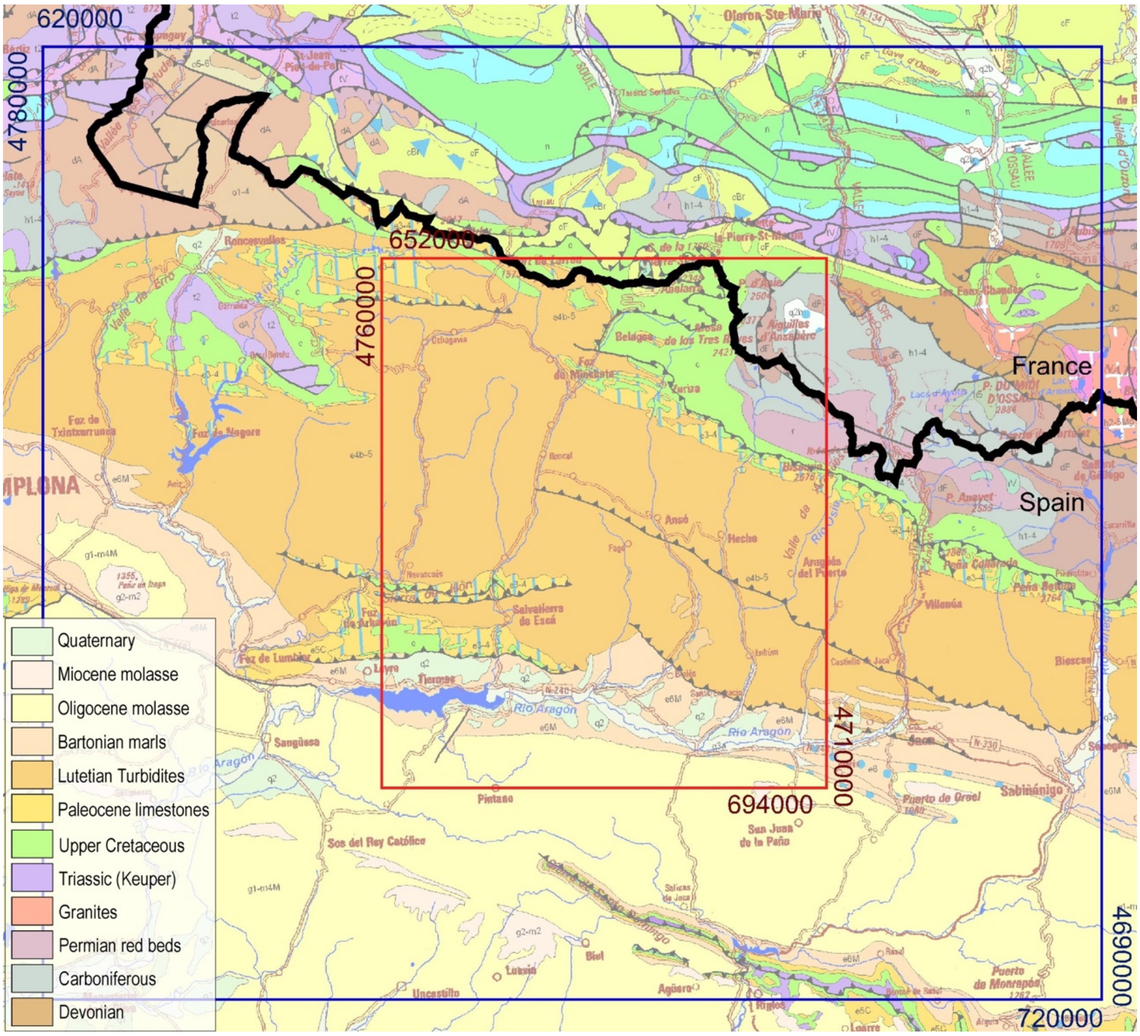

Fig. 4. Geological map (Barnolas et al., 2008; Ternet et al., 2008) of the study area (indicated by the red rectangle).

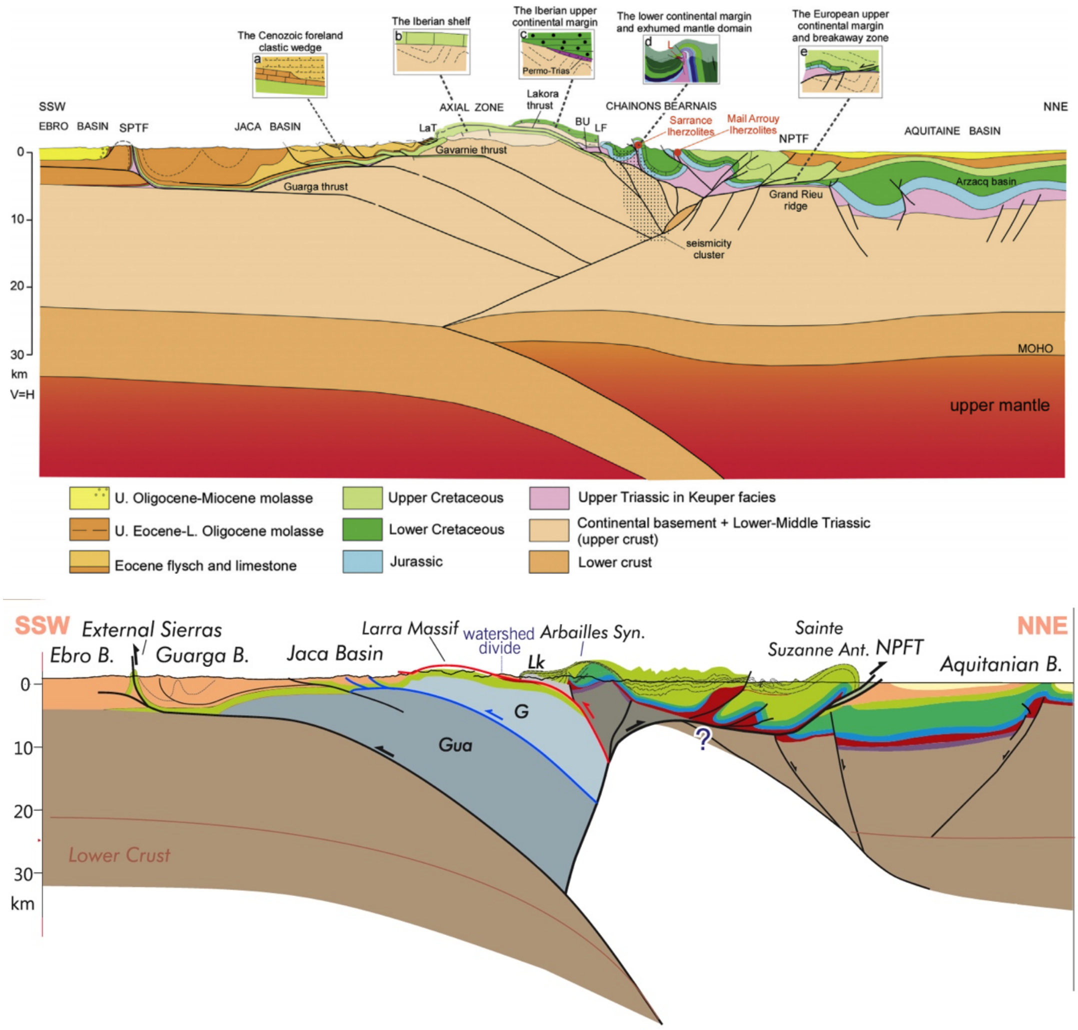

Fig. 5. Crustal-scale cross-section across the western Axial Zone following recent interpretations. Top; by Teixell et al. (2016). Bottom; by Garcia-Senz et al. (2020).

Basement thrusts merge upwards at the bottom of the Mesozoic succession (Upper Cretaceous marls and limestones to the North and Middle-Upper Triassic evaporites to the South) and are related to kilometric-scale fault-bend folds. Outcropping Paleozoic units are located in the hangingwall of the two uppermost thrusts in the system (Teixell, 1996, Teixell et al., 2016; Fig. 4): the Lákora-Eaux-Chaudes thrust to the North and the Gavarnie thrust to the South.

The foreland of the Gavarnie thrust is characterized by the wide synclinorium of the Jaca Basin (i.e. the Guarga sinclinorium), filled up by Eocene and Oligocene synorogenic sediments. The northern limb of the Guarga synclinorium is known as the Internal Sierras (Fig. 4). They consist of a fold-and-thrust system that affects the Upper Cretaceous to Paleogene units overlying the basement. This thrust system (the Larra-Monte Perdido thrust system) is dominantly south-verging and presents a main décollement found at the Zuriza marls and Marboré sandstones unit (Labaume et al., 1985; Teixell, 1992). Additional décollements are identified at the base of the Upper Cretaceous sequence (Calizas de los Cañones limestones; Rodríguez Mendez, 2011) that is clearly involved in the Larra-Monte Perdido thrust system at the western termination of the Axial Zone (Teixell et al, 1989). The Larra-Monte Perdido thrust system in the Internal Sierras is southwards tilted, located above a south-dipping basement panel at the frontal tip of the Gavarnie basement thrust (Séguret, 1970; Labaume et al., 1989; Teixell, 1992; Izquierdo-Llavall et al., 2013). The dip of this basement panel changes along-strike, decreasing westwards at the western termination of the Axial Zone. The Larra-Monte Perdido thrust system branches northwards with the Lakora-Eaux-Chaudes basement thrust (Teixell, 1996, 1998) and extends at depth several tens of kilometers to the South of the Internal Sierras (as attested by well data; Labaume and Teixell, 2018).

The southern limb of the Guarga synclinorium consists of several imbricates emerging in the hangingwall of the South Pyrenean Frontal thrust (the Sierras Exteriores; Almela and Ríos, 1951; Puigdefàbregas, 1975; Millán et al., 1995, 2000). The Sierras Exteriores crop out 7-17 km to the South of the GeoEra project area (Fig. 4). Thrusts forming this frontal structure detach on Triassic evaporites and deform a Mesozoic-Paleogene sequence that is made of Upper Cretaceous shallow marine limestones, Upper Cretaceous-Lower Eocene red sandstones and shales and Middle Eocene platform limestones (the Guara Fm; Puigdefàbregas, 1975; Millán et al., 1994). The structure deforming these units consists of a NW-SE-trending and west-plunging anticline (the Santo Domingo anticline) that interferes with a set of oblique, NW-SE to N-S trending anticlines (Fig. 3; Millán et al., 1994; Poblet and Hardy, 1995). During their development, these NW-SE to N-S folds experienced significant clockwise vertical axis rotations (Pueyo et al., 2002; Soto et al., 2006; Muñoz et al., 2013; Mochales et al., 2012; Oliva-Urcia et al., 2012; Ramón et al., 2012; Pueyo-Anchuela et al., 2012) which are nevertheless negligible to the West of the Santo Domingo anticline (Larrasoaña et al., 2003; Pueyo et al., 2002; Oliva-Urcia et al., 2012).

The Guarga synclinorium is filled by a 4 km thick succession of Ypresian-Lutetian turbidites in the North (Fig. 3, 4; the Hecho Group, Mutti and Sgavetti, 1987; Mutti et al., 1988). These turbidites onlap southward the underlying Lower and Middle Eocene platform limestones (Puigdefàbregas, 1975; Labaume et al., 1985; Barnolas and Teixell, 1994; Muñoz et al., 2013) and are in turn overlain by Upper Eocene deltaic marls (Puigdefàbregas, 1975; Dreyer et al., 1999) and Upper Eocene to Lower Miocene continental sequences. These units are traversed by several NW-SE to E-W-trending thrusts including the Oturia, Jaca, Sierra de Illón and Sierra de Leyre thrusts (see Fig. 28).

The axis of the Guarga synclinorium roughly coincides with the cut-off of the basement units in the hangingwall of the Guarga basement thrust (Labaume et al., 2016; Labaume and Teixell, 2018). This thrust uplifts the northern part of the Jaca Basin and the western Axial Zone (Gavarnie thrust) and represents the lowermost of the thrust units involving the Paleozoic. In between the Guarga and Gavarnie units, different authors define a variable number of basement thrusts based on the interpretation of available seismic data (Cámara and Klimowitz, 1985; Teixell, 1996; Casas-Sainz, 2005; Labaume et al., 2016; Labaume and Teixell, 2018). There is no consensus on the number, names, geometries and ages of these basement thrusts nor in their lateral relationships.

3 METHODOLOGY AND PREVIOUS INFORMATION

3.1 Overview of the workflow

As a general rule, we have followed the methodological approach proposed in this project in D6.4 "**Optimized 3D reconstruction workflow based on gravimetric, structural and petrophysical data**" where additional details have been extensively described. This workflow is based on three main pillars; gravimetric data, robust petrophysical (density) data and serial cross sections, and three different levels depending on the data processing level can be established (Figure 6):

1) Level 1 considers the raw data from different sources. First, structural, stratigraphic and cartographic elements derived from field work and/or from data repositories are processed and synthetized in GIS platforms (Q GIS and ArcGIS). In second place, gravimetric data measured in the field and post-processed plus harvested data from bases (standard reductions are performed in this level) with in-house software. And finally, the petrophysical properties of the lithologies involved are estimated. Data come from field records, from well logging (mostly non-accessible) or obtained from FAIR databases. In our study case, we also included the interpretation of seismic sections in this level.
2) Level 2 involves a certain degree of data processing. The gravimetric data are processed to obtain the Bouguer anomaly as well as regional and residual components or other enhancement techniques (vertical and horizontal derivatives, etc.). Cross sections, if possible balanced, are built from the structural and stratigraphic information as well as from seismic section interpretation. In this level petrophysical data (density) are also grouped and processed together depending upon the final selection of stratigraphic horizons to be modelled.
3) Level 3 is focused on modelling. 2D and/or 3D, sequentially or alternatively (the 2D step may be skipped in areas with extensive or at least sufficient subsurface information), in level 3 an integrated 3D structural model is build merging all data together - the petrophysical and geological data (formation and structural trends, bed dips, stratigraphic thicknesses, etc.) together with the measured gravimetric field. The integration of the geological data to obtain the initial 2D or 3D geological model can be performed in several software platforms. In this working package we used Gravmag and Oasis for the 2D modeling (balancing cross sections with the gravimetric and petrophysical information) and Move by Petroleum Experts (former Midland Valley Ltd.) to build a 3D model with geological attributes (depth geometry, contacts, faults, etc.).
4) Further processing during the generation of 3D models with attributes includes the forward modelling and inversion of potential field data. Because a number of reasons that delayed the project milestones, in this report we show the forward modelling and the inversion of the basement topography using the GM-SYS 3D module of Oasis Montaj (from Seequent).

Figure 6 (next page): Synthetic workflow for 3D modeling used in this project.

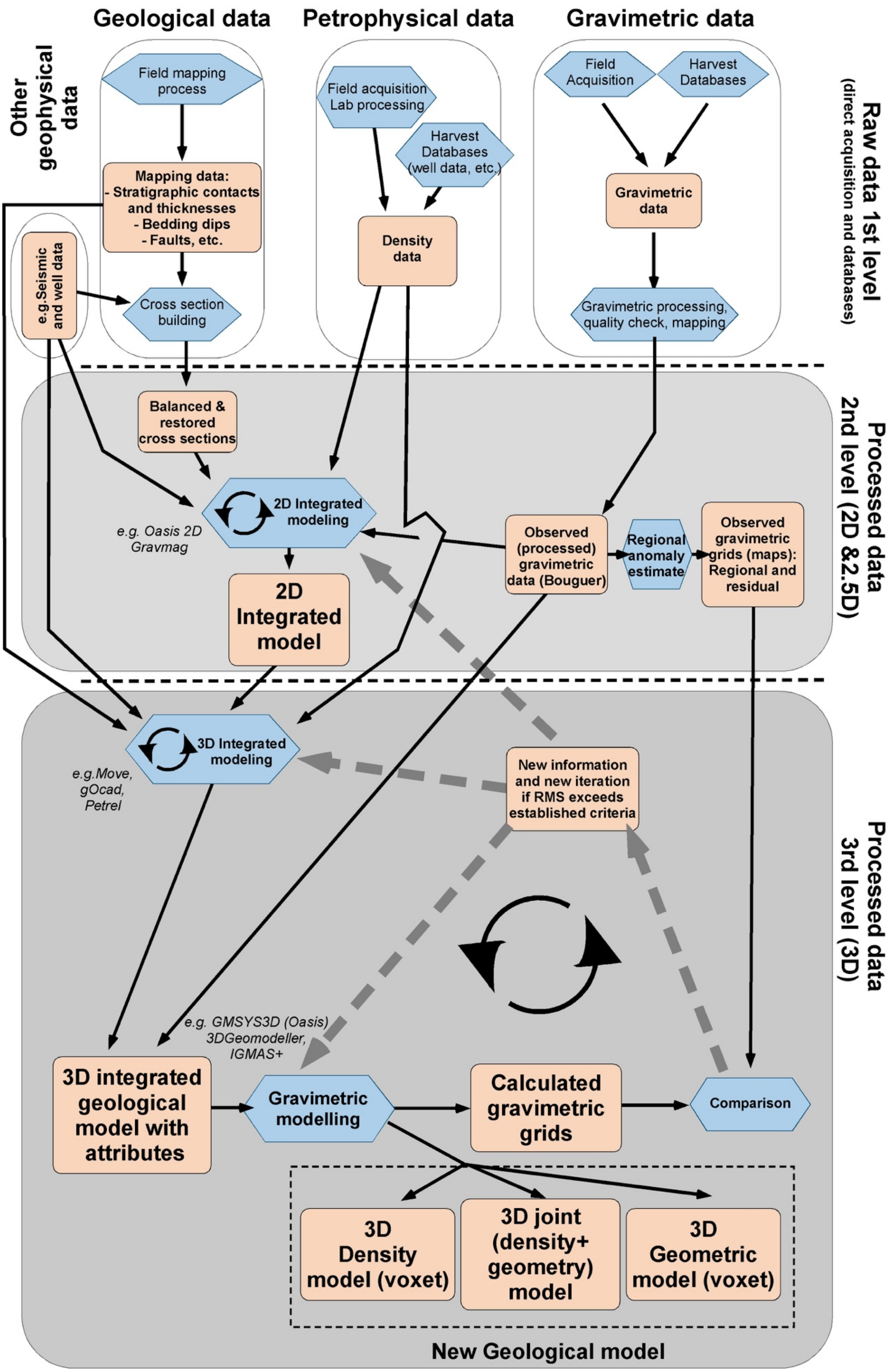

Geological data
Petrophysical data
Gravimetric data
Other geophysical data
Raw data 1st level
(direct acquisition and databases)
Field mapping process
Mapping data:
- Stratigraphic contacts and thicknesses
- Bedding dips
- Faults, etc.
Cross section building
e.g.Seismic and well data
Field acquisition Lab processing
Harvest Databases (well data, etc.)
Density data
Field Acquisition
Harvest Databases
Gravimetric data
Gravimetric processing, quality check, mapping
Processed data 2nd level (2D &2.5D)
Balanced & restored cross sections
2D Integrated modeling
e.g. Oasis 2D Gravmag
2D Integrated model
Observed (processed) gravimetric data (Bouguer)
Regional anomaly estimate
Observed gravimetric grids (maps): Regional and residual
Processed data 3rd level (3D)
3D Integrated modeling
e.g.Move, gOcad, Petrel
New information and new iteration if RMS exceeds established criteria
e.g. GMSYS3D (Oasis) 3DGeomodeller, IGMAS+
3D integrated geological model with attributes
Gravimetric modelling
Calculated gravimetric grids
Comparison
3D Density model (voxet)
3D joint (density+ geometry) model
3D Geometric model (voxet)
New Geological model

3.2 Projection, GIS and boundary boxes

The European Terrestrial Reference System 1989 (ETRS89) was used as the geodetic Cartesian reference frame. Besides, all data were referred to the Universal Transverse Mercator (UTM) projection system and, specifically, in the UTM 30T North zone. Therefore, all georeferenced files accompanying this deliverable (D6.2) used this projection and reference system. The project boundaries are: X: 652000, Y: 4760000 (NW corner) and X: 694000, Y: 4710000 (SE corner) (Fig 7 red quadrangle). A larger portion was selected to avoid border effects in the model building (Fig 7 blue quadrangle); X: 620000, Y: 4780000 (NW corner) and X: 720000, Y: 4690000 (SE corner).

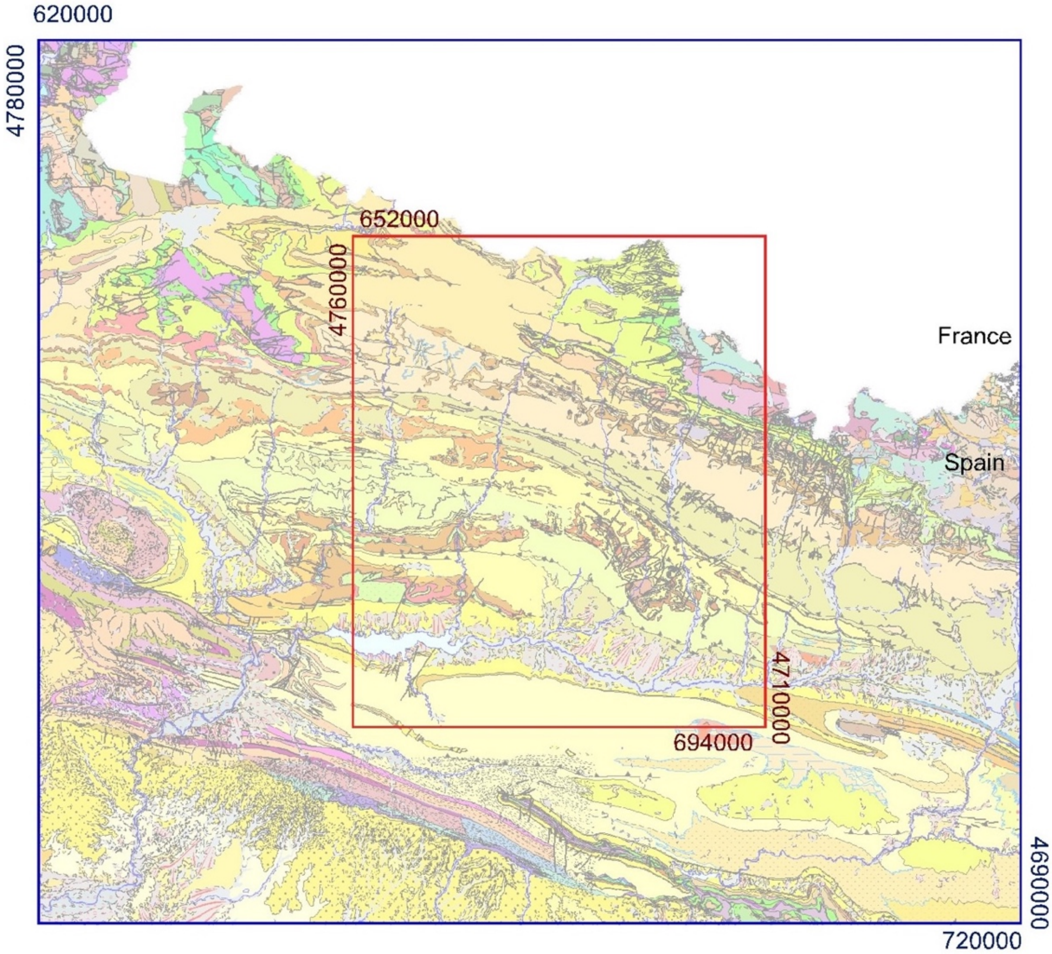

Figure 7. Southwestern Pyrenees project boundaries (ETRS89 UTM30T-N). Geological map derived from Harmonized Digital Geological Map.(1:50.000), GEODE Plan (Pyrenean and Ebro Basin regions) (Robador et al., 2011 and 2019).

Geological information in 2D (geological map and cross sections, petrophysical and gravimetric stations, etc.) were handled in standard GIS platforms like ArcGIS and Q.GIS (Sherman et al., 2004). The Move software (by Petroleum Experts, formerly Midland Valley Exploration) was used (licensed under IGME) for the integration in 3D of the geological and geophysical information (seismic sections).

3.3 Seismic and wells

Almost 350 seismic sections (reflection) were acquired in the wider area of the project (blue rectangle in Fig. 8) during the 70's, 80's and 90's. Seismic acquisition was partially driven by the discovery of the Serrablo gas field to the East of the project box (between the red and blue rectangles, see Fig. 8). Unfortunately, only ca. 50% of them were available for the modelling of the subsurface in the frame of this project because of access problems to the data. Besides, we could only recover high-resolution images (600 ppp) of most of them and very few in digital SGY format (23 profiles, Table 1). Both high resolution images and SGY profiles are in double time domain and reach maximum depths of 4 to 4.8s, the imaging being very poor below 2.5s. All in all (table 1), in the frame of this project, we interpreted 172 seismic sections (22 in SGY format and 119 in HR TIFF one). In total, more than 2300 km of seismic sections were studied. Studied data came from different repositories; mostly from the Geophysical Data Repository (SIGEOF) by IGME (https://info.igme.es/SIGEOF/) and also from the Technical Archive of Hydrocarbons (ATH), depending upon the Spanish Ministry of Ecologic Transition and Demographic Challenge (https://geoportal.minetur.gob.es/ATHv2/). A few sections were also provided by closer collaborators from the universities of Barcelona, Zaragoza and Montpellier. In any case, the shot points navigation data was always available. Additionally, 26 exploration wells were also available in the study area (Fig. 7) from public databases (SIGEOF) or from other public repositories (ENRESA database). The considered exploration wells have variable lengths (from ~1950 m up to 5370 m) and traverse the Cenozoic cover, with several deep boreholes also traversing the Mesozoic sequence and the top of the Paleozoic basement. Sonic logs from four of the considered wells were accessible and were used to carry out the depth conversion of the seismic profiles. Unfortunately, and despite the large number of boreholes in the western Pyrenees, formation density logs (gamma-gamma) were not accessible for any single well.

	Existent (all)	Available			No access
		SGY	TIFF	Total	
Number of sections	347	23	119	142	205
Percentage	100%	6.3%	34.3%	40.9%	59.1
Km of coverage		529 (23%)	1795 (77%)	>2000	unknown

Table 1: Basic seismic reflection information

As a general rule, the spatial distribution of available sections is uneven and heterogeneous and many of them display a low-medium quality with a heterogeneous degree of seismic signal processing. Because of this, we decided to split the project model (in the wider sense) in five different sectors (sectors 1 to 5). Sectors were defined based on structural criteria. Sectors 1, 2 and 3 are located to the East, show a dense seismic coverage and are well connected by along-strike seismic profiles. Sector 1 extends throughout the eastern part of the Guarga syncline. Sector 2 (to the North of sector 1) extends from the Internal Sierras to the Yebra de Basa anticline, in the area located between the Tena and Aragüés valleys. Sector 3 was defined to the West of sector 2 and extends from the Aragüés to the Ansó valleys. To the West, sectors 4 and 5 extend through the western Jaca Basin. Seismic data in this area is scarcer and poorly connected to sector 3. The GeoEra project area considers seismic data from sectors 2, 3 and 4, covering the gap of seismic data between the eastern and western areas. In fact, this was why we proposed, as one of the main goals of the project, to harmonize this information by means of the feedback with the gravity data.

Due to the poor quality results, initial trials to digitalize the TIFF sections into SGY files (for example using Image2seg software by Farrán, 2008) were ruled out and we decided to manually adjust the sections in the software package Move (by Petroleum Experts , formerly Midland Valley). Move was the main tool for:

- Integrating all relevant information (Digital Elevation Model, DEM), geological mapping, structural data (dips), seismic sections, boreholes, previous cross sections, etc.
- Projection of outcrop traces and bedding attributes from geological maps on the DEM as well as the analysis of outcrop traces.
- Manually final adjusting of misfits and drawing the identified reflectors (see the seismic stratigraphy section). Interpretation of seismic reflection profiles was supported by three oil exploration wells available in the target zone (Aoiz-1, Roncal-1, Sangüesa-1, by Lanaja, 1987), plus 23 additional ones, most of them in the Serrablo Gas field (see figure 10 for location and figure 12 for correlation panel between the lithological logs).
- Depth conversion of seismic profiles (Tiff and Segy files) and the stratigraphic horizons interpreted along them
- Construction of geological cross sections (including the structural projection of relevant data; seismic reflectors, bedding dips, outcropping traces, etc.).
- Construction of reference surfaces (faults and stratigraphic horizons) from the depth-converted seismic interpretations and constructed cross-sections. Projection and construction of ancillary cross sections. Final fusion of horizons.

Time-to-depth conversion of the seismic reflectors was based on the sonic logs only available in 4 boreholes; Roncal-1 in the target area and other three wells (Aoiz-1, Sangüesa-1 and Pamplona Sur-1) located to the West. The scarcity of sonic logs precluded the building of a 3D velocity model and a 2D time-to-depth conversion was done instead. For this purpose, the 2D depth conversion tool in Move was used. The location of some key seismic reflectors (top of the Eocene carbonates, top of the Keuper evaporites and top of the Paleozoic basement) was double-checked with the lithological record (well depths) after depth conversion. A good fit was generally observed.

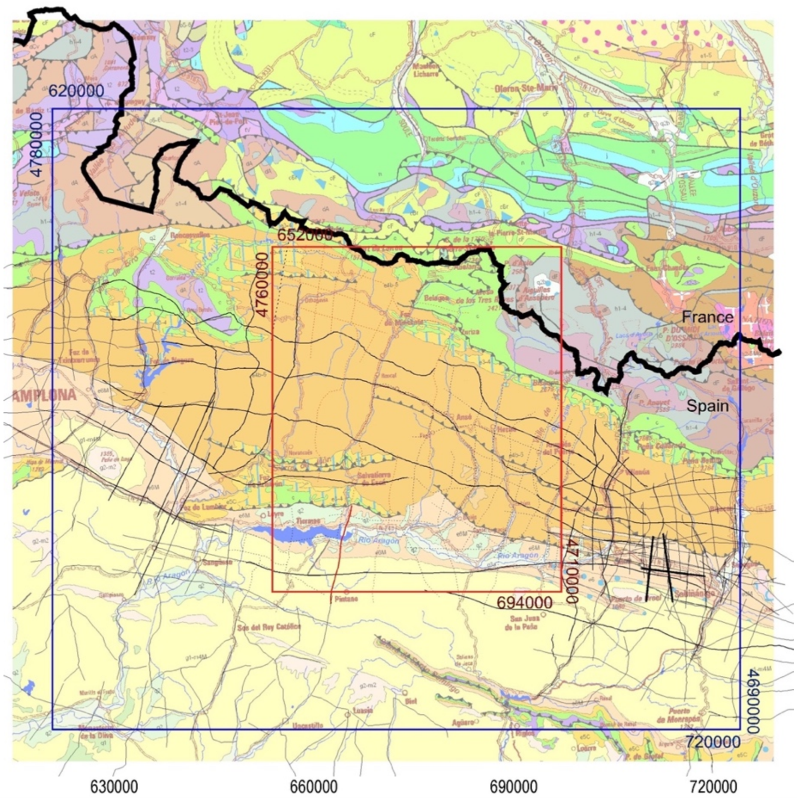

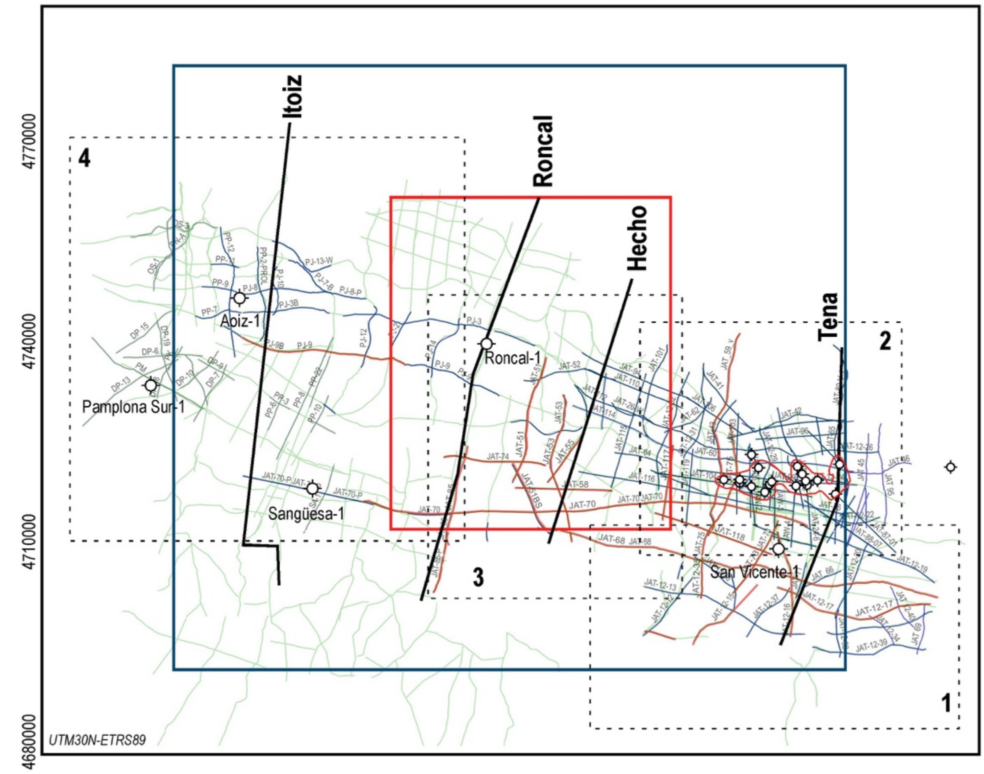

Figure 8. Subsurface information in the study area with (upper) and without (lower) geology. Blue sections; available in TIFF format, red sections available in SGY format, green sections; non available (access problems). Oil exploration boreholes are also shown. The red target square is the main target area, the blue one is the accompanying one. Seismic projects limits (from 1 to 4) as well as the balanced section are also identified.

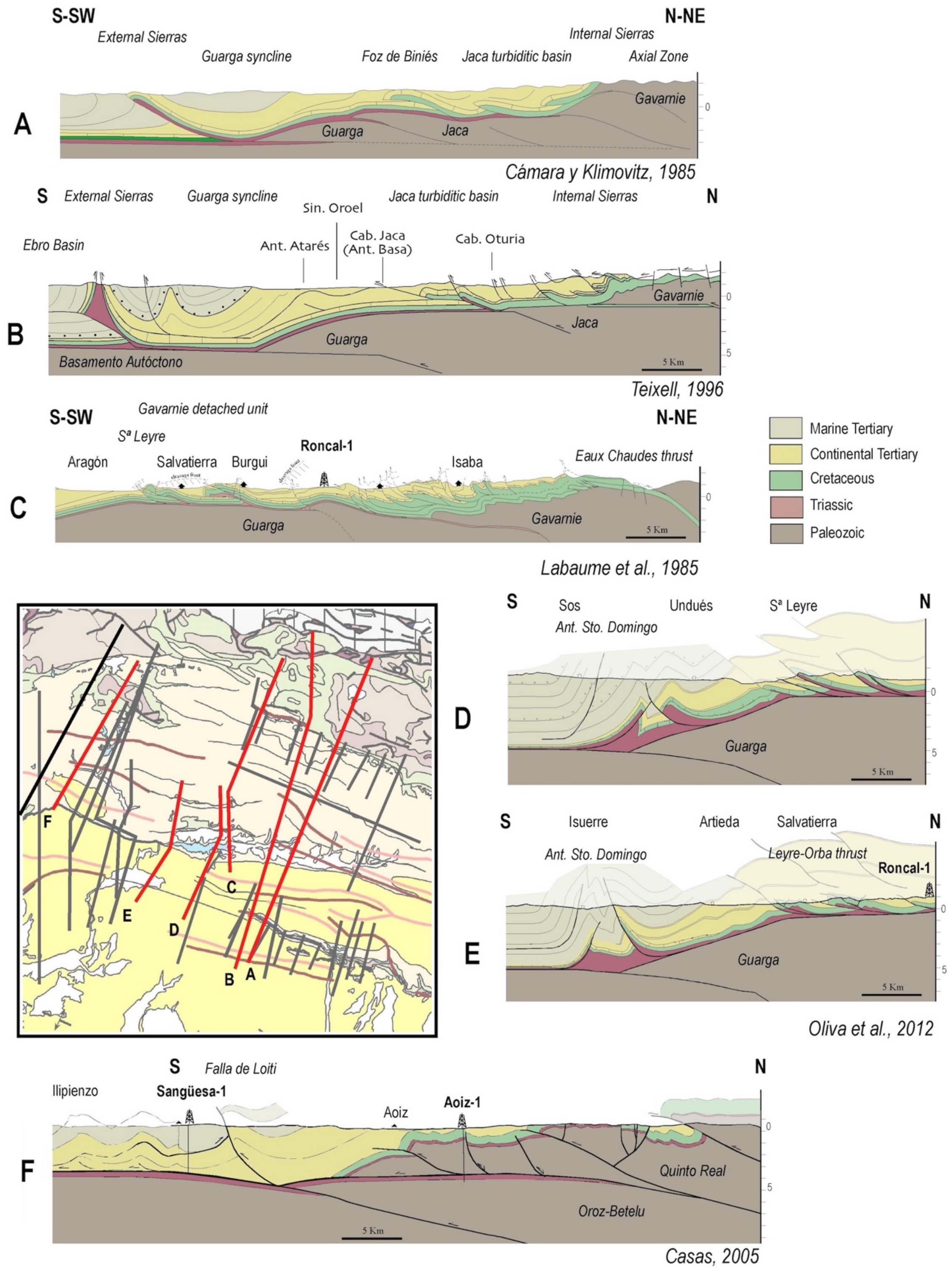

Figure 9. Some relevant (mostly balanced and restored) geological cross sections in the western Pyrenees displaying the most important basement thrusts and cover structures.

3.4 Structural geology

Beyond the 1:50.000 scale maps (MAGNA plan by IGME) and subsequent harmonization at larger scales (Robador et al., 2011 and 2019), several academic and research studies have bee performed in the Southwestern Pyrenees during the last decades (Puigdefàbregas, 1975; Teixell, 1992; Millán 1996 and 2006; Oliva-Urcia, 2000, Pueyo, 2000; Montes, 2002 and 2009) and have provided excellent synthetic maps to identify the main structural features.

Furthermore, numerous research papers had focused on the subsurface geology of the southwestern Pyrenees and abundant cross sections are available (Cámara and Klimovitz, 1985; Labaume et al., 1985; Nichols, 1984 and 1987; McElroy, 1990; Turner and Hancock, 1990; Turner, 1996; Millán, 1996; Schellart, 2002; Pueyo-Anchuela, 2003; Casas 2005; García-Sansegundo, 2014; Cámara and Flinch, 2017), but unfortunately, balanced and restored cross sections are limited (Teixell, 1996; Larrasoaña et al., 2003; Casas and Pardo, 2004; Pueyo et al., 2004; Meresse, 2010; Oliva-Urcia et al., 2012; Labaume et al., 2016; Anastasio et al., 2020), see figure 9.

3.5 Cross sections

We constructed three new NNE-SSW-trending cross-sections distributed along the Jaca basin (Fig. 10), from East to West: Tena, Hecho and Roncal valleys cross-sections. These cross-sections were used together with the cross-section by Casas-Sainz (2005) and the depth-converted interpretation of the seismic profiles to construct the main horizon and fault surfaces used in the 3D model. Two of the cross-sections (Hecho and Roncal valleys cross-sections) traverse the area of the GeoEra project.

Cross-sections were entirely constructed using the software Move (Petroleum Experts). Section traces were defined as parallel to the vertical planes that statistically best fit bedding poles in the cross-section areas. Using this trace selection method, the Hecho valley cross-section was defined as straight all along its trace whereas the Roncal and Tena valley cross-sections consist of three and two sub-traces displaying slight trend variations. Cross-sections were built based on (Fig. 10):

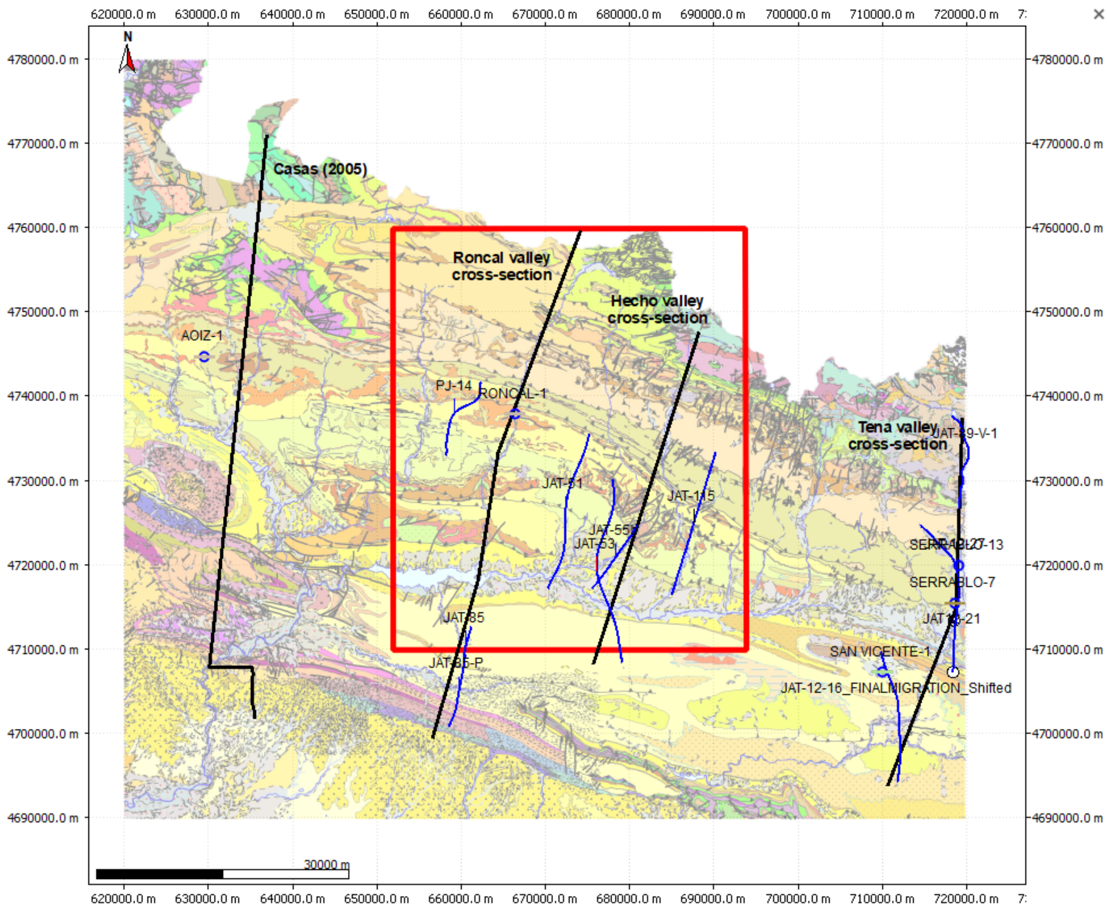

Figure 10. Geological map of the study area with location of the constructed cross-sections (black solid lines). Key wells and seismic profiles considered for cross-section construction are also shown.

- The 1:50000 geological maps of the area (Magna series, see references above). The stratigraphic horizons and outcropping faults mapped in the cross-section areas were digitized and the intersection between them and the section traces was considered for cross-section construction. Additionally, we also considered the 3D geometry of certain horizons and faults to define geometries above the cross-section topography: cross-sections run along the main valleys (where the acquisition of structural data was easier) and the horizons and faults at the valley slopes could at some areas be projected to section traces. This allowed a partial reconstruction of the eroded geometries which is fundamental for cross-section balancing.

- The available bedding data. Bedding data at distances below ~ 2 km from cross-section traces were preferentially considered for cross-section construction. Bedding data were generally projected as parallel to fold axis and belonged to different source datasets: structural data from the Magna series geological maps and from previous academic works (Puigdefàbregas, 1975; Millán, 1996; Pueyo, 2000; Larrasoaña, 2000; Oliva-Urcia, 2000&2004; Montes, 2002; Pueyo-Anchuela, 2013; Izquierdo-Llavall, 2014).

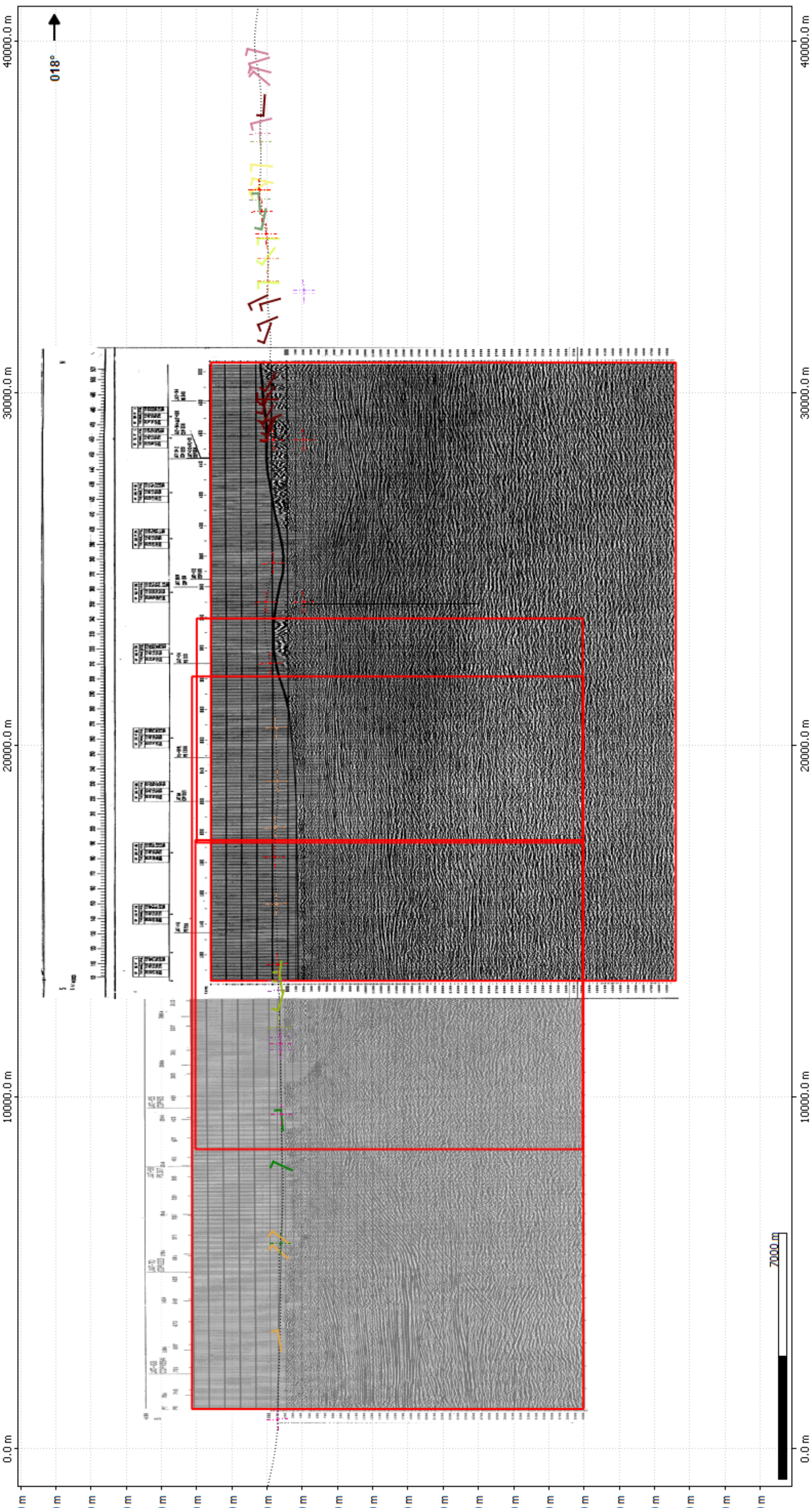
018°
0.0 m
10000.0 m
20000.0 m
30000.0 m
40000.0 m
8000.0 m
7000.0 m
6000.0 m
5000.0 m
4000.0 m
3000.0 m
2000.0 m
1000.0 m
0.0 m
-1000.0 m
-2000.0 m
-3000.0 m
-4000.0 m
-5000.0 m
-6000.0 m
-7000.0 m
-8000.0 m
-9000.0 m
-10000.0 m
-11000.0 m
-12000.0 m
-13000.0 m
7000 m

Figure 11 (previous page). Data considered for the construction of the Hecho valley cross-section. Crosses in the topographic profile indicate the intersection of outcropping stratigraphic horizons and faults with the cross-section trace. Dip data are projected from neighboring zones. The depth structure is mostly based on the depth-converted seismic profiles shown in the figure that were projected perpendicularly to the cross-section trace (previous page).

- Well data. Well top data from wells Roncal-1, San-Vicente-1, Serrablo-7 and Serrablo-1 were taken into account (Lanaja, 1987). Roncal-1, Serrablo-7 and Serrablo-1 are located along the traces of the Roncal and Tena valleys cross-section respectively, whereas the San-Vicente-1 well was projected to the Tena valley cross-section trace from a distance of 5.5 km (Figs. 10 and 12). The cross-section by Casas-Sainz (2005) is constrained by the Aoiz-1 well. Remaining wells were taken into account for horizon tying across the available seismic profiles, this horizon tying being also considered along cross-sections.

- The depth-converted seismic profiles. Seismic profiles in the GeoEra project area are in general terms less abundant than in the surrounding areas and had to be projected from longer distances (Fig. 10). For the constructed cross-sections, we considered the seismic lines JAT 85, JAT 85P, JAT51, PJ14, JAT53, JAT55, JAT55b, JAT115, JAT12-16, JAT12-21, JAT12-27v and JAT89v1 (see location and projection distances in Fig. 11) that were perpendicularly projected to cross-section traces.

To interpolate between the available dip data we used the kink method and considered the stratigraphic thickness variations reported by previous studies. The construction process was facilitated by the varied Model Building tools in the Move software package.

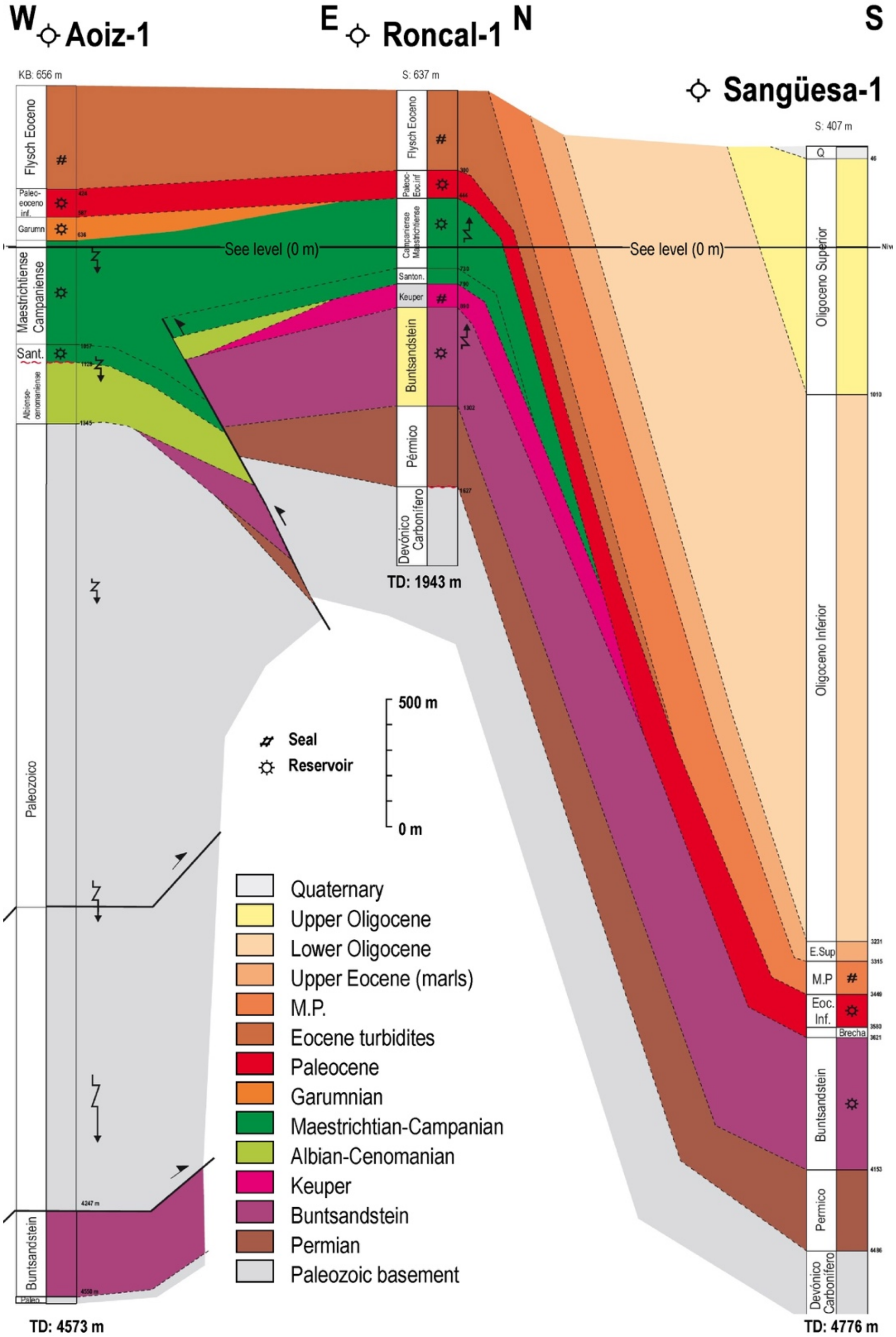

Figure 12. Correlation panel of Aoiz-1, Roncal-A and Sangüesa-1 boreholes (Pueyo et al., 2010 & 2012).

3.6 Gravimetry

The study area comprised more than 4400 gravimetric stations from previous databases (SITOPO compilation). In the Pyrenean area, these data were already harmonized together with the French ones (Ayala et al., 2016) (Figs. 13 yellow points). However, these data had a strongly uneven distribution and the lowest density of information was centered in the GeoERA target zone. Therefore, significant efforts were done to mitigate this problem and to homogenize the data distribution (Fig. 14). Considering our experience in previous and recent Pyrenean and Ebro Basin projects (Calvín et al., 2018; Izquierdo-Llavall et al., 2019; Santolaria et al., 2020; Ayala et al., 2021) focused on regional characterization, a 1km x 1 km net was adopted for the regional characterization of the Bouguer anomaly in the target (red) study area. Apart from the SITOPO database, we also harvested 975 gravimetric stations from previous IGME projects; to the South in the Santo Domingo anticline (Calvín et al., 2018) and some more points to the SE in the Guara Range (Santolaria et al., 2020). In this group we also included some data from mining studies in the SW corner of the study area (Granda-Sanz and Granda-París, 2014).

In total, about 3100 new gravimetric stations, close to 2400 within the study area, were obtained in the field during the project life in different campaigns that took place from November 2018 (Fig. 14) to November 2020. More than 700 additional stations were taken in Spring-Summer 2021 to the East of the study area to harmonize the Bouguer map and to complement future studies. 213 days in the field allowed to obtain the whole dataset. The development of these campaigns was strongly affected by the crash of one of the gravimeters in summer 2019, the very early snow in November 2019 as well as the pandemic situation that severely limited the mobility and field activities during 2020. It is worth mentioning that more than 700 gravimetric stations were acquired in rough Pyrenean terrains since the upper NE corner comprises altitudes and mountain landscape that almost reach 3000 m. Hiking with the equipment along mountain trails was necessary to get a homogeneous distribution of the data (Fig. 14) but the data acquisition rate was significantly lower (5.7 stations/day) compared to the mean of all standard campaigns (15.7 stations/day). In total (databases, previous projects and newly acquired data), we have used more than 8,500 gravimetric stations for building the Bouguer and residual anomaly maps (Fig, 13) in the accompanying project (blue) area (11,000 km^2). This implies about 0.8 stations(km^2), although the density in the core (red zone; ca. 2,000 km^2) exceeds 1 station/km^2, in agreement with the project goals.

Three different gravimeters were used in this project; a CG5 by Scintrex, a Lacoste&Romberg and ZLS by Burris corporation (this last one owned by the University of Zaragoza) (Fig. 15). Although the L&R is a vintage instrument, all three devices guarantee reading resolutions, at least down to 0,005 mGal, more than enough for the needs of the project goals. Repeatability of gravity readings was check during the campaign in about ≈7% of the stations performed to ensure the internal consistency of the dataset. Differential GPS was used to accurately locate the stations, and particularly their elevation (centimetric resolution). Two TRIUMPH-1 GNSS receivers (Fig. 15) were used for this purpose. The reference base stations used for differential correction corresponds to the IGN and Aragon permanent network of GNSS receivers (https://www.ign.es/web/ign/portal/gds-gnss-estaciones-permanentes) in particular using the locality of JACA as the main reference.

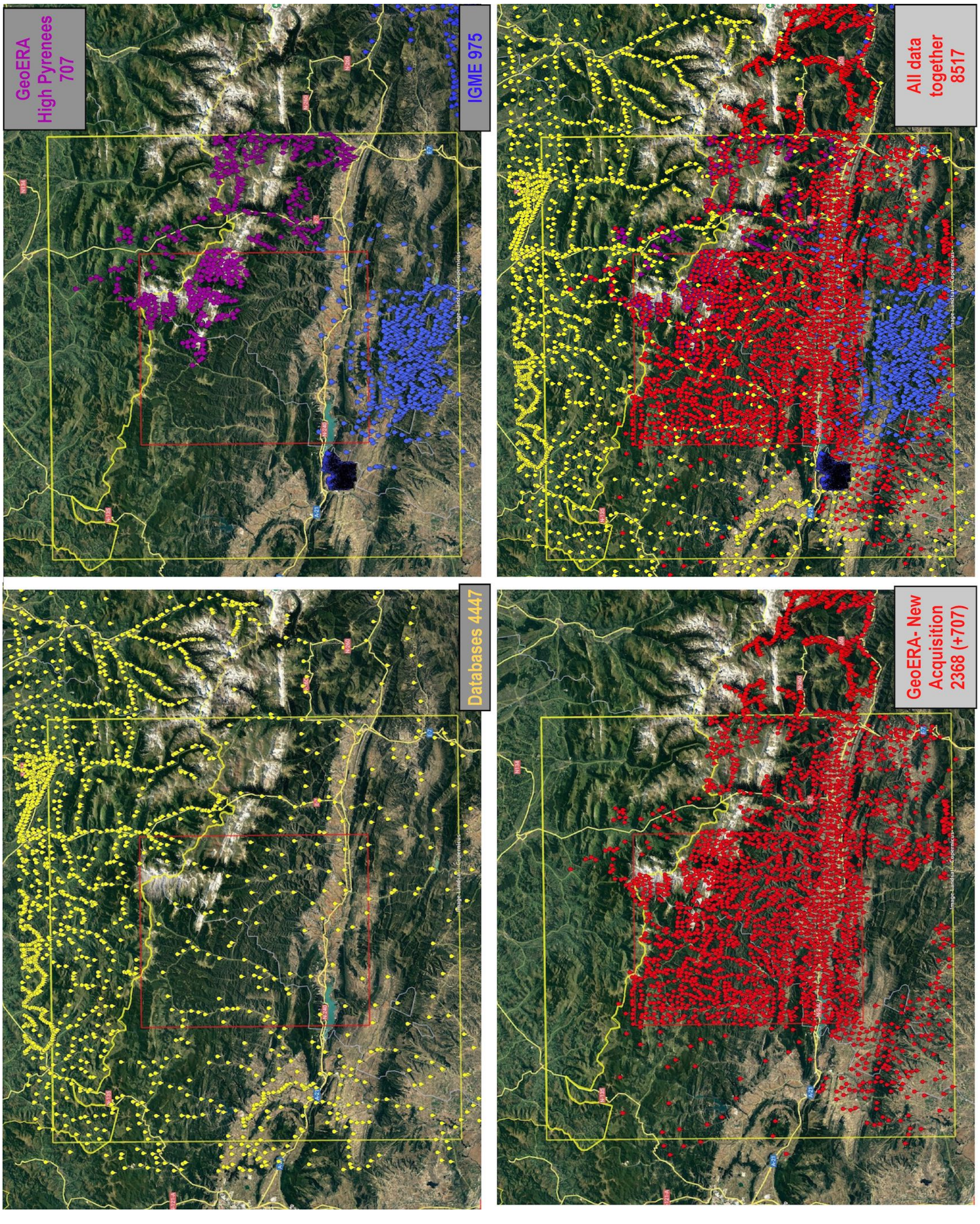

Figure 13. Gravimetric data used in the project

With respect to the relative gravity measurements, they were referred to the Spanish net for absolute gravity (REGA, Vaquero and Sainz-Maza, 2011) through six gravity bases located in the South Western Pyrenees, four of them in the northern part of the project area:

Base	code	g (mGal)	Lat	Long	Height (masl)
Jaca	NAPJ18*	980143.42	42° 34' 01,7''	- 0° 33' 14,1''	808.6204
Artieda	NGV 97	980227.44	42° 36' 35,0''	- 0° 59' 56,0''	505.8717
Sabiñánigo	NAPJ34	980141.30	42° 31' 04''	-0° 21' 52''	788.9057
Isaba*	NGV 97*	980191.4210	42° 51' 33''	-0° 55' 35''	774.13

The first three belong to the Spanish net of the nivelation (REDNAP; https://www.ign.es/web/ign/portal/gds-redes-nivelacion), and the Isaba one was created and tied up (*) to the absolute network by a standard "M" loop in the frame of this project for practical purposes. Two additional bases were located in the southern part of the study area and were previously linked together with the absolute gravity network (Calvín et al., 2018 and Pueyo et al., in review):

Base	code	g (mGal)	Lat	Long	Height (masl)
Luesia*	LUE	980161.2975	42° 22' 19''	-1° 01' 34''	791.71
Ayerbe	AYE	980195.7546	42° 16' 44''	-0° 41' 26''	573.69
Zaragoza (ESD-UZ)	UZAZ	980224.10	42° 38' 37''	-0° 53' 56''	219.85

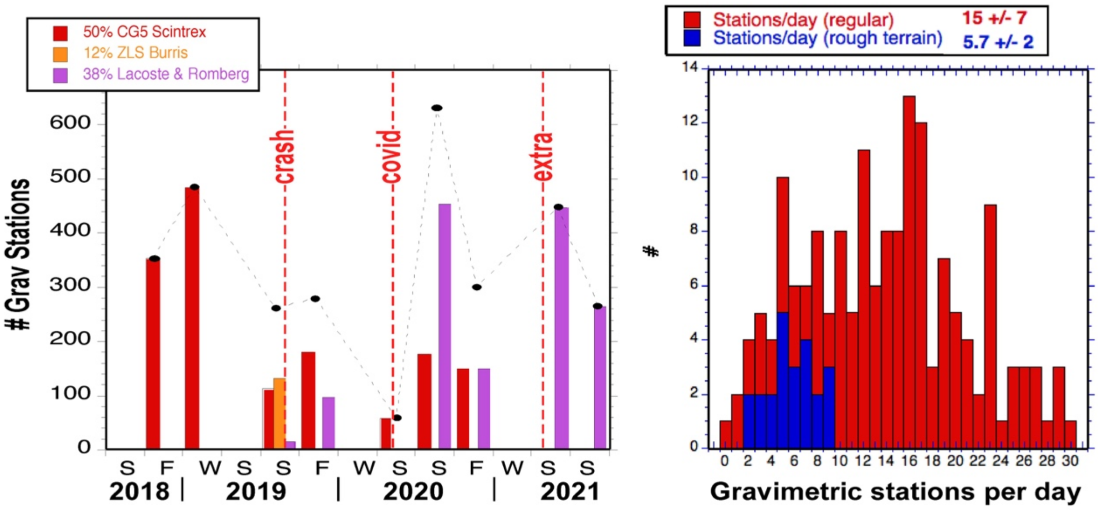

Figure 14. Data acquisition. Gravimetric campaigns in the GeoERA The three different gravimeters are shown in different colors. Main disruptive facts are indicated in the plot as well as the development of additional (extra) campaigns in the Eastern zone during spring and summer 2021. Acquisition averages per day (regular and rough terrains are split).

Figure 15. Gravimetric data acquisition during the project life. Bottom right photograph shows the three gravimeters used during the intercalibration campaign (ZLS Burris, CG5 Scintrex and Lacoste and Romberg from top to down).

Standard gravimetric acquisition and processing (reductions) procedures were applied to all gravimetric surveys (for a more detailed information see D6.4 "**Optimized 3D reconstruction workflow based on gravimetric, structural and petrophysical data**"). The standard Geodetic Reference System GRS80 (Moritz, 1980) was used to calculate the Bouguer anomaly after applying the free-air correction (Hinze et al., 2005), the Bouguer correction (density reduction 2670 kg/m^3) and the terrain correction (Hammer, 1939). In this respect, the near terrain correction was directly estimated in the field (Hammer's arcs of 17m and 53m) and the medium (170m) to far terrain corrections were derived from available digital elevation models (100 x 100m and 500 x 500m sampling grids respectively) up to 167 km.

3.7 Petrophysics

Several petrophysical data were available from previous research and academic works done in the study area. Most part of them were based on density determinations carried out in paleomagnetic and AMS samples: 9 sites (with more than 300 individual density determinations) belong to the Internal Sierras (Oliva-Urcia et al., 2009) and 197 additional sites (300 density determinations) are distributed along four N-S sections across the study area (Esca, Veral, Subordan and Aragón valleys) and were developed in the course of a PhD focused on the analysis of the anisotropy of magnetic susceptibility (Pueyo Anchuela, 2012) as well as some extra data from the Jaca Basin (Pueyo, 2000). Besides, additional density data were obtained during recent gravimetric studies south of the project area in the External Sierras (Calvín et al., 2018; 35 sites with 125 density determinations) and closer rock formations in the Southeast corner were also considered in the modelling (Santolaria et al., 2014, 2020). In any case, we decided to improve the density database focusing on less-represented rock formations (e.g. Paleozoic formations). Therefore, we performed new density estimations in two different types of petrophysical samples

- Type 1: Large hand-samples (a few dm^3) were obtained in 44 new sites in Paleozoic rocks. These samples were cut in cubic boxes (edges about 8-10 cm) and thus, normalized laboratory essays (see below) could be applied to derive robust density estimations. In these outcrops, auxiliary magnetic susceptibility measurements were taken (more than 40 readings) with a SM20 device (GZ Instruments).
- Type-2: Several unpublished paleomagnetic samples from the ongoing UKRIA4D project (42 sites and 185 measurements) and other samples stored in the IGME's Pmag-Lithotech were also used to improve the density database in Cretaceous to Eocene formations.

In type 1 samples, the apparent density estimation was applied following the European standard UNE EN 1936:2006 (Natural stone test methods - Determination of real density and apparent density, and of total and open porosity [CEN/TC 246 - Natural stones; CEN/TC 246/WG 2 - Test methods]) at the IGME laboratories (Tres Cantos, Madrid). In type 2 (paleomagnetic) samples, density was estimated in two different ways; application of the Archimedes buoyance principle and the estimation of the rock volume with a vernier caliper on cylindrical samples. For that purpose, only regular (cylindrical sections) and complete samples (whole, unbroken, etc.) were used. Any broken, incomplete, irregular or cracked specimen was ruled out. Apart from the weighting of the sample (m), the maximum and minimum diameters (Ø) and heights of the specimen (H) are measured with a Vernier caliper. Afterwards both measurements are averaged out ($Ø_m$ and H_m) and the volume was rapidly calculated: $V = \pi (Ø_m/ 2)^2 \cdot H_m$, as well as the density $\rho = m / (\pi [Ø_m/ 2]^2 \cdot H_m)$. Additional details can be found in D6.4, § 2.3 Petrophysics.

In total, we have acquired or compiled as well as harmonized and processed together, density data from 329 sites evenly distributed in the main target area (Fig. 16). 243 sites were recovered from previous works, and 86 new sites (193 determinations) were performed within the project life.

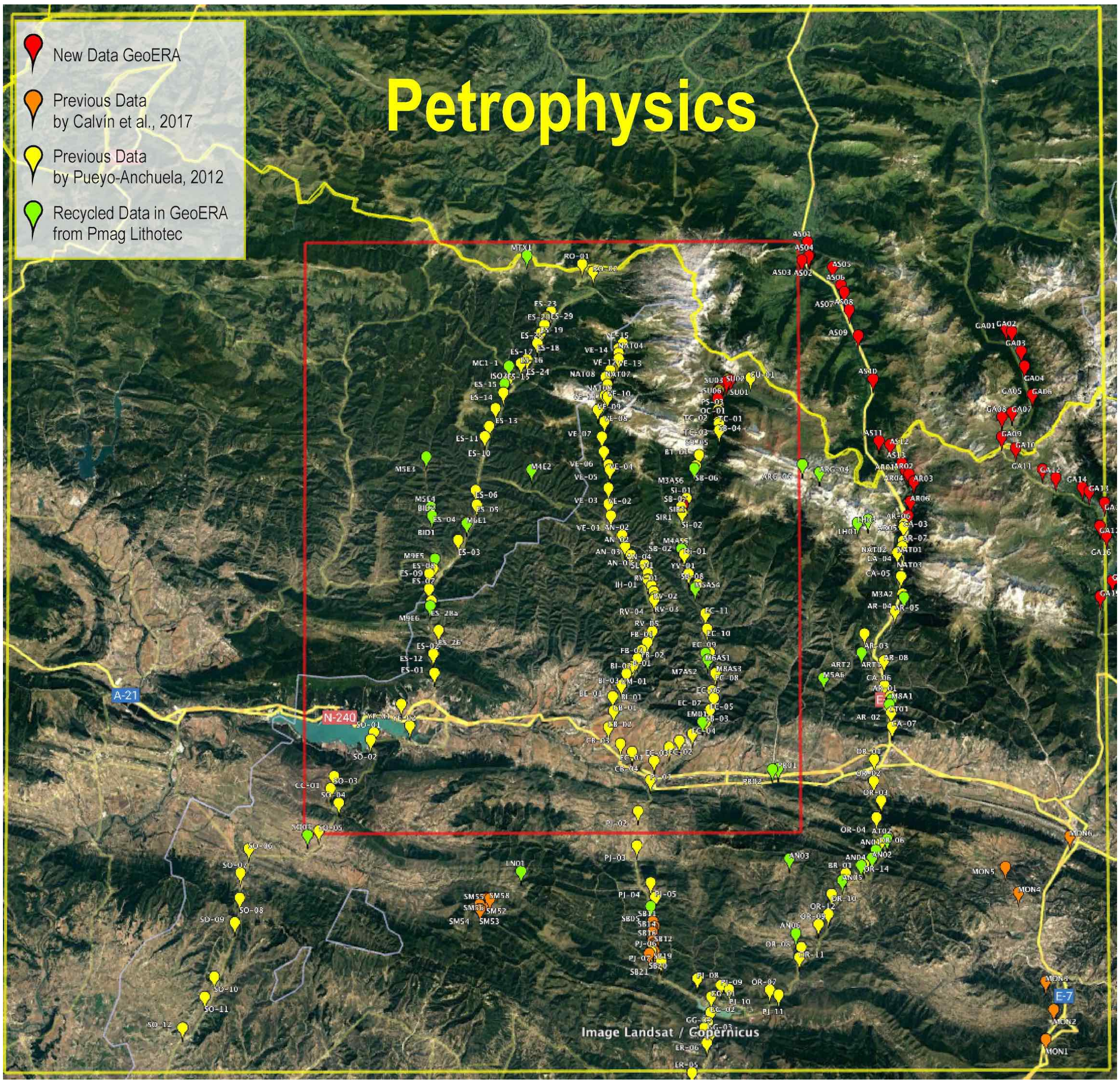

Figure 16. Petrophysical (density) data used in the GeoERA proyect.

Synthetic histograms and full statistical parameters were estimated separately (stratigraphic formations with indication of lithology) as well as grouping the stratigraphic units with structural sense; Jaca molassic basin (Campodarbe Fm), Lutetian-Bartonian marls (Arro-Larrés marls Fm, Arguis-Pamplona marls Fm and Belsué-Atares Fm), Jaca Turbiditic Basin (Hecho Group, tubidites), Internal Sierras (Paleocene and Upper Cretaceous limestones and siltstone fms; Zuriza, Millaris, Marboré, Cañones, etc…) and finally, the basement Paleozoic rocks (Permian and Carboniferous to Devonian sequences).

3.8 2D and 3D modelling

Altogether, these three different datasets (gravimetric, petrophysical and structural) allow to refine the geometric model of the subsurface. Two main modeling techniques can be applied; forward modeling and inversion (additional details can be found in D6.4, § 3.2 2D & 3D modeling). The basic principle of the forward modelling is simple; following the Newton's law of universal gravitation, the initial geometry of the model plus the petrophysical properties allow calculating its geophysical response (calculated gravimetric anomaly) which is compared with the observed anomaly (actual observation). Analyzing the misfits and the subsequent modification of the initial geological model is a manual or semi-automatic feedback processes (trial and error process) that eventually will end up in an acceptable model where all properties are consistent and balanced (geometry, petrophysical and gravimetric). Forward modelling can be performed in 2D and/or 3D. Usually, the Oasis Montaj is the reference software package in recent IGME projects (Izquierdo-Llavall et al., 2019; Santolaria et al., 2020; García-Senz et al., 2020) but we have also used the classic Gravmag program (Pedley, 1991) in some working areas (Mochales et al., 2007; Calvín et al, 2018).

On the other hand, the inverse modelling of gravimetric data consists of allowing the selected algorithm (there are several available solutions) to automatically modify the model (geometry and/or physical properties) to minimize the difference between observed and calculated anomalies. Several physical laws (gravitation, mechanics, etc.) and geometrical rules (governing the stratigraphic and deformed bodies) are involved and the inverse problem is not straight-forward. Therefore, some assumptions have to be taken because a precise and unique formulation showing the way the data have to be transformed to replicate the model does not exist. The formulation overview is described in length by Blakely (2005), a reference publication on inversion of geophysical data and a historical synopsis on inversion of gravimetric data can be found in Nabighian et al. (2005). In a practical sense, we can let the calculation run free but there is the risk that the results might not have any geological meaning. Alternatively, we can introduce several constraints (well logs, interpreted seismic profiles, surface geology, robust petrophysical data, etc.) to guide the software on how geometry or petrophysical properties can be modified. By doing so, the resulting parameter minimized observed versus calculated misfits while being consistent with the geological and geophysical observations.

In the southwestern Pyrenees we have used the software Gravmag for the 2D forward model of the two balanced sections (Hecho and Roncal ones) and the Oasis Montaj for the 3D forward modelling inversion of the basement geometries.

4 RESULTS AND DISCUSSION

4.1 3D model based on 2D seismic sections and wells

In this subsection we summarize the most significant results concerning the interpretation of more than 140 reflection seismic sections (> 2000 km) that hardly represents 2/5 of the actual coverage. Besides, we define the correlation between the seismic stratigraphy (main identified horizons) and the surficial stratigraphy by means of some key sections as well as the four available sonic logs. The adopted time-to-depth conversion is also discussed.

4.1.1 Seismic stratigraphy and selection of modeled volumes

Several seismic reflectors could be identified in the study case (Fig. 17), although a few of them represent key levels for the interpretation since they can be followed in many sections of the project. From down to top they are:

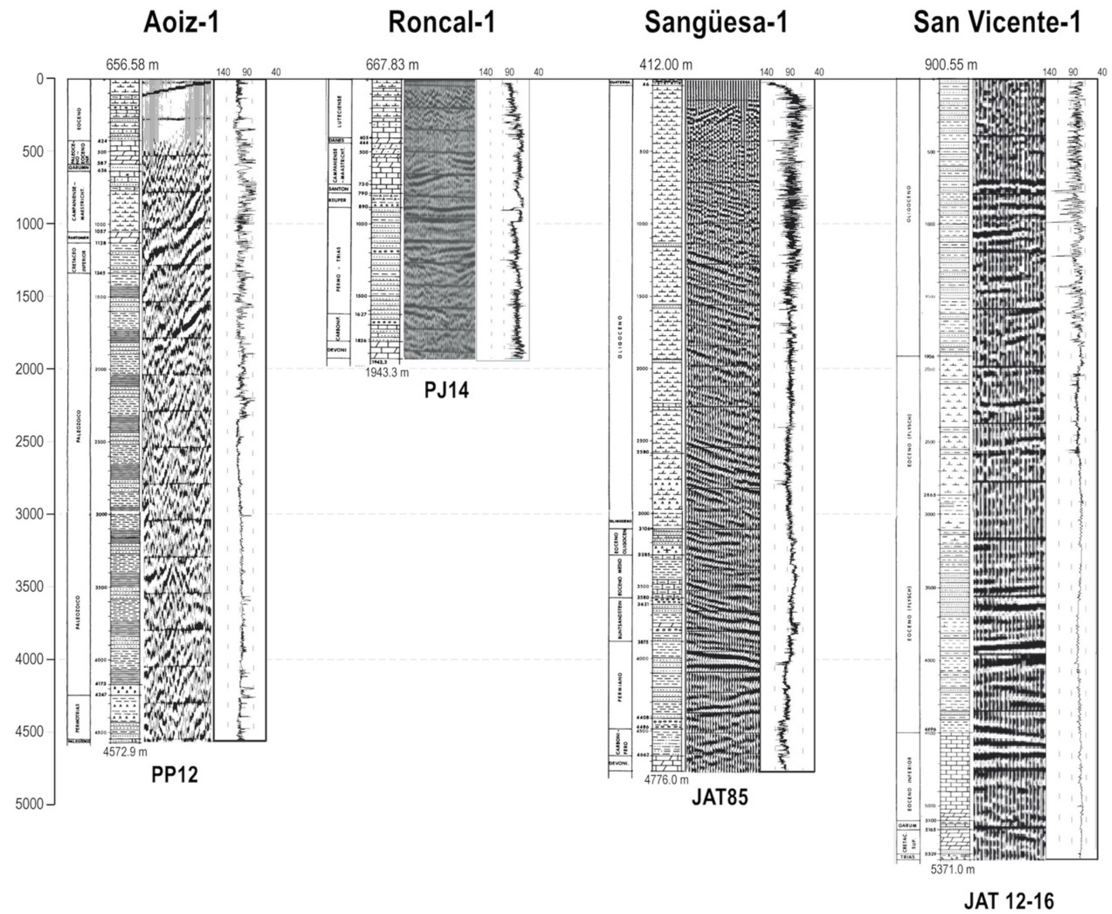

Figure 17. Key boreholes in the Project. Seismic stratigraphy, sonic logs and the original chronostratigraphic and lithological record (in Spanish) by Lanaja (1987)

- Paleozoic Top (Devonian-Carboniferous): the basement (s.l.) is usually represented by transparent seismic facies that can be identified in its top by characteristic and almost ubiquitous reflectors that have helped the definition of the basement geometry.

- The red beds from the Upper Permian and/or the Buntsandstein Lower Triassic facies also display distinctive seismic facies, being imaged as a medium to high reflective sequence.

- Cañones limestones. The base of these limestones witnessed for an important sedimentary hiatus in Southwestern Pyrenees since they unconformably overlie the Paleozoic basement cropping out in the Axial Zone. This high-density and elastic rock formation helps delineating the base of the Internal Sierras calcareous sequence as well as the top of the Keuper facies, which is absent to the North but very relevant to the South in the Jaca Basin and in the External Sierras.

- The rest of the Upper Cretaceous calcareous sequence (Marboré sandstones) as well as the Paleocene Lower-Eocene-limestones also show characteristic reflectors that can be followed underneath the very thick turbiditic facies (Hecho Group) and allow linking the subsurface geometry with the outstanding outcrops of the Internal Sierras.

- Some relevant and very thick megabeds (like the Villanúa one) can be also tracked in some seismic sections. Although their lateral extent is not so continuous as other Mesozoic and Cenozoic units.

- The Garum facies, across the Cretaceous/Paleocene boundary, crop out in the External Sierras to the South, display also distinct seismic reflectors and help tracking the top of the thinned Cretaceous sequence underneath the Jaca Basin to the South of the project area

- The Sabiñanigo Sandstones (northern Jaca Basin), approximately across the Lutetian/Bartonian boundary is a key reflector located between two identical seismic facies; the Arro/Larrés marls (Lutetian) and the Arguis-Pamplona ones (Bartonian) and was a key reference to reconstruct the geometry in this part of the basin as well as to relate the Lutetian turbiditic marls (Arro) with its equivalents to the South (Guara platform limestones) in the External Sierras.

- The very thick molassic sequence (Campodarbe formation) displays a large set of seismic facies where lateral (N-S and E-W) changes are very frequent. However, the availability of several seismic reflectors are key to define the geometry of the Jaca Basin.

Considering these reflectors, the average density values, the outcropping geological units and the goals of the project, we have defined six stratigraphic horizons for the 3D model (Fig 17):

(1) Top of Basement. In the absence of Permian red beds, the top of the Carboniferous or the top of Devonian is defined as the top of the basement.

(2) Top of Permian-Triassic red beds. Indicates the top of the Permian red beds (if present), otherwise this horizon is coincident with the top of the basement unit.

(3) Keuper top. Its occurrence is limited to the South-Central part of the model and it is absent in the Internal Sierras and turbiditic trough.

(4) Top of Paleocene limestones. This pretectonic layer also includes the entire Upper Cretaceous sequence (bottom to the base of the Cañones limestones, or top of the Keuper facies if present).

(5) Top of the Hecho group. Limits the upper extend of the turbidites in the northern part of the region. To the South and to the top, this sequence changes laterally to the Arro (Larrés) Lutetian marls and to the Guara limestones in the southernmost units (External Sierras) beyond the scope of this project.

(*) Due to their complex geometric relationships, sequences 4 and 5 have been merged for the gravimetric modeling. The average densities of these two units differ ~ 0.02 g/cm^3 which justifies their join interpretation in the 3D model used for the gravity forward and inverse modeling.

(6) Top of the Bartonian Arguis-Pamplona marls. This unit helps delineating the geometry of the Jaca molassic Basin underneath the Guarga synclinorium. The package defined between this and the underlying horizon includes the Arro/Larrés Marls, Sabiñánigo sandstone and Pamplona Marls.

(7) Top of Campodarbe. Only outcropping south of the main target zone, in the southernmost units (External Sierras) but with a cartographic expression that must be considered for the joint modeling.

4.1.2 Seismic Interpretation

Seismic interpretation required the identification of seismic facies across the studied seismic profiles. From well top data and their correlation trough seismic lines and to surface unit boundaries, six main seismic units are differentiated, from top to bottom: (1) the detrital sequence including the Campodarbe Group and the Belsué-Atarés Sandstone, (2) the marly sequence encompassing the Arguis-Pamplona and Arro and Larrés marls, (3) the Hecho Group turbidites, (4) the Upper Cretaceous to Middle Eocene carbonates, (4) the Keuper evaporites, (5) the Permian-Lower Triassic red beds and (6) the Paleozoic basement (older than the Permian).

The uppermost detrital unit (Campodarbe Group and Belsué-Atarés Sandstone) includes a lower reflective sequence and an upper more transparent unit. Reflectors in the lower part are generally discontinuous and describe growth geometries across the Guarga syncline where seismic profiles image strong thickness variations in the Campodarbe Group. The Pamplona and Arro/Larrés Marls are imaged as a transparent or semitransparent package whereas the Hecho Group turbidites are represented by a transparent to chaotic seismic unit. Both units show a progressive southward thinning, the Hecho Group turbidites grading to higher reflectivity carbonates in the southern limb of the Guarga syncline. They are underlain by the Upper Cretaceous to Middle Eocene carbonates. This carbonated sequence is clearly imaged in most seismic profiles as a highly reflective package consisting of high amplitude, continuous and parallel reflectors. Underlying the carbonates, the Keuper evaporites are identified in the southern part of the studied cross-sections. The Keuper unit is imaged as discontinuous, transparent to chaotic seismic facies that indicate the presence of salt. It shows strong thickness variations, being absent in the northern part of the study area and attaining its maximum thickness across the hinge zone and southern limb of the Guarga syncline. Internal higher-reflectivity reflections probably correspond to dolostone layers (Muschelkalk unit) interlayered within the salt. The Permian-Lower Triassic red-beds are a medium to high reflective sequence, well-tied in the Roncal-1 borehole. This unit shows thickness variations that inform on the location of inherited Triassic extensional faults across the studied area. Besides, Permian-Lower Triassic red-beds are also well imaged in the footwall of the Guarga and Oroz-Betelu thrusts where they consist of a 0.1 – 0.2 s thick unit of high amplitude and parallel reflectors. This high reflective package has been tracked along the available seismic profiles and used for the interpretation of the location, geometry and lateral continuity of the main basement thrusts. Permian-Triassic and Cretaceous units unconformably overlie the Paleozoic basement that is characterized by poor reflectivity and chaotic seismic units.

Apart from seismic facies themselves, seismic interpretation was also guided by surface geology. which was helpful for deciphering the along-strike tracking of cover thrusts. The interpretation at depth of cover thrusts largely relied on the geometry of the high reflectivity and generally well-imaged Cretaceous to Middle Eocene sequence.

Figure 18 (next page). Four examples of seismic sections (JAT12-16, JAT85P, JAT115 and JAt12-27) with and without the interpretation. The interpreted ones display the most relevant seismic reflectors used in this project

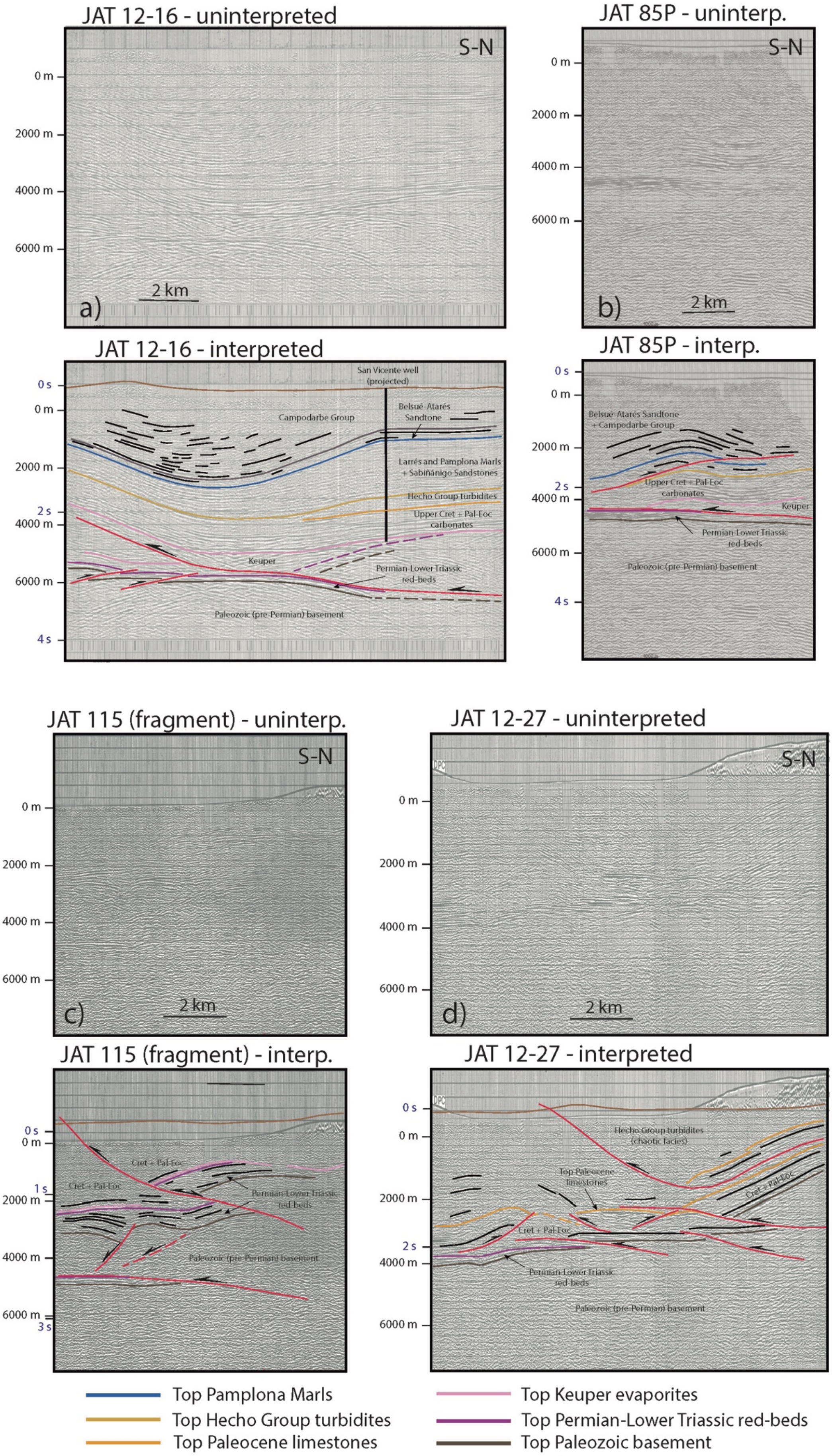
JAT 12-16 - uninterpreted
S-N
0 m
2000 m
4000 m
6000 m
2 km
a)
JAT 85P - uninterp.
S-N
0 m
2000 m
4000 m
6000 m
2 km
b)
JAT 12-16 - interpreted
0 s
0 m
2000 m
2 s
4000 m
6000 m
4 s
San Vicente well (projected)
Campodarbe Group
Belsué-Atarés Sandtone
Larrés and Pamplona Marls + Sabiñánigo Sandstones
Hecho Group turbidites
Upper Cret + Pal-Eoc carbonates
Keuper
Permian-Lower Triassic red-beds
Paleozoic (pre-Permian) basement
JAT 85P - interp.
0 s
0 m
2000 m
2 s
4000 m
6000 m
4 s
Belsué-Atarés Sandtone + Campodarbe Group
Upper Cret + Pal-Eoc carbonates
Keuper
Permian-Lower Triassic red-beds
Paleozoic (pre-Permian) basement
JAT 115 (fragment) - uninterp.
S-N
0 m
2000 m
4000 m
6000 m
2 km
c)
JAT 12-27 - uninterpreted
S-N
0 m
2000 m
4000 m
6000 m
2 km
d)
JAT 115 (fragment) - interp.
0 s
0 m
1 s
2000 m
4000 m
6000 m
3 s
Cret + Pal-Eoc
Cret + Pal-Eoc
Permian-Lower Triassic red-beds
Paleozoic (pre-Permian) basement
JAT 12-27 - interpreted
0 s
0 m
2000 m
2 s
4000 m
6000 m
Hecho Group turbidites (chaotic facies)
Top Paleocene limestones
Cret + Pal-Eoc
Cret + Pal-Eoc
Permian-Lower Triassic red-beds
Paleozoic (pre-Permian) basement
Top Pamplona Marls
Top Hecho Group turbidites
Top Paleocene limestones
Top Keuper evaporites
Top Permian-Lower Triassic red-beds
Top Paleozoic basement

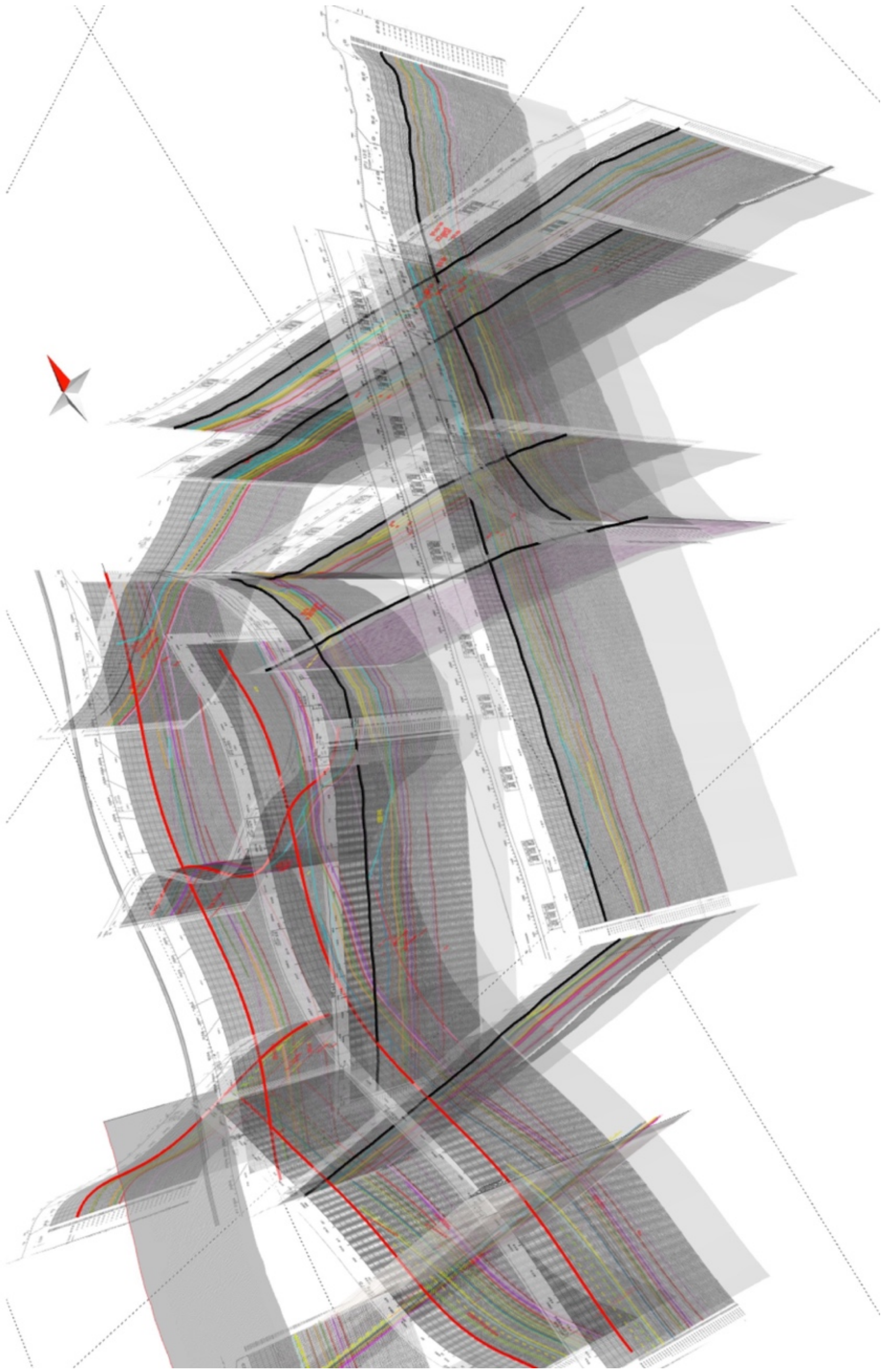

Figure 19. 3D view of the seismic sections in the SE corner of the target area (red box &.zone 3 in Fig.8).

4.1.3 Velocity model

Although the interpretation of the seismic sections was always carried out in two-way travel time (sg), the time-to-depth conversion was needed to integrate the seismic information together with other borehole and structural data in the space domain. Despite the large number of boreholes drilled in the Serrablo Gas field (> 15 among the Serrablo and Jaca series plus Villanovilla-1), none of their sonic logs were available for this study. The only sonic logs we had access to were: Roncal-1, Sangüesa-1, Aoiz-1 and Pamplona-Sur-1 (Fig. 20 and Fig. 8 for location). Accordingly, the construction of a 3D velocity voxet, as in other Pyrenean projects (Santolaria et al., 2020), was discarded this time. Among the four sonic logs, Sangüesa and Aoiz (more than 4000 m each) have the longest record and give the more consistent results. They both show a linear correlation between double-time and depth values, consistent with an approximately constant velocity through the drilled stratigraphic section. Pamplona-Sur-1 was identified as an outlier and consequently was ruled out for further calculations. The combined linear regression of the three datasets was used for the conversion: Depth = 60m + 2190 TWT (R^2=0.99), which gives a one-way velocity of 4,380 m/s similar to other Pyrenean studies. It is clear that the lack of more abundant and reliable sonic logs implies an inherent and significant uncertainty in the depth estimation from the seismic sections that may reach some few hundreds of meters depending on the depth.

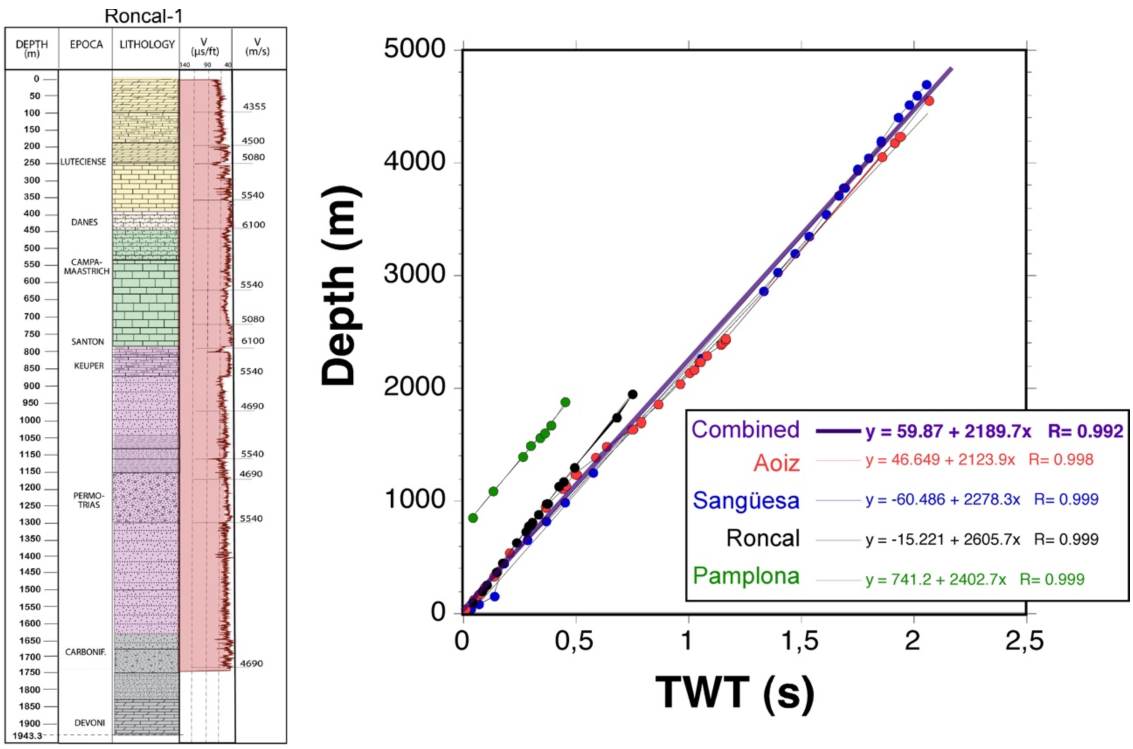

Figure 20. Velocity model from the four available sonic logs. The Roncal detailed data are also shown.

4.2 Gravimetric data

4.2.1 Bouguer anomaly map.

The new gravimetric dataset acquired in the frame of this project has helped to considerably increase the homogeneity and resolution of the Bouguer anomaly for the Southwestern Pyrenees (Fig. 21) comparing to previous updated maps (Ayala et al., 2016) with half density of information and much more uneven distribution (Fig. 13).

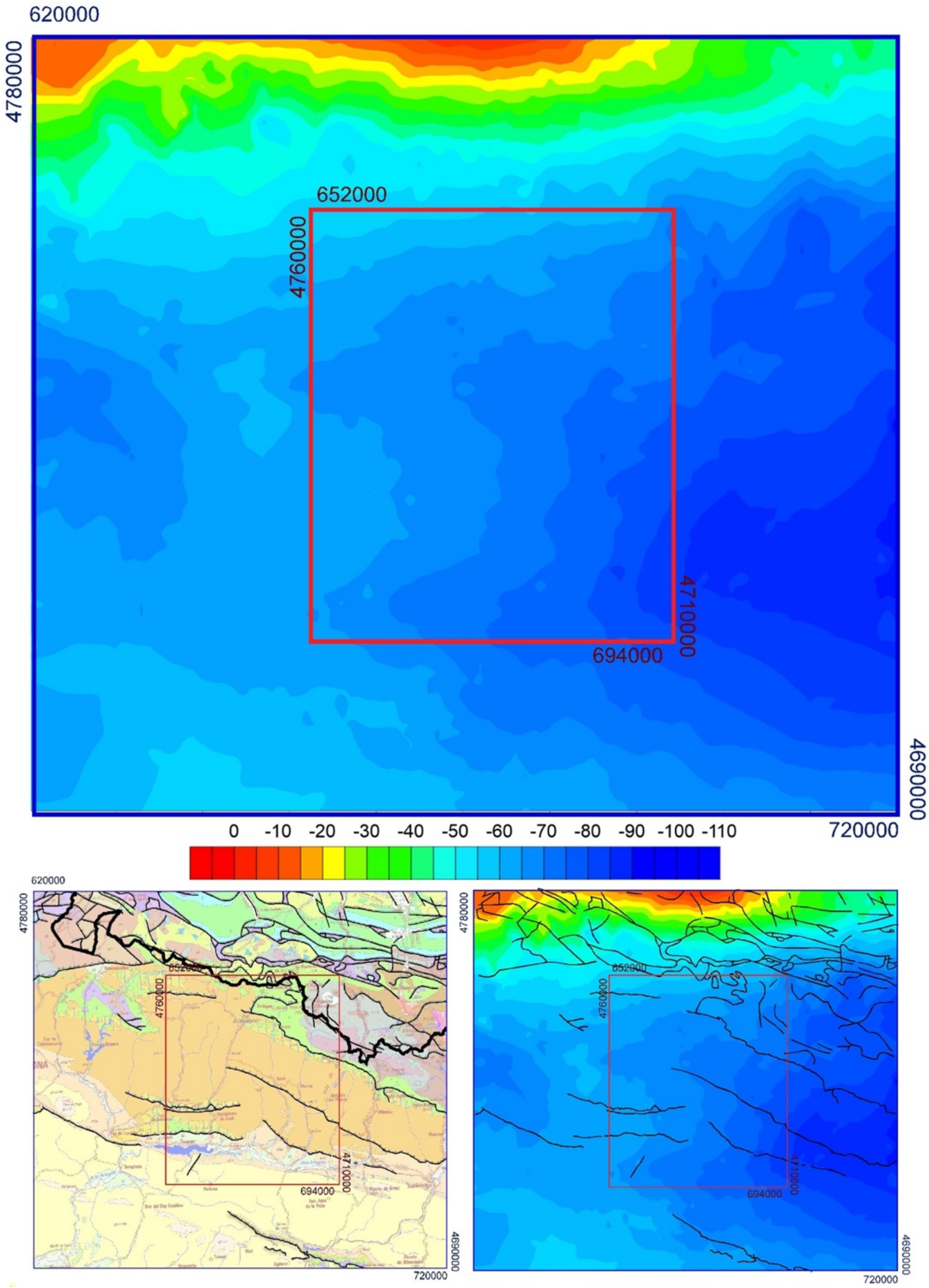

Figure 21: New Bouguer anomaly map for the Southwestern Pyrenees including main structural features

The new Bouguer anomaly map displays some distinct features at a regional scale; the remarkable N-S gradient intensely conditioned (García-Senz et al., 2020 and references therein) by the geometry of the lower crust and the mantle (responsible for the maximum values in the Bouguer map to the North), caused by the geometry of the subduction of Iberia underneath Europe and the exhumed mantle. In this N-S trend the thinning of the Iberian plate can be also described to the South. Besides, this area of the Pyrenees is also characterized by a smoother but consistent E-W gradient triggered by the architecture of the basement rocks; the Axial zone (to the East of the map) vanishes to the West (trend 282° and plunge 11° following Teixell and Arboleya, 1996) and basement rocks show up again in the so-called Basque Paleozoic Massifs far to the Northwest. Finally, South of the Axial zone there is a clear pattern of Pyrenean N120E structures that match very well the structural grain defined by numerous and well-known outcropping structures from the Jaca turbiditic basin until the External Sierras front to the South. All these major anisotropies of the crust are partially emphasized in the vertical and horizontal derivatives of the Bouguer map (Fig. 23).

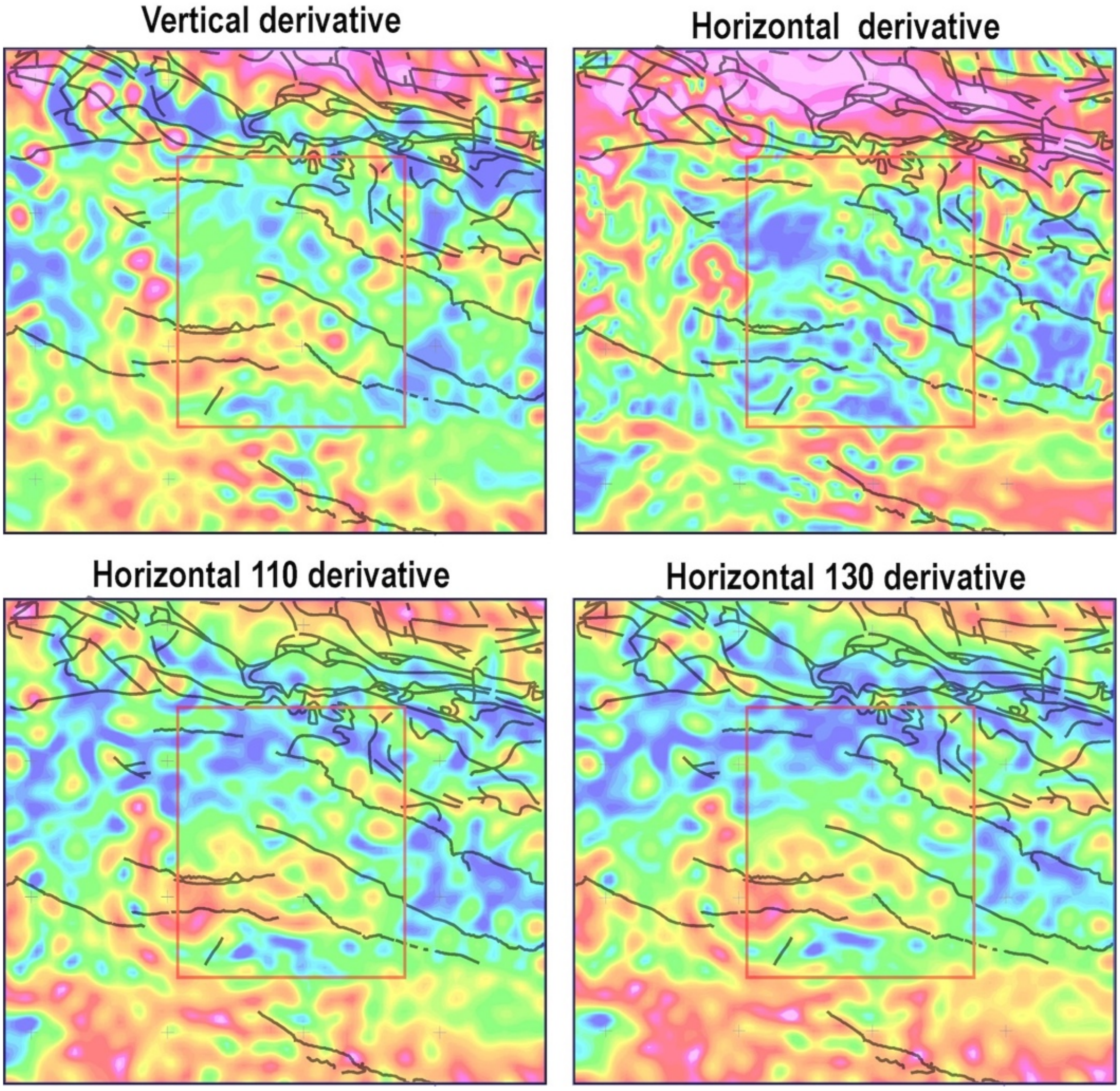

Figure 22: Vertical and horizontal derivatives of the Bouguer anomaly map. Structurally addressed horizontal derivatives along N110E and N130E trends are also introduced.

The first derivatives (gradients) of the Bouguer gravity anomalies show the rate gravity is changing in any spatial direction and are useful to resolve small and shallow variations in the gravity field that otherwise could go unnoticed. They act as a low frequency filters enhancing short wavelength structures as lineaments faults, thrusts and distinctive lateral lithological changes often related to non-outcropping structures. The derivatives in the SW Pyrenees highlight part of the aforementioned regional features and some additional ones. Apart from emphasizing the Pyrenean N120E trend of the structures in the eastern and southern sectors of the study area, they also depict a noisier SW-NE trend in the northwestern portion. Another remarkable feature is the basement uplift (positive) centered in the main target zone (SW of the red box) which is related to the particular W-E gradient of this region.

4.2.2 Regional and Residual anomaly maps

Additional and standard enhancement methods of the Bouguer anomaly have been also carried out. The basic regional (long way-length) subtraction and the evaluation of the residual components (Fig. 23) was performed by three different approaches; the upward continuation at 10 km above the surface, the best polynomial fitting (third order in this case) and the isostatic approach.

The three semiautomatic estimations of the regional field gave similar results. As it could be expected, irregular hyperbolic paraboloids describe the regional Bouguer anomaly, and reflects the non-coaxial superposition of lower and upper crust geometries. The precise geometries of those hyperbolic paraboloids slightly change from one to another, the 3rd order polynomial approach is the most distinctive one; the double curvature intersection is clearly displaced to the South. On the other hand, the range of the anomalies is very different; ≈ 70 mGal for the upward continuation, 130 mGal for the polynomial and about 35mGal for the isostatic one.

The residual anomaly derived from the isostatic filter has been ruled out for further interpretations since it ranges along more than 80 mGal and hardly characterizes correlations with many surficial geological features (except for the northern Pyrenean zone and some features to the East). The polynomial and upward continuation residuals display a negative anomaly correlating to the Axial zone and also with the outcrops of the Basque Paleozoic massifs. In any case these residuals range 50 and 40 mGal respectively pointing to the effect of much deeper components. Comparable residuals from closer Pyrenean projects usually range below 35 mGal (ca. 15 in Calvín et al., 2018; ca. 30 in Santolaria et al., 2020; ca. 35 in Ayala et al., 2020) or 20 mGal to the South in the Ebro Basin and Iberian Ranges in comparable regional studies.

These observations point out to the effect of complex and non-coaxial deformation patterns at different crustal depths and preclude the modeling of the residual anomalies as in other projects. Therefore, we have decided to carry out a double fold approach:

1) To perform the 2D forward modeling at a crustal scale (see section §5.1 “2D joint modeling”) in two out the three balanced cross sections incorporating crustal information from previous studies.

2) To focus on the inner target (red) area and to evaluate the residuals in a smaller portion. Although this region is also affected by non-coaxial deformation (upper crust), this decision is supported by the lower, but not totally neglectable, effect of the lower crustal levels (see next section)

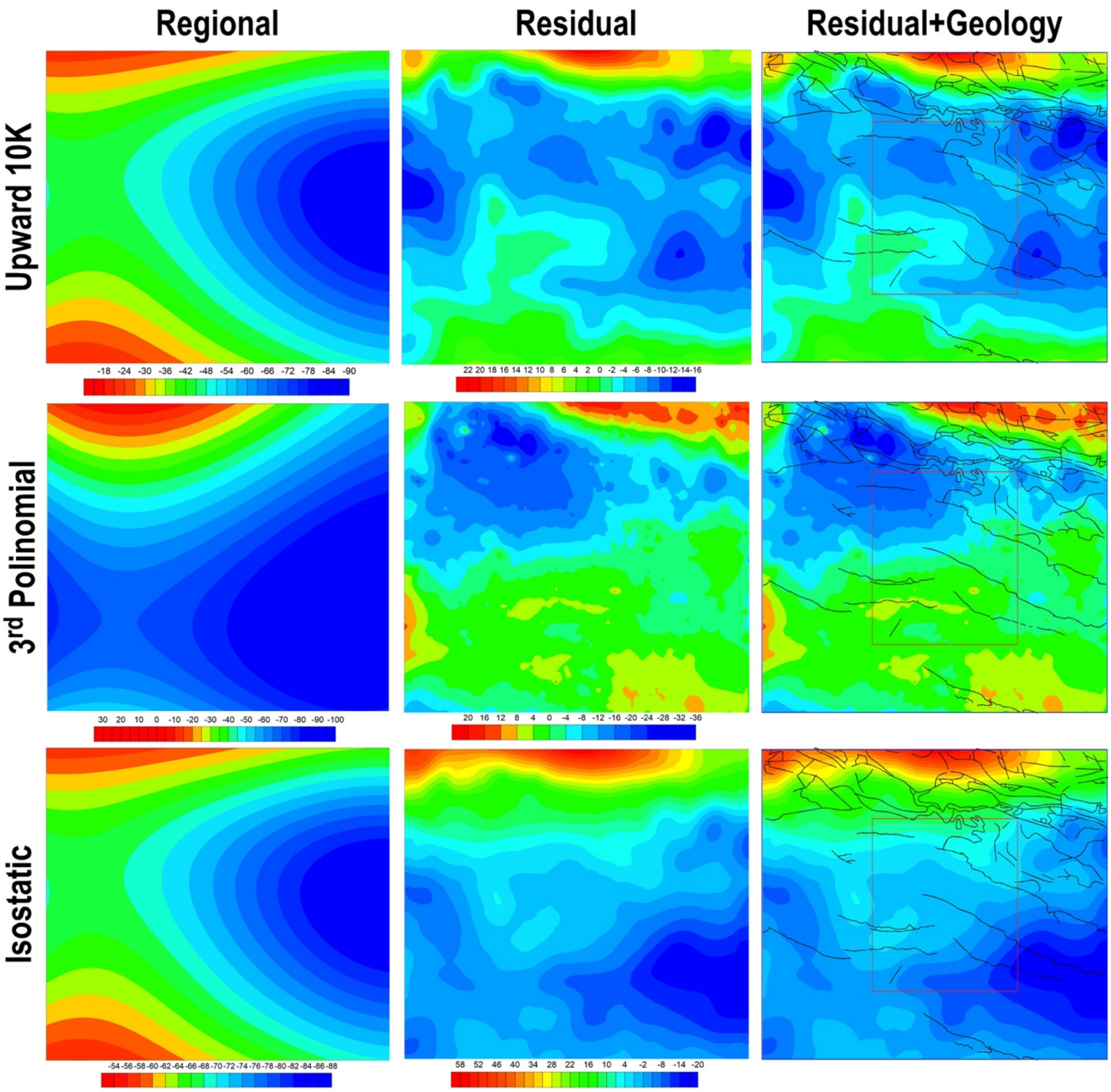

Figure 23: Regional (semiautomatic) anomaly maps in the Western Pyrenees (large blue area). Their residuals are also plotted together with the main structural features

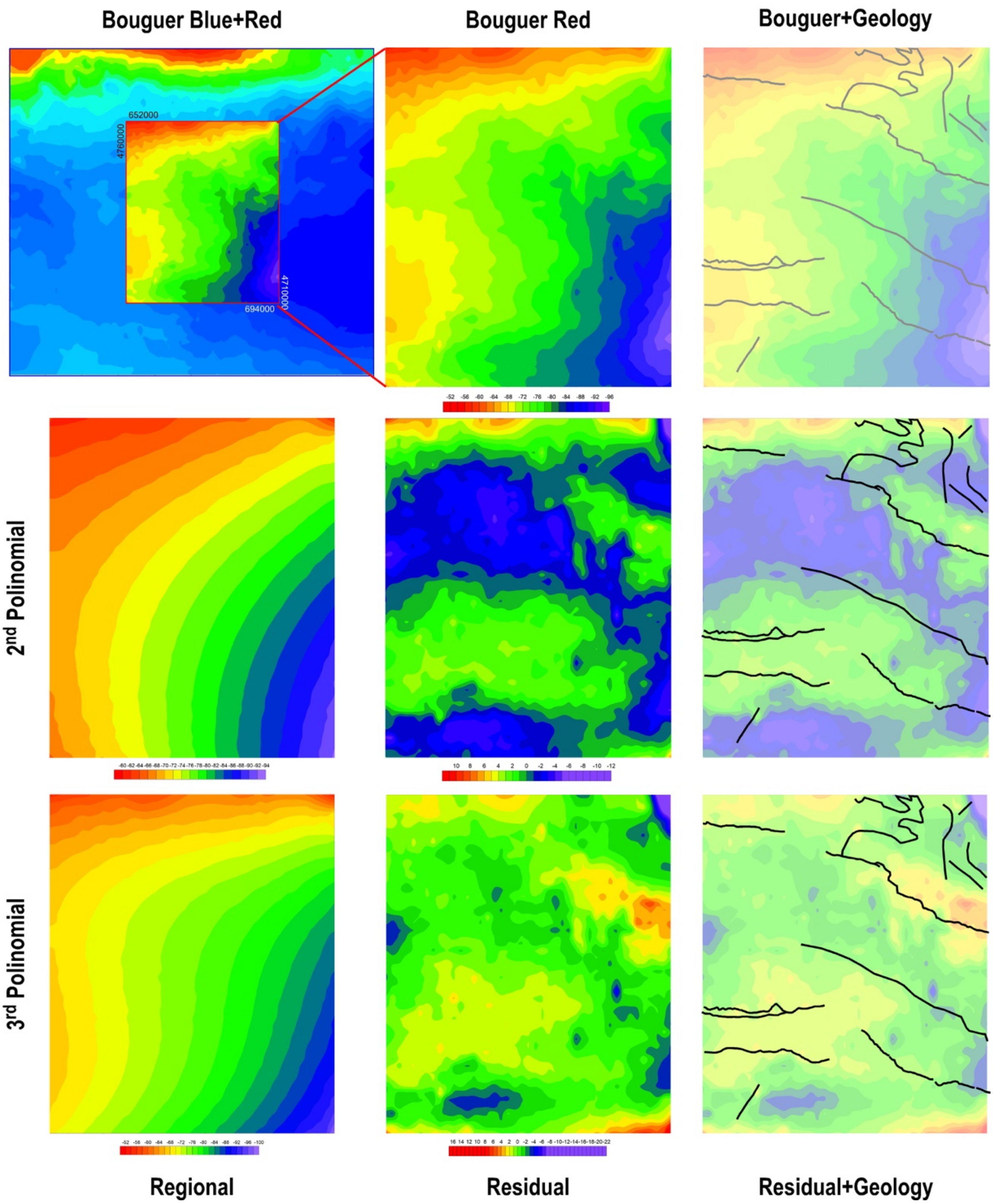

Figure 24: Regional and residual anomaly maps (2nd and 3rd) in the Western Pyrenees (red area) in comparison with surface and subsurface elements

The Bouguer anomaly of the core zone (red quadrangle in figure 24) ranges between -52 to -96 mGal (much less than the blue square; 10 to -110 mGal). We have applied two different polynomial fittings (2^{nd} and 3^{rd} orders) to derive the correspondent regional anomaly maps and their residuals for a first evaluation. These residuals are now much more bounded (24 and 40 mGal) in agreement to other Pyrenean projects. Besides, there is a strong correlation between the residuals (both, 2^{nd} and 3^{rd} orders) and the main outcropping structures. South of the Axial zone (NE corner) a relative positive anomaly seems to delineate the hanging wall of the buried portion of the Gavarnie thrust (due to the higher density of the Paleozoic rocks). At the other corner (SW), another relative positive anomaly fits very well with the Leyre and Illon thrust sheets that also attest for a basement high. The outcrop of the Oturia cover thrust seems to adapt its trend to this basement high.

As a preliminary check, we have projected together the topography of the basement on top of the residual maps (Fig. 25). There are many similarities between both maps, like the basement high definition at Leyre-Illón, the possible hanging wall geometry of the Gavarnie thrust underneath the cover structures of the Internal Sierras and the base of the Jaca turbiditic basin, etc. However, the correspondence is not total in other portions of the target area. We have also included a map displaying the uncertainty of the seismic coverage. This is a simple approach that consists in contouring the estimation of the distance to the neighbors with data. Thus, the largest the distance, the highest the uncertainty in the model definition. The highest degree of discrepancy between the residual maps and the basement topography falls within the areas where the uncertainty of the intial 3Dmodel is larger (lack of seismic data). Therefore, all these observations support the modeling of the gravimetric anomalies in the target (red) zone as an plausible way to retrieve the basement geometry and other geological elements (particularly in those areas with poorer seismic coverage).

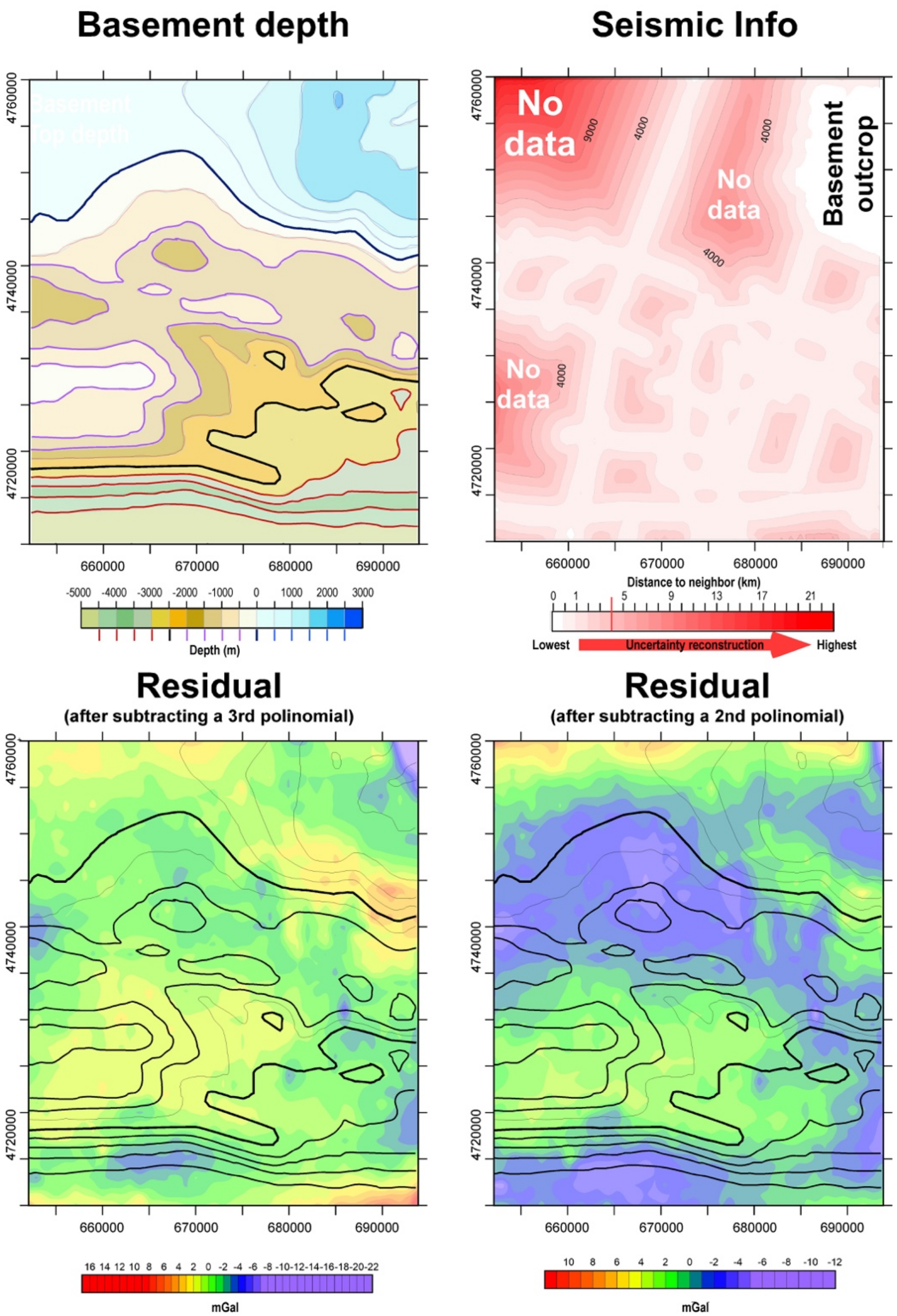

Figure 25: Comparison of residual anomaly maps with the basement depth from the 3D model. The coverage of seismic information is also shown as an estimate of the 3D model uncertainty based on seismic and geologic data

4.3 Petrophysical data

The petrophysical data harvested or acquired in the frame of this project (Fig. 26) have been grouped according to the selection of modeled stratigraphic volumes; Paleozoic (includes Permian, Carboniferous and Devonian rocks from the Axial Zone), the Internal Sierras (Upper Cretaceous and Paleocene limestones, calcarenites and mudstones), the Hecho Group turbidites, the Bartonian mudstones (Arguis-Pamplona Fm.) and the molassic rocks (Campodarbe sandstones and siltstones). Detailed histograms are displayed in figure 27.

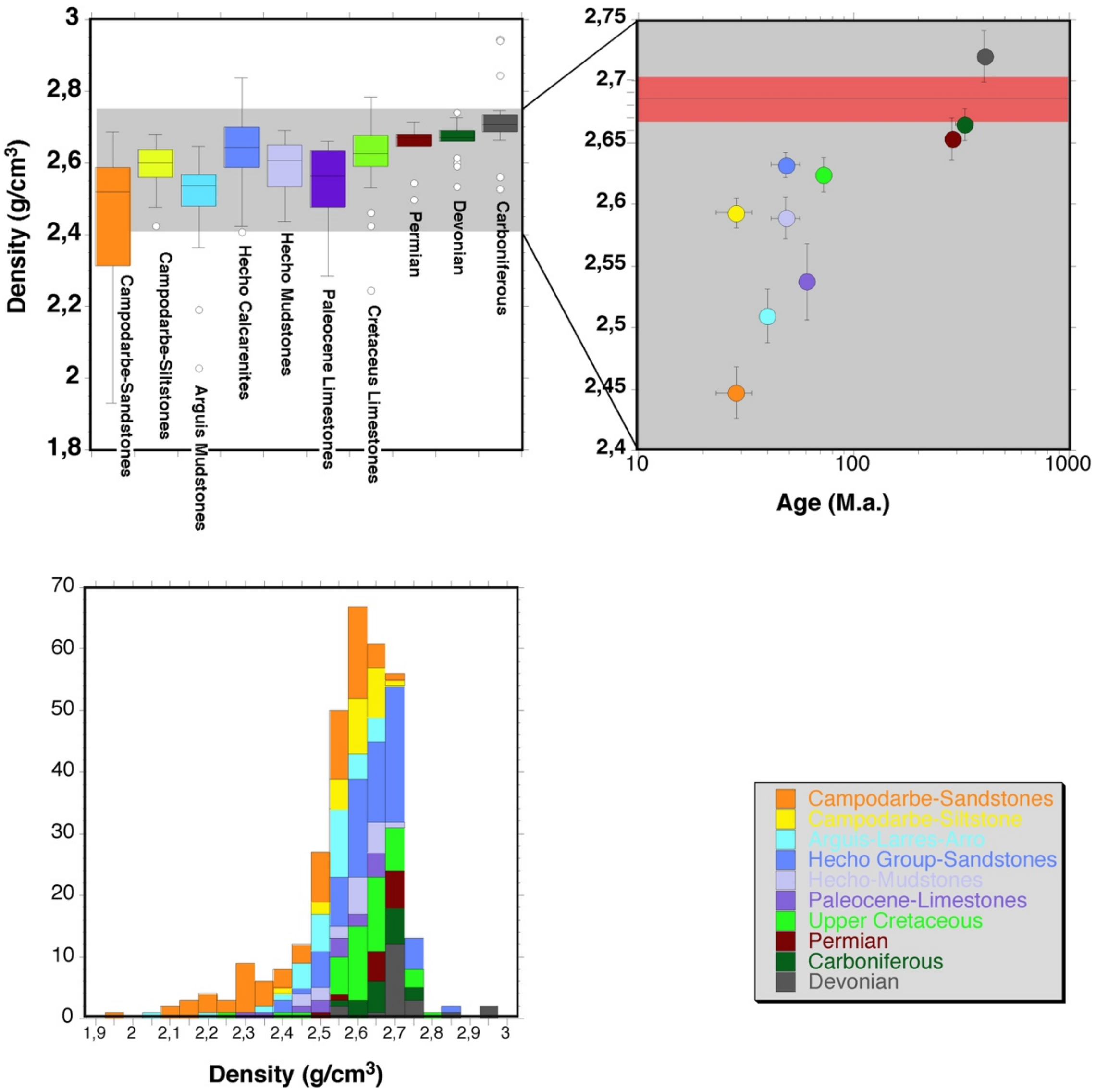

Figure 26: Joint petrophysical box-plot, global histogram and pseudo-log versus time for the modelled volumes. Density is plotted together with the standard error and the red box is the Paleozoic mean.

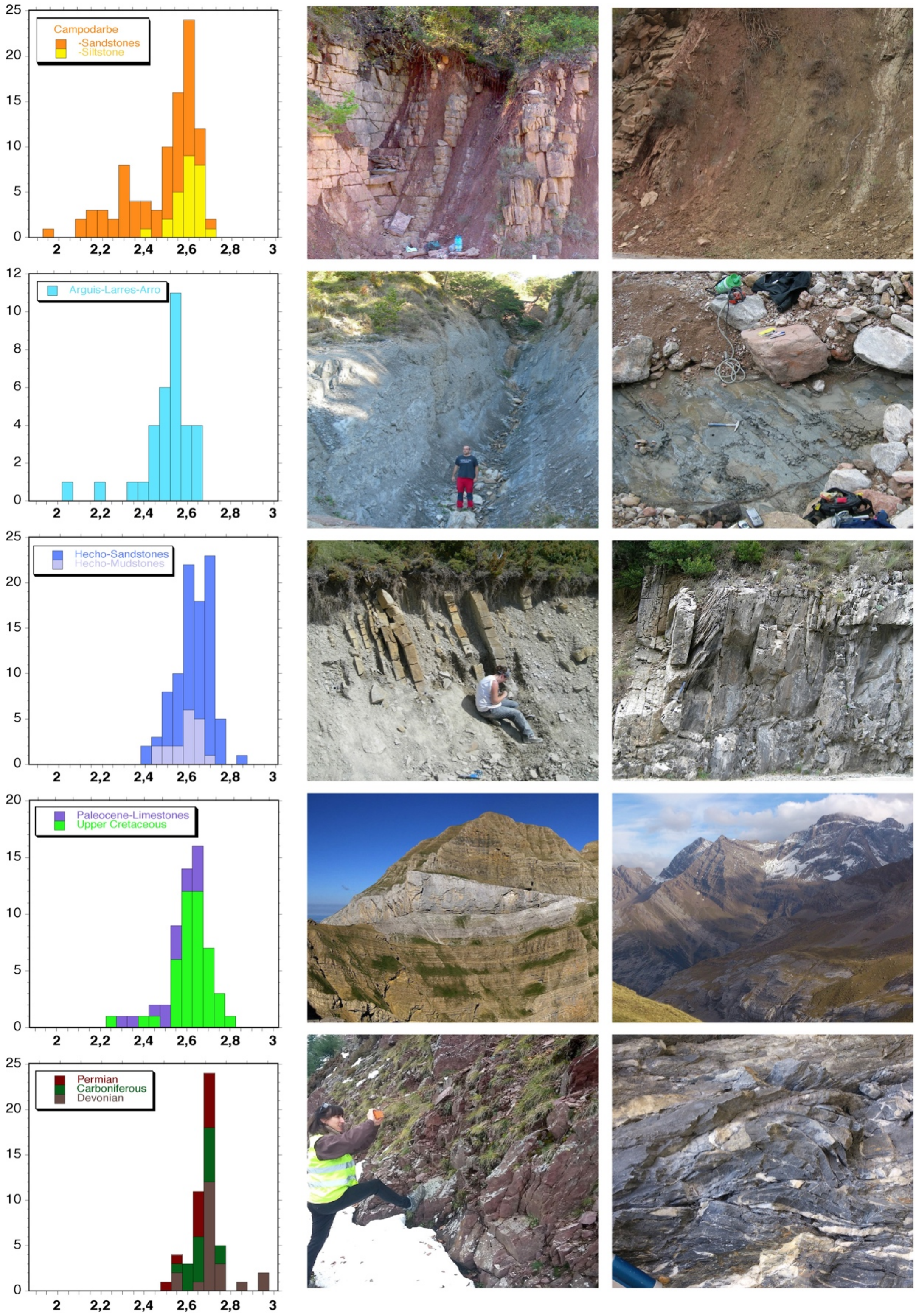

Figure 27: Specific petrophysical histograms for the modelled horizons and some outcrop and landscape pictures of those rock formations.

The maxima densities are found in the Devonian limestones (2.720 g/cm^3) and the minima in the molassic sandstones (2.447 g/cm^3), although the non-outcropping Keuper evaporic facies display the absolute minimum record (2.28 g/cm^3). The lack of data in the target area has forced us to retrieve this value from the Central Pyrenees (Santolaria et al., 2014 & 2020) and from the External Sierras to the South (Calvín et al., 2018) which is also coherent to data from the Iberian ranges (2.27 g/cm^3; Pueyo et al., 2016; Izquierdo-Llavall et al., 2019). The density contrast between the basement rocks and the Internal Sierras and Turbiditic Basin units is significant but not remarkable, this is partially due to the increasing burial conditions (and subsequent density enhancement) of these units to the North before the Gavarnie Thrust emplacement time. This process and the associated temperature are witnessed by the development of pressure solution cleavage (Choukroune & Séguret, 1973; Labaume et al., 1985) and numerous thermometer data across the turbiditic basin (Izquierdo-llavall et al., 2013).

Variable	Mean Age	Age Error	Type	Min	Max	Data	Sites	Mean	Median	RMS	Std Dev	Variance	Std Error	Skewness	Kurtosis
Campodarbe-Sandstones	28,5	5,4	Pmag	1,931	2,687	136	69	2,447	2,519	2,452	0,171	0,029	0,021	-0,845	-0,155
Campodarbe-Siltstone	28,5	5,4	Pmag	2,423	2,679	56	26	2,593	2,600	2,594	0,064	0,004	0,012	-0,933	0,547
Jaca Molassic				**1,931**	**2,687**		**94**	**2,487**	**2,554**	**2,492**	**0,164**	**0,027**	**0,017**	**-1,161**	**0,584**
Arguis-Larres-Arro	39,8	0,2	Pmag	**2,027**	**2,646**	**87**	**33**	**2,509**	**2,537**	**2,512**	**0,126**	**0,016**	**0,022**	**-2,160**	**5,454**
Hecho Group-Sandstones	48,6	7,4	Pmag	2,408	2,837	145	74	2,632	2,644	2,633	0,083	0,007	0,010	-0,572	0,178
Hecho-Mudstones	48,6	7,4	Pmag	2,437	2,691	21	18	2,589	2,608	2,590	0,073	0,005	0,017	-0,776	-0,255
Jaca Turbiditic				**2,408**	**2,837**		**92**	**2,624**	**2,627**	**2,625**	**0,083**	**0,007**	**0,009**	**-0,510**	**0,082**
Paleocene-Limestones	61,0	5,0	Pmag	2,285	2,660	18	14	2,537	2,563	2,540	0,117	0,014	0,031	-1,018	-0,026
Upper Cretaceous	72,7	0,7	Pmag	2,245	2,784	365	44	2,624	2,626	2,625	0,091	0,008	0,014	-1,774	5,518
Internal Sierras				**2,245**	**2,784**		**58**	**2,603**	**2,621**	**2,605**	**0,104**	**0,011**	**0,014**	**-1,483**	**2,807**
Permian	287,5	12,5	Pmag/Hand sample	2,498	2,714	17	13	2,653	2,671	2,654	0,063	0,004	0,017	-1,571	1,337
Carboniferous	328,9	30,0	Hand sample	2,534	2,741	24	17	2,665	2,670	2,665	0,053	0,003	0,013	-0,930	0,443
Devonian	406,3	13,0	Hand sample	2,528	2,944	24	21	2,720	2,708	2,722	0,097	0,009	0,021	0,702	1,288
Paleozoic				**2,498**	**2,944**		**51**	**2,684**	**2,686**	**2,686**	**0,081**	**0,007**	**0,011**	**0,738**	**3,106**

Table 2: Detailed statistical parameters of the grouped petrophysical data used in this study

Additional and standard density data had to be considered for the deeper upper crust (2.7 g/cm^3), the lower crust (2.9 g/cm^3) and the upper mantle (3.3 g/cm^3) during the 2D forward modeling of the Bouguer anomaly.

4.4 Geological structure

4.4.1 Map of main structures

The surficial geology displays excellent outcropping conditions and the nine official geological maps (MAGNA Plan by IGME, scale 1:50.000) covering the studied area are all available (116-Garralda, 117-Ochagavía, 118-Zuriza, 142-Aoiz, 143-Navascués, 144-Ansó, 174-Sangüesa, 175-Sigüés and 176-Jaca; Carbayo et al., 2008a2&b, Teixell et al., 1994; Puigdefàbregas et al., 2008; Del Valle et al., 2008; Teixell et al., 1996; Hernández et al., 2006; de Rojas y Latorre, 2006; Teixell and Barnolas 1994 respectively). Besides, the harmonization of the geological maps (so called GEODE Plan for continuous and digital cartography) allow for the digital files for both, the Pyrenean and the Ebro Basin (Robador et al., 2011 and 2019), to be harvested from IGME repositories. Harmonized Spanish/French cartography of the Pyrenean region (Barnolas et al., 2005, scale 1:400.000) was also used as background map in this project as well as the pioneer structural map of Choukroune and Seguret, 1973. Additionally, several academic and research studies performed in the Southwestern Pyrenees during the last decades (Puigdefàbregas, 1975; Teixell, 1992; Millán 1996 and 2006; Oliva-Urcia, 2000, Pueyo, 2000; Montes, 2002 and 2009) have provided excellent synthetic maps to identify the main structural features. Most of this information was already georeferenced or it was georeferenced using Quantum GIS open software. We carefully analyzed and hierarchized all structural elements (thrusts, folds, and other faults) highlighting the most relevant structures.

There are a number of relevant basement structures that can be linked to cover ones in the study area, from upper to lower (older to younger) and from East to West they are (Figs. 28 and 29):

- The Lakora thrust (not outcropping in the target zone, but the the NW) is related to the Larra Monte Perdido cover system that only affects the Internal Sierras sequence (detached in the Maastrichtian Zuriza mudstones) and the lower levels of the turbiditic Hecho Group (Urzainqui thrust)
- The Gavarnie thrust, whose hanging-wall outcrops in the Axial Zone (NE corner) which is related to the Oturia cover thrust that trends SE-NW in the central portion of the model.
- The Broto-Bielsa thrust (outcrops to the East in the Axial zone) linked to the Yebra de Basa anticline that laterally passes to the Jaca-Javierregay cover thrust. To the West, it is likely linked to the Illón cover thrust. Underneath, the Fiscal thrust is a minor basement structure to the East (only seen in the Tena section) and maybe linked to the eastern portion of the Yebra de Basa anticline (Labaume and Teixell, 2018)
- The Sigüés basement thrust can be related to the Atarés anticline and the Leyre thrust cover structures
- The Oroz-Betelu thrust. It is only defined in the western sections (Roncal and Hecho) as well as in the Itoiz one (Casas, 2005). Its hangingwall basement cut-off is clearly imaged in seismic profiles and defines a striking NE-SW salient to the West of the Tena cross-section. In the GeoEra target area, this basement thrust strikes roughly E-W and its cover expression is the tight Botaya anticline, an E-W trending and tight anticline affecting the Jaca Molassic Basin Oligocene rocks
- Finally, the Guarga thrust, the youngest in the temporal sequence and the deeper in the structural (piggy back) sequence, is responsible for the re-activation of the External

Sierras thrust system in Oligocene-Miocene times and represents the Pyrenean sole thrust.

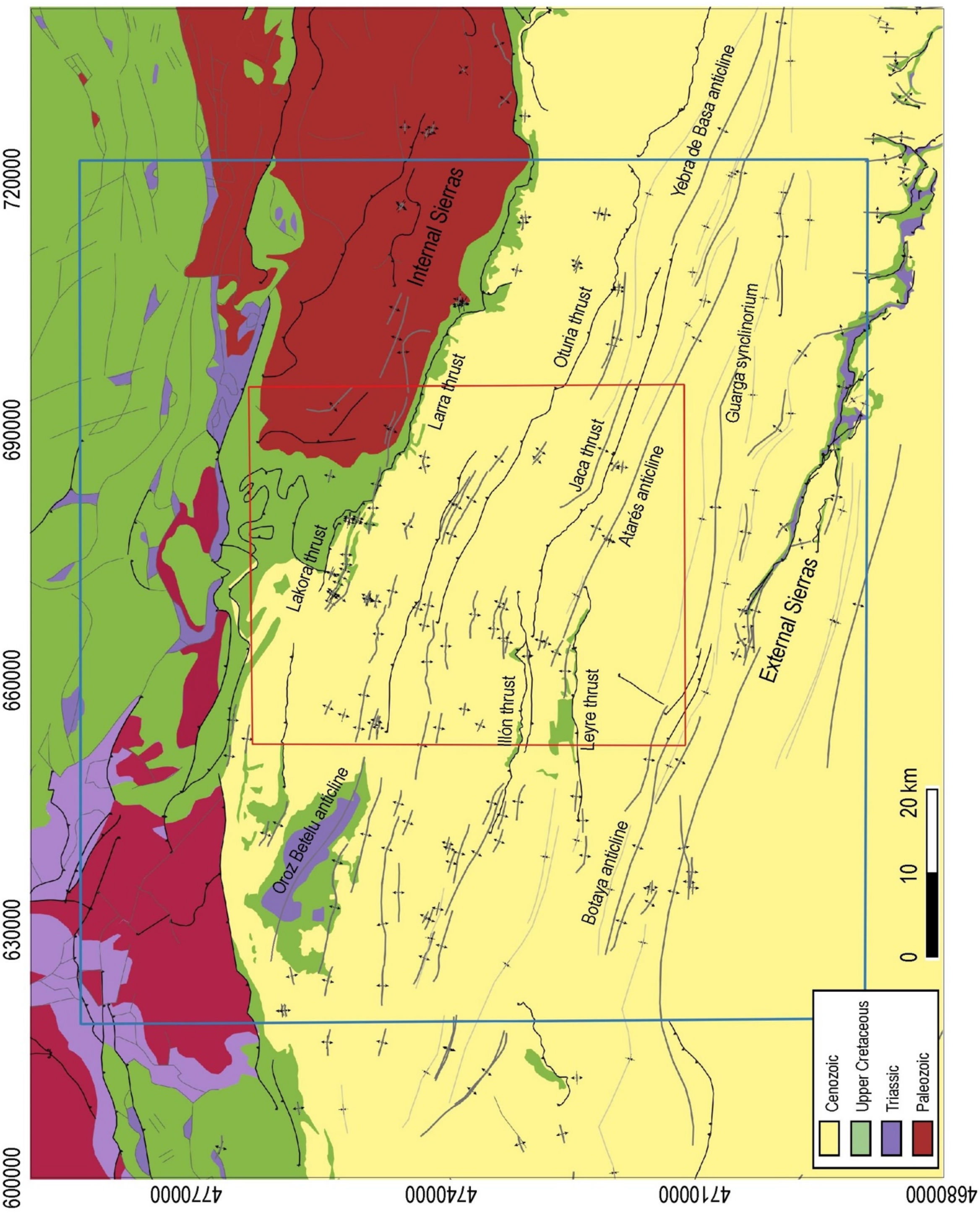

Figure 28: Synthetic structural map of the study-area.

4.4.2 Serial Balanced Cross sections

<u>Tena valley cross-section</u>

The easternmost cross-section depicts a thick Jaca Basin with Cenozoic units thinning drastically along its northern part. Meso-Cenozoic units are ~ 4 to 5.5 km-thick in an area of ~ 37 km, considered from the southern limit of the cross-section to the North. They are deformed by three main surface structures, from the North to the South: the Oturia thrust, the Yebra de Basa anticline and the Guarga syncline. The Cenozoic sequence shows thickness variations that indicate a progressive southwards migration of depocenters trough time. The Hecho Group turbidites are thicker (~ 3.5 km) in the footwall of the Oturia thrust and pinch-out along the Guarga syncline axis. Overlying them, the transitional marls and sandstones (Larrés-Arro and Pamplona-Arguis marls and Sabiñánigo sandstones) are thicker in the Yebra de Basa anticline and northern limb of the Guarga syncline and thinner in the southern syncline limb whereas the younger continental units reach their maximum thickness across the Guarga syncline axis. The Guarga syncline is an open fold characterized by shallowly dipping limbs and detached from the basement along the Upper-Middle Triassic evaporites. The Upper Cretaceous to Lower-Middle Eocene units at the lower part of the folded sequence describe an approximately 5 km-long flat-lying hinge zone. They are overlain by the younger Cenozoic units that registered a progressive migration of the Guarga syncline axis to the South.

The basement flooring the thick Meso-Cenozoic units of the Jaca Basin in the Tena transect is found at a depth of ~3 km underneath the Oturia thrust and deepens progressively to the South, reaching a maximum depth of ~6 km underneath the southern limb and the Guarga syncline axis. Variations in basement depths in this portion of the cross-section are provoked by a main basement thrust: the Guarga thrust. The Guarga basement thrust has been depicted as a shallowly North-dipping fault. Basement units in its hangingwall are deformed by a kilometric-scale fault-bend fold that includes a northern and a southern basement panels dipping ~ 5 and 20º to the South, respectively. The basement cut-off in the hangingwall of the Guarga basement thrust is located along the Guarga syncline axis. The basement thrust is interpreted to accommodate a significant displacement (> 10 km) which is transferred to the cover along the South Pyrenean Frontal Thrust (which emerges few kilometers to the South of the southern limit of the cross-section). As previously mentioned, basement and cover structures in the southern portion of the Tena cross-section are decoupled along the Middle-Upper Triassic evaporites that crop out along the South Pyrenean Frontal thrust, are ~ 1 km-thick underneath the Guarga syncline axis and pinch-out or become very thin to the North of the Yebra de Basa anticline. In this northern area, seismic and surface data evidence a change in the main décollement which is located along the Upper Cretaceous units (the Zuriza marls and Marboré sandstones and, more locally, the Cañones limestones), with additional décollements found at the base and within the Hecho Group turbidities. The Yebra de Basa anticline is at surface a tight, South-verging anticline with a large vertical to overturned southern limb and a shallowly North-dipping northern limb. Well-tied seismic reflectors at depth show that the Upper Cretaceous – Lower Eocene sequence underlying the turbidities is nevertheless subhorizontal to shallowly South-dipping underneath both the northern and southern limbs of the Yebra de Basa anticline. This decoupling between the surface and the deep structure has been interpreted as a fish-tail type structure. The Upper Cretaceous and Paleocene-Lower Eocene units at depth are affected by a thrust system involving fore- and back-thrusts and fault-bend anticlines. Thrust flats within the Cretaceous are imaged in the seismic profiles. They would connect to basement thrusts and transfer shortening to the overlying Cenozoic units that are decoupled along the multi-layered Hecho Group turbidites.

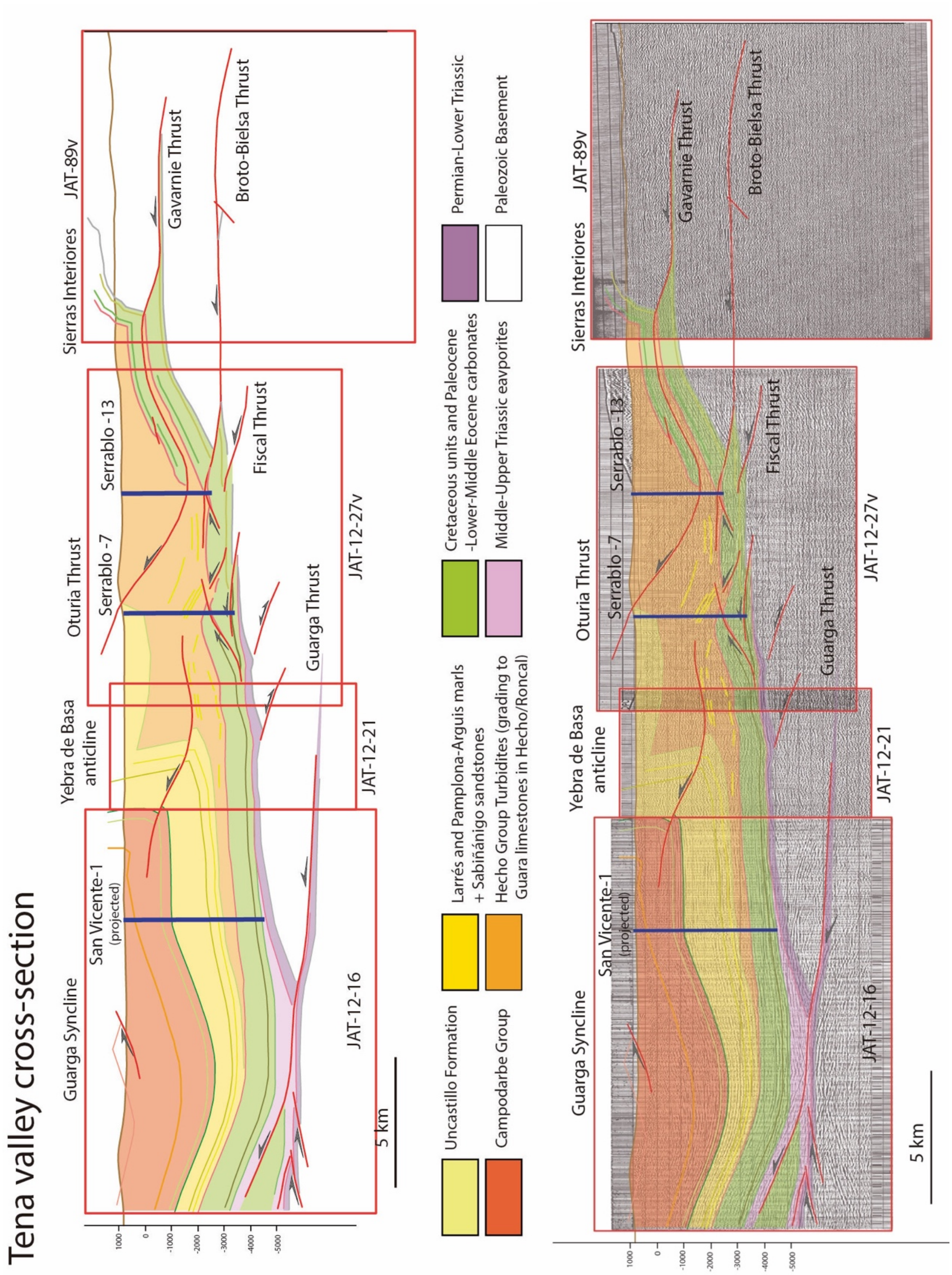

Fig. 29a. Tena Valley balanced cross-section shown with and without the seismic information.

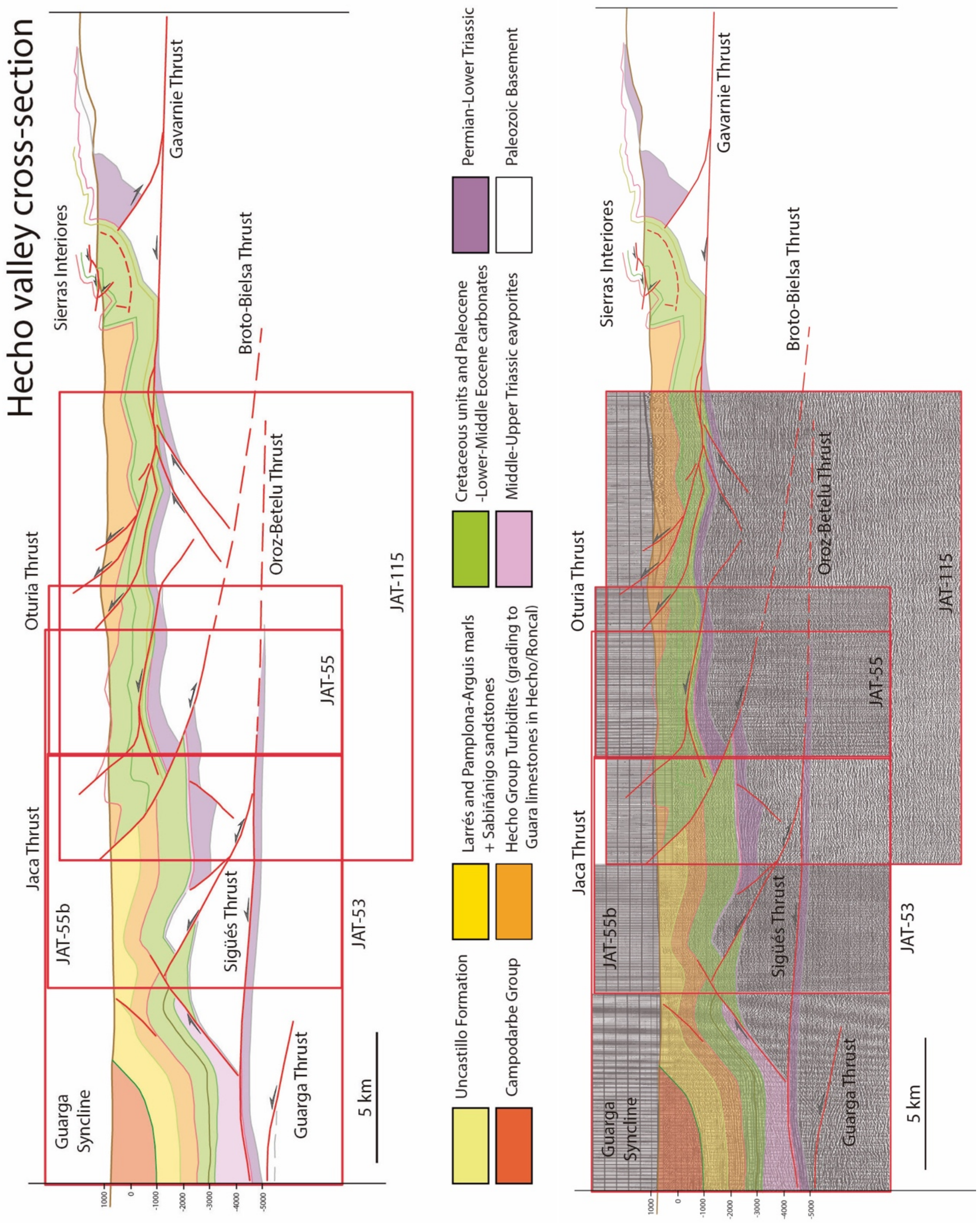

Fig. 29b. Hecho Valley balanced cross-section shown with and without the seismic information.

To the North of the Yebra de Basa Anticline, the Oturia thrust superposes the Hecho Group turbidites onto the Larrés-Arro marls. The map view inspection of the units overlying the Larrés-Arro marls in the Oturia thrust foot-wall evidences an apparent thinning of the Pamplona marls towards the fault surface, which allows constraining the age of the thrust. The structure of the Hecho Group turbidites in the Oturia thrust hangingwall is defined by metric to kilometric scale south-verging folds displaying vertical to overturned southern limbs and shallowly to moderately North-dipping northern limbs. The details of these folds are not represented in the cross-section in Figure 29. Underlying these folded turbidites (transparent in the seismic reflection profiles), seismic data image a prominent panel of reflectors that dip ~ 25 º to the South. Based on well and surface data, we interpreted these reflectors as Upper Cretaceous-Lower Eocene carbonates and marls. The sequence is repeated by the Oturia thrust which is in turn folded and southwards tilted. Considering previous interpretations (Labaume and Teixell, 2018), the Oturia thrust is interpreted to branch at depth with the Gavarnie basement thrust. A displacement of ~ 7 km has been suggested for this basement thrust with a major thrust flat at the base of the Upper Cretaceous sequence (consistent with surface data to the East, in the Gavarnie window). The Gavarnie-Oturia thrust is folded by the underlying Broto-Bielsa thrust that shows a shorter displacement and a basement, fault-related anticline in its hangingwall.

Basement cut-offs in the hangingwalls of the Gavarnie and the Bielsa-Broto thrusts are separated by ~ 5 km. They produce a significant basement stacking in a short distance which allows explaining the rapid thinning of the Meso-Cenozoic units in the northern part of the cross-section: they are ~ 4 km-thick in the foreland of the Bielsa-Broto thrust but absent 7-8 km to the North (contact between the Axial Zone and the Internal Sierras).

<u>Hecho valley cross-section</u>

The main difference between the Hecho and Tena transects is that the basement flooring the Jaca Basin is located in a shallower position in the Hecho cross-section. Consequently, the cover sequence is significantly thinner: Upper Cretaceous-Cenozoic units have a maximum thickness of ~ 4 km in the southern limit of the cross-section and thin progressively towards the North. The Upper Cretaceous is underlain by a reflective sequence showing thickness variations that we interpreted as Permo-Triassic in age.

At surface, the Meso-Cezonoic is affected by several south-directed thrusts that laterally disappear or branch and that correlate to the Jaca and Oturia thrusts further East. To the South of the Jaca thrust, surface and seismic data show two open NW-SE-striking anticlines: the northern anticline ends laterally to the East and connects along-strike to the Foz de Sigüés structure (Leyre thrust) whereas the southern anticline correlates along-strike to the Ceresola-Atarés anticline in the East. Further South, stratigraphic units lay horizontally along the hinge zone of the Guarga syncline. Cenozoic units (the Hecho Group turbidites, the transitional marls and sandstones and the overlying continental sequence) are thinner than in the Tena cross-section and reach their maximum thickness across the Guarga syncline axis (~ 3 km). The basement flooring the Jaca Basin is imaged by seismic lines at a depth ranging between 1 and 3 km in the central portion of the cross-section although it deepens up to 4.5 km underneath the Guarga syncline and shallows in the northern part of the transect where it crops out. Vertical offsets in the position of the top of the basement have been interpreted to be related to five main basement thrusts, from the North to the South (and from the top to the base of the thrust system): the Gavarnie, Broto-Bielsa, Sigüés, Oroz-Betelu and Guarga thrusts. The Gavarnie Thrust is depicted as a short-cut in the foot-wall of an extensional fault that bounds the Permian-Triassic, Hecho sub-basin to the south. This basin has a width of ~ 7 km and shows a rough halfgraben geometry with Permian-Triassic units thickening to the South. Permian-Triassic inheritance is negligible along the Tena section but probably exerted a strong control on the location and orientation of Cenozoic thrusting in the western Axial Zone (where Permian-Triassic basins crop out immediately to the North of the Internal Sierras). The Gavarnie thrust in the Hecho cross-section connects at surface to the Oturia thrust that here shows a displacement that is shorter than in the Tena transect. Mesozoic and Cenozoic units in the hangingwall of the Gavarnie thrust are affected by the thin-skinned Larra fold-and-thrust system, cropping out in the Internal Sierras.

As the Gavarnie thrust, we interpreted the Sigüés thrust as a basement short-cut in the foot-wall of an inherited Permian-Triassic normal fault whereas the Bielsa-Broto thrust is imaged by seismic reflection profiles as an inverted normal fault. The Bielsa-Broto thrust connects at surface to the Jaca thrust that superposes the Hecho Group turbidites onto the transitional marls. Basement and cover units in its hangingwall are folded and affected by two north-directed back-thrusts and a south-directed thrust, all they three accommodating a minor displacement. The basement cut-off in the hangingwall of the Bielsa-Broto thrust is located about 17 km to the South of the basement cut-off in the hangingwall of the Gavarnie thrust. This distance decreases up to ~ 5 km in the Tena transect, where basement thrust stacking is consequently more significant. The mapping of this observation would be translated into two cut-off lines diverging to the West. The southern cut-off line (basement cut-off in the hangingwall of the Bielsa-Broto thrust) would be approximately E-W-trending, oblique to main cover structures that run NW-SE, whereas the northern cut-off line (basement cut-off in the hangingwall of the Gavarnie thrust) would be NW-SE-trending, parallel to the strike of the Internal Sierras. Cross-sections depict a westwards moderate increase in the displacement of the Bielsa-Broto basement thrust between the Tena and Hecho valleys (oppositely to the Gavarnie Thrust). The Sigüés thrust, in the footwall of the Bielsa-Broto thrust, does not crop out at surface along the Hecho transect but would underlie to the Atarés anticline deforming Cenozoic units at surface. Immediately to the South, the Yesa anticline is interpreted to be related to a back-thrust detached into Middle-Upper Triassic evaporites (the Yesa back-thrust). This décollement seems to be absent or very thin to the North of this structure but seismic profiles show it thickens underneath the Guarga syncline where it is 1-1.5 km-thick. As observed in the Tena cross-section, the thickening of the Middle-Upper Triassic décollement provokes an increase in the decoupling between cover and basement structures from the Guarga syncline to the South.

Underlying the whole described structure, we identified a subhorizontal basement thrust (the Oroz-Betelu thrust) displaying a long thrust flat at the base of the Upper-Middle Triassic evaporites. The trust surface is found at a depth of 4-5 km. It is folded in the hangingwall of an underlying basement structure that we interpreted as the lateral analogue of the Guarga Thrust. The displacement of this lowermost basement thrust would be probably much less significant than in the eastern Tena cross-section whereas the Oroz-Betelu thrust seems to accommodate a significant shortening that would be transferred to the cover units in the External Sierras. The Oroz-Betelu thrust has been identified and drilled to the West of the Hecho transect (in the Aoiz well; Casas-Sainz, 2005) but it is not recognized in the East (Tena cross-section). Seismic profiles clearly image the basement cut-off in the hangingwall of this thrust. Tracking of this feature allows identifying that this basement structure initiates to the West of the Aragon valley transect where the related basement cut-off line is strongly oblique (NE-SW) to cover structures.

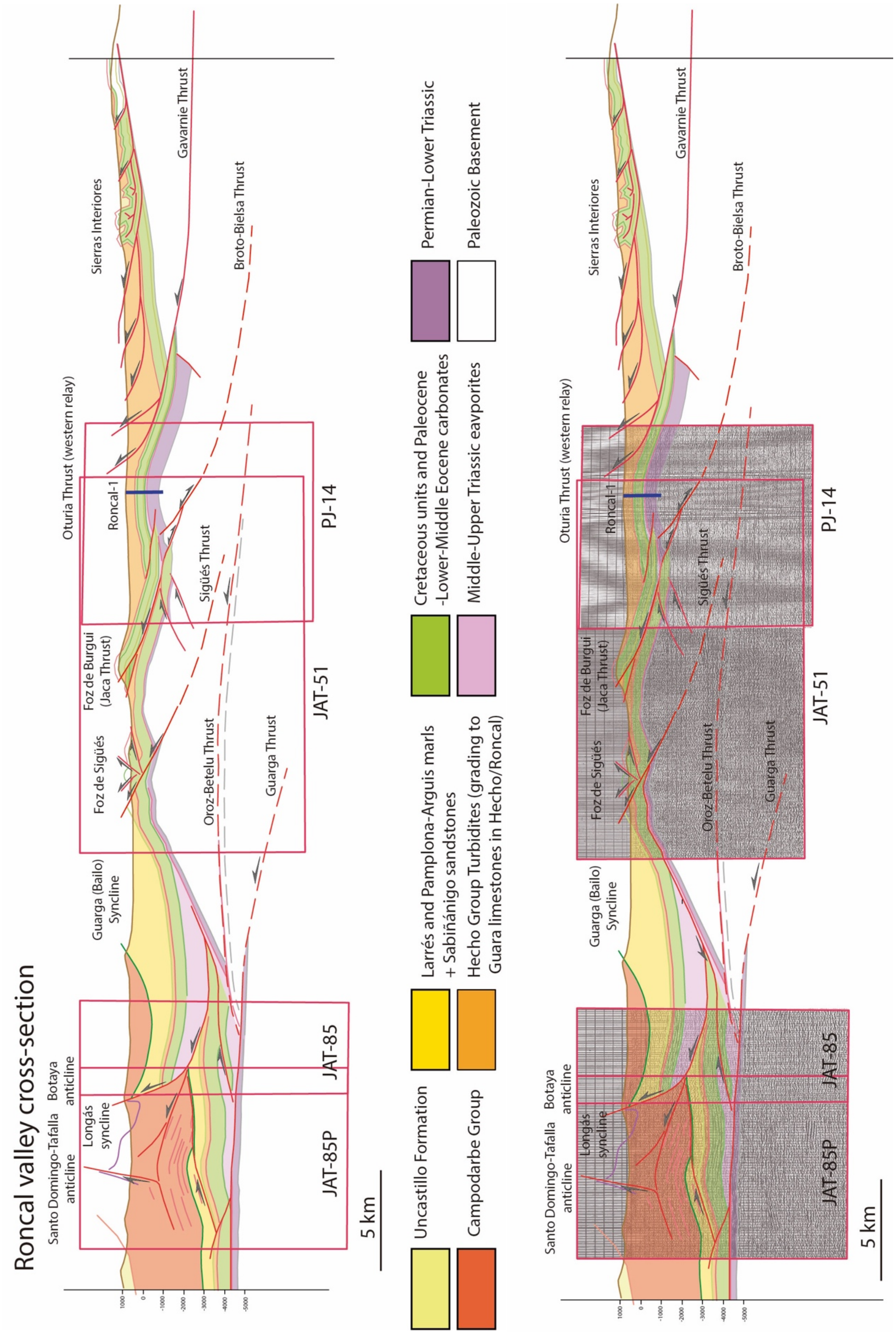

Fig. 29c. Roncal Valley balanced cross-section shown with and without the seismic information.

Roncal valley cross-section

The basement flooring the Jaca Basin along the central portion of the Roncal transect is at an even shallower position (< 1 km) than in the Hecho transect (1 to 3 km). Surface outcrops to the North of the Guarga syncline (here also named as the Bailo syncline) are dominated by the Hecho Group turbidities that are in general terms thinner than in the previous cross-sections. The Hecho turbidites grade across-strike to the Guara limestones Fm to the South and are overlain by the transitional marls and sandstones and the younger continental sequence. Thickness variations in these units are consistent with a southward migration of depocenters trough time: the thickest Hecho Group is found to the North of the Guarga syncline, whereas the thickest transitional and continental sequence are identified at the northern limb and to the South of the Guarga syncline, respectively. It is in this part of the cross-section where the Cenozoic reaches its maximum thickness (~ 4 - 4.5 km). Mesozoic-Lower Eocene carbonated units underneath are represented by a reflective package that is turn underlain by an also reflective sequence in the central part of the cross-section. Well data (Roncal-1 well, located along the trace of the cross-section) indicate that this lowermost sedimentary unit corresponds to Permian-Triassic red beds.

At surface, Meso-Cenozoic units are affected by several south-directed thrusts and north-directed back-thrusts that laterally correlate to the Jaca and Oturia thrusts to the East. To the South of the Jaca thrust, the previously mentioned Sigüés thrust (identified at depth in the Hecho cross-section) emerges at surface in the Foz de Sigüés structure (Leyre thrust). This structure disappears to the East of the Hecho valley, where it probably branches to the Jaca Thrust. South of the Sigüés/Leyre thrust, surface and seismic data image an open syncline (the Bailo syncline, laterally correlating to the Guarga syncline) bounded to the South by a tight and faulted anticline (the Botaya anticline). Further South, a south-verging syncline-anticline pair crops out (the Longás syncline and the Santo Domingo-Tafalla anticline, following Oliva-Urcia et al., 2012). The southern limb of the anticline is subvertical to steeply south-dipping and it is separated from the northern limb by a steeply-dipping back-thrust.

The basement flooring the Meso-Cenozoic units is imaged at a depth < 1 km underneath the central portion of the cross-section (Oturia, Jaca and Sigüés/Leyre thrusts areas) although it deepens up to 4.5 km underneath the Guarga syncline and Santo Domingo-Tafalla anticline and shallows in the northern part of the cross-section where it crops out. As for the Hecho cross-section, vertical offsets in the position of the top of the basement have been interpreted to be related to the same five basement thrusts, from the North to the South: the Gavarnie, Broto-Bielsa, Sigüés, Oroz-Betelu and Guarga Thrusts. The Gavarnie Thrust shows a limited displacement and connects to the Oturia thrust at surface. The basement and the Meso-Cenozoic cover in its hangingwall are tilted an average of ~ 10º to the South. Mesozoic and Cenozoic units to the North are in turn affected by the thin-skinned Larra fold-and-thrust system which involves multiple décollements: a lower décollement at the Paleozoic-Mesozoic boundary or the basal Upper Cretaceous unit (the Cañones limestones)(following Rodríguez et al., 2014) , an intermediate décollement along the Zuriza marls and an upper décollement at the base of the Hecho Group turbidites. The upper décollement provokes a strong decoupling between the strongly folded turbidites (affected by metric to kilometric-scale folds that are not represented in the cross-section) and the underlying Paleocene-Lower Eocene limestones. The intermediate décollement relates to the South-verging, tight and almost isoclinal folds that crop out in the lateral equivalent of the Internal Sierras whereas South-verging thrusts and fold-bend anticlines developed above the lower décollement.

As in the Hecho cross-section, the Bielsa-Broto thrust along the Roncal valley is interpreted as an inverted normal fault. Permian-Triassic units in the hangingwall of the inverted fault are traversed by the Roncal-1 well which also cut-across a thin portion of Keuper evaporites. We interpreted these evaporites as a main décollement in the Foz de Burgui-Illón Range structure (lateral analogue of the Jaca thrust) that is represented in the cross section as a fault-bend fold in the hangingwall of a main south-directed thrust. The thrust shows a long flat along the Keuper evaporites, this flat connecting at depth to the Broto-Bielsa inverted normal fault. To the South, the Sigüés-Leyre thrust is related to a basement anticline in its hangingwall and emerges at surface in the Foz de Sigüés structure that we depicted as a pop-structure limited by two south-directed thrusts to the South and two north-directed back-thrusts to the North. Basement cut-offs in the hangingwalls of the Gavarnie, Broto-Bielsa and Sigüés thrusts are separated by ~ 10 km.

Cross-sections depict a westwards increase in the displacement of the Bielsa-Broto thrust between the Hecho and Roncal valleys whereas the Gavarnie and Sigüés thrusts show an approximately constant displacement in both sections. Underlying the whole described structure, we interpreted the Oroz Betelu basement thrust at a depth of ~ 4 km. This thrust is folded by the Guarga thrust, at ~ 4.5-5 km depth. The basement cut-off in the hangingwall of the Oroz-Betelu thrust is located along the axis of the Bailo syncline (Guarga syncline) and it is at a distance of ~ 10 km from the basement cut-off in the hangingwall of the Sigüés-Leyre thrust (this distance is shorter in the Hecho cross-section).

Shortening in the Oroz-Betelu and Guarga thrusts would be transferred to the Botaya and Santo Domingo-Tafalla anticline and related thrusts. A strong decoupling between seismic reflectors at depth and surface bedding data is identified in this portion of the cross-section. Folds at surface are tight, bedding and thrusts being steeply dipping. Conversely, seismic reflection images a gently folded, reflective package at a depth of 3-4 km underneath the tight surface folds. To explain this decoupling, we interpreted the frontalmost folds and thrusts as a complex fishtail type structure involving a lower décollement at the Middle-Upper Triassic evaporites and additional décollements at the transitional, marly units and the lower and intermediate part of the continental sequence. As stated for the Hecho cross-section, the thickening of the Middle-Upper Triassic décollement in the Oroz-Betelu forelimb and foreland provokes an increase in the decoupling between cover and basement structures from the Bailo (Guarga) syncline to the South.

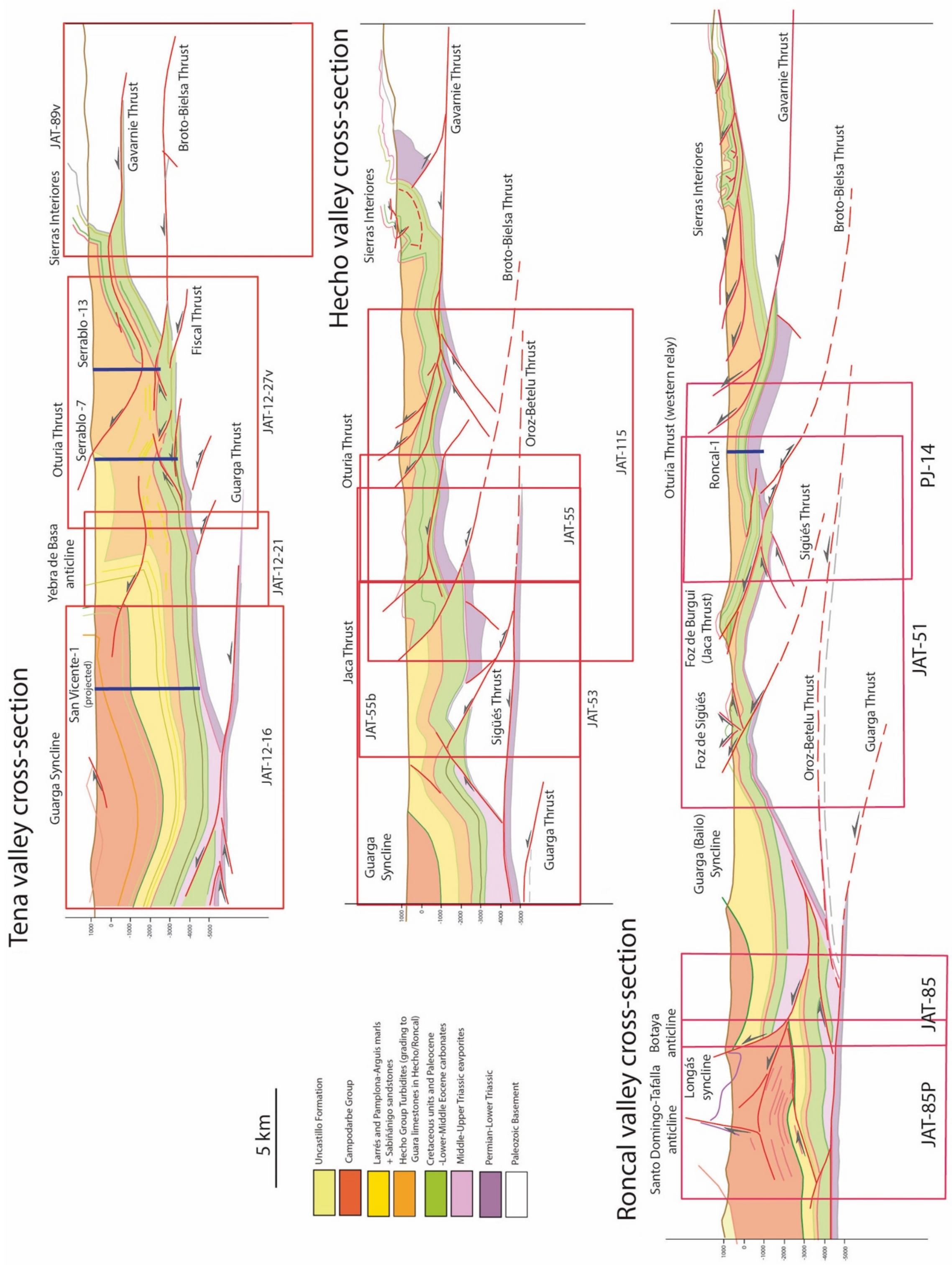

Fig. 29d. Tena, Hecho and Roncal balanced cross-section without seismic information.

4.5 3D model of the South Western Pyrenees

The 3D model of this portion of the Western Pyrenees is limited to the target area defined in the red quadrangle (Figs. 4, 8, etc.). The primary data to build the stratigraphic and structural (thrusts) surfaces were:

- The digital elevation model (DEM)
- The geological mapping; stratigraphic and fault contacts, projected into the DEM to characterize the outcropping areas in 3D
- The identified seismic reflectors (Fig. 8) after the time-to-depth conversion
- The lithological log of the Roncal-1 well
- The two balanced cross-sections; Roncal and Hecho

Due to the limited number of subsurface information (Fig. 25), especially critical in the Northern (NW) and southwestern corners of the project, additional information from auxiliary sections was also used. This was favored by the excellent outcropping conditions (and geological maps) and the abundant bedding dips. The Roncal and Hecho sections were laterally displaced considering structural elements (e.g. plunging of the Axial zone westwards). In any case, an unknown but significant uncertainty is located in the areas with lack of information. Further improvements of this model should consider the building of additional balanced sections.

For simplicity, the final selection of stratigraphic horizons comprises:

- Top of the basement; Carboniferous (or Devonian in the outcropping zone)
- Top of Permian
- Top of Upper Triassic (Keuper facies), only present in the southern half of the project
- Top of Paleocene Limestones, thus this horizon envelops the entire Internal Sierras Upper Cretaceous sequence
- Top of Hecho Group, simplifying the complex internal deformation of this layer
- Top of Bartonian marls
- Top of Campodarbe

Unravelling the structural relationships among thrust faults was critical for the model consistency. The main thrusts in the target area are:

- The Larra thrust system in the Internal Sierras (NE corner). It was not considered in the 3D model. This thrust system is formed by small-scale thrust slices showing frequent along-strike relays and lateral terminations. The lateral continuity of the thrusts is much smaller than the spacing of the cross-sections and seismic profiles used for building the 3D model, which are thus insufficient for the proper reconstruction of the Larra thrust system 3D geometry.
- The Gavarnie- Oturia thrust
- The Broto-Bielsa basement thrust and its related Illón cover thrust (Foz de Burgui)
- The Sigüés basement thrust and its related Leyre cover thrust (Foz de Burgui)
- The deeper Oroz-Betelu thrust and related cover structures (Botaya and Sto. Domingo anticlines)
- The Pyrenean basal Guarga thrust
- The Yesa back-thrust. It is detached into the Keuper evaporites, along the forelimb of the Oroz-Betelu basement thrust.

Digital files of all these geological elements are available in deliverable D6.1 uploaded in the GeoERA reservoir under FAIR principles (Toro et al., 2021).

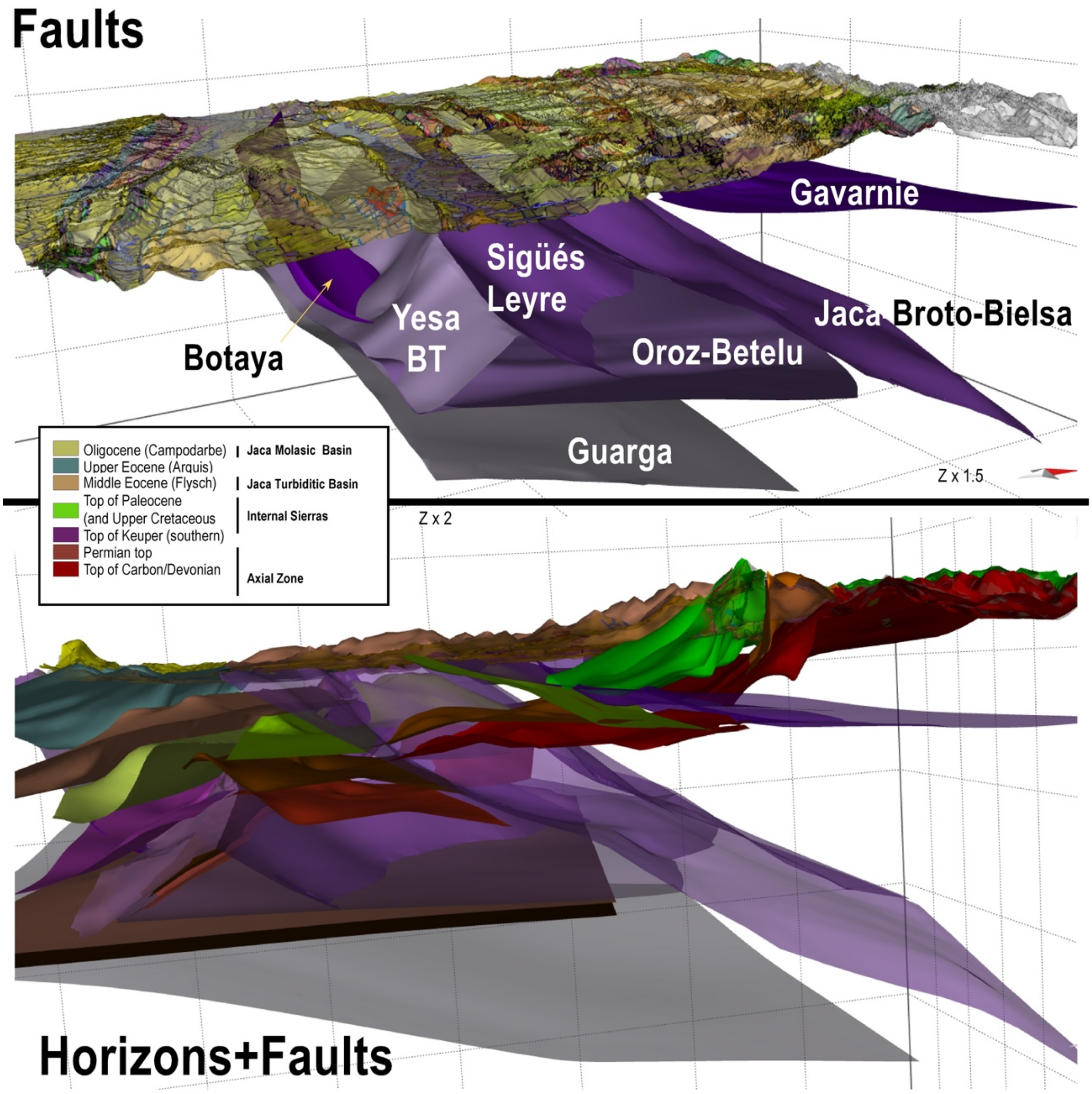

Fig. 30. 3D model of the Southwestern Pyrenees

5 2D AND 3D MODELLING IN THE WESTERN PYRENEES

5.1 2.5 D forward modeling (Gravmag)

Modelling of gravimetric anomalies allows to check the consistency of the seismic model. The 2.5 D modelling is based on the idealization of geological bodies by means of polygons having particular shapes and densities in 2-D (cross-section) and a certain lateral extension in the direction perpendicular to the cross-section (half-width parameter). Each geological body in a cross-section is characterized by one polygon with an initial density that gives a particular gravimetric response. The combination of all gravimetric signatures of all bodies in a cross section produces a gravimetric anomaly (so called “calculated”) that can be compared with the actual curve (“observed”) obtained from the gravimetric anomaly map or directly from a transect in which measurements are projected onto the cross-section. Forward modelling of gravimetric anomalies can be done using either the residual gravimetric curve or the total Bouguer anomaly. In the first case, the gravimetric anomaly is obtained after filtering (eliminating) the regional gravimetric anomaly from the Bouguer anomaly. Therefore, the long-wavelength trend, originated by deep-seated bodies is subtracted and the remaining anomaly (residual gravimetric anomaly) reflects the changes in density of only the upper few km of the crust. Note that the depth to which the geological bodies must be modelled to answer for this gravimetric anomaly is not a fixed level, but depends on the particular conditions of each cross-section.

Normally, the regional anomaly responds to the changes in thickness of the continental crust, whose density contrast with the lithospheric upper mantle is about 400 Kg/m3. Since the regional anomaly can be modelled by means of a first-order, two-order or three-order regular surface, this is the usual way of modelling gravimetric anomalies. However, it is sometimes difficult to separate the regional anomaly from the total Bouguer anomaly, as it is the case in the SW Pyrenees (see §4.2.2. Regional and Residual anomaly maps). This kind of situations occurs when there is for example an important thickness of low-density sediments in foreland basins, as occurring in many sectors of the Ebro Basin (Mezcua et al., 1996; Del Río el al., 2013). The facts contributing to create an apparent regional anomaly linked to near-surface deposits are: (i) the thickness of sediments, that can reach more than 5000 m in the above-cited example, (ii) the density of this sedimentary pile, contrasting in more than 200 Kg/m3 with the standard density of most sedimentary rocks, (iii) the lateral extension (i.e. the volume) of the low-density sedimentary body and its gentle ends (either by thrusting or by pinchout) towards its borders, that create a long-wavelength anomaly similar to those obtained by changes in the thickness of the continental crus. (iv) the interference of non-coaxial deformation patterns at different depths. In places where an interference between long-wavelength anomalies is expected, for example because of the changes in thickness of the continental crust combined with the existence of a thick foreland basin (as in the study case), it is convenient to model the total Bouguer anomaly, in order not to filter as a regional anomaly gravimetric features that are caused by these upper crust, surficial bodies.

Therefore, in the SW Pyreenan case study, we have modelled the Roncal cross-section considering the total gravimetric Bouguer anomaly. This allows to reliably reproduce the geometry of the crust also considering the minor anomalies resulting from the uppermost geological bodies. The reason for this choice is that in the study area there is a combination of shallow and deep sources whose effects are very difficult to separate by means of mathematical procedures such as the construction of regular surfaces. There are two main sources of anomalies that preclude this separation: (i) the Ebro foreland basin to the South of the studied area, that shows a considerable thickness of low-density deposits and cover a vast area; this creates a negative effect that is superimposed to the thinning of the continental crust towards the South, that in its turn, creates a positive effect that partially compensates the former, and (ii) the existence of high-density bodies of mantellic origin (density contrast between 300 and 500 Kg/m3 with the surrounding host rocks) that are emplaced at high levels within the crust. The anomalies caused by these bodies are of intermediate wavelength because of their shallow emplacement level and their connection with the mantle at the depth, therefore their effects are difficult to classify either as “residual” or “regional” anomalies. Therefore, our choice has been to model the total Bouguer anomaly paying particular attention to small changes that can be classified as residual anomalies caused by subtle changes in the uppermost crustal bodies.

5.1.1 Roncal section

In our case, the existence of geological cross-sections, well constrained by means of the delimitation of seismic horizons and boreholes helps a reasonable characterization of the upper levels down to 7-7 km. For deeper crustal levels we have considered previous deep reflection seismic studies (Daignières et al, 1994), receiver function signals (de Lis Mancilla and Diaz, 2015), magnetoteluric studies (Campanyá et al., 2012), modelling of gravimetric and magnetic signal (García-Senz et al., 2020) as well as previous deeper interpretations based on balanced cross sections (Teixell, 1998; Casas and Pardo, 2004; Casas, 2005). Both datasets together allowed us building an initial cross section for the entire crust and, thus checking the feasibility of the solutions proposed and the maximum and minimum depth to the top of the bodies.

Density contrasts in the outcropping geological bodies are also well constrained. For the crustal levels at depth, values of 2700 Kg/m3 and 2900 Kg/m3 have been chosen for the upper crust and lower crust (below the base of the Paleozoic sedimentary units) respectively. For the outcropping units, densities of the different materials are based on measurements of samples, whose results can be found in Table 2. Finally, a feedback process with the seismic-constrained section (given the error margins for horizons) has been established. In this way, the gravimetric model has been used to correct or modify the cross-sections and in its turn can be considered as a solid proposal.

The Roncal cross-section shows a gradual thickening of the continental crust (from 30 to 50 km) towards the Axial Zone of the Pyrenees, that explains the overall negative Bouguer anomaly towards this zone. It is worth noting the non-direct correspondence between the thickening of the continental crust and the Bouguer anomaly, that only shows a very gentle low. This is due to the two-step geometry of the base of the continental crust, that shows a large flat area corresponding with the southernmost edge of the Axial Zone. Conversely, in the northernmost sector of the Ebro Basin, the homogeneous gradient of the Bouguer anomaly is explained by progressive thickening of the upper crust and gradual deepening of the lower crust to the North. The thickening of the Paleozoic from the southern margin of the Axial Zone towards its center can be explained by the stacking of basement thrust sheets in the Axial Zone. Minor (residual) anomalies can be explained by the outcrops of Cretaceous units, that pinpoint the main thrusts. These anomalies, although small regarding their absolute values, are interesting because they result from the interaction to different extent of the relatively dense Cretaceous-Paleocene limestones and the underlying low-dense Upper Triassic, Keuper facies. The most remarkable features in terms of absolute values is the Mauléon positive anomaly (more than 70 mGal), corresponding with the North Pyrenean fault and the emplacement of mantellic bodies, whose top, in this case is 10 km deep, in agreement with recent interpretations (García-Senz et al., 2020). The thickness of the crust progressively increases from this area towards the North but it is poorly constrained in our cross-section.

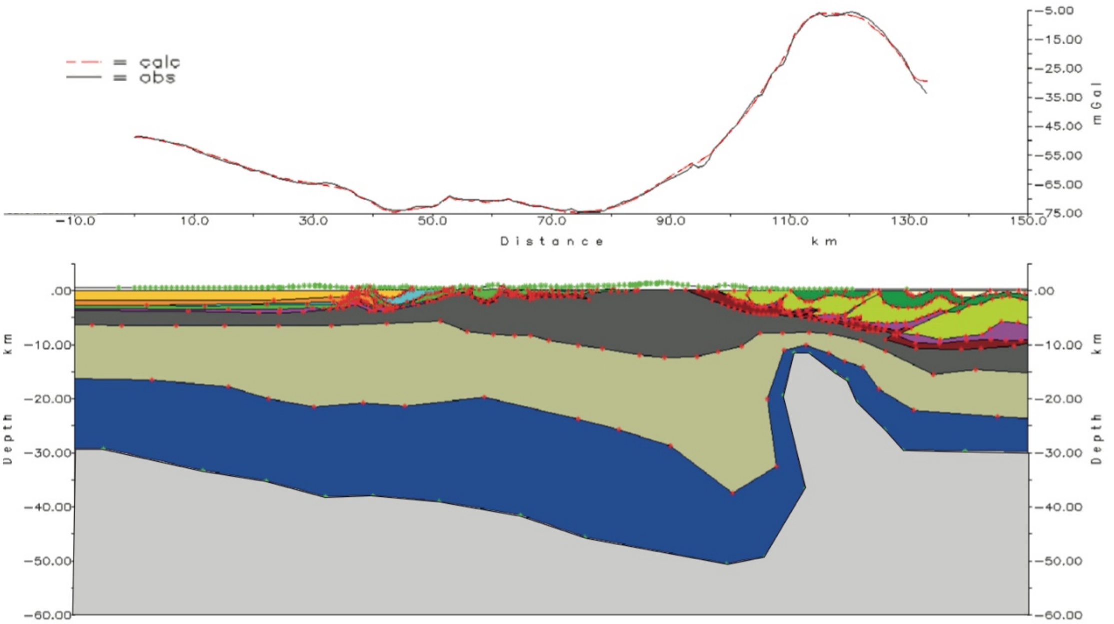

Gravimetric /stratigraphic unit.	Fill Style	Density (g/cm3)	Gravimetric /stratigraphic unit.	Fill Style	Density (g/cm3)	Gravimetric /stratigraphic unit.	Fill Style	Density (g/cm3)
Mantle		3.300	Permian + Triassic		2.550	Campodarbe (Sandstones)		2.447
Lower Crust		2.900	Triassic		2.280	Campodarbe (Siltstone)		2.593
Upper Crust		2.700	Paleocene- Upper Cretaceous		2.603	Other Jaca Molassic deposit		2.487
Paleozoic		2.684	Eocene - Bartonian		2.509			
Paleozoic - Permian		2.653						

Fig. 31a. 2.5D Forward modeling of the extended Roncal section in Gravmag

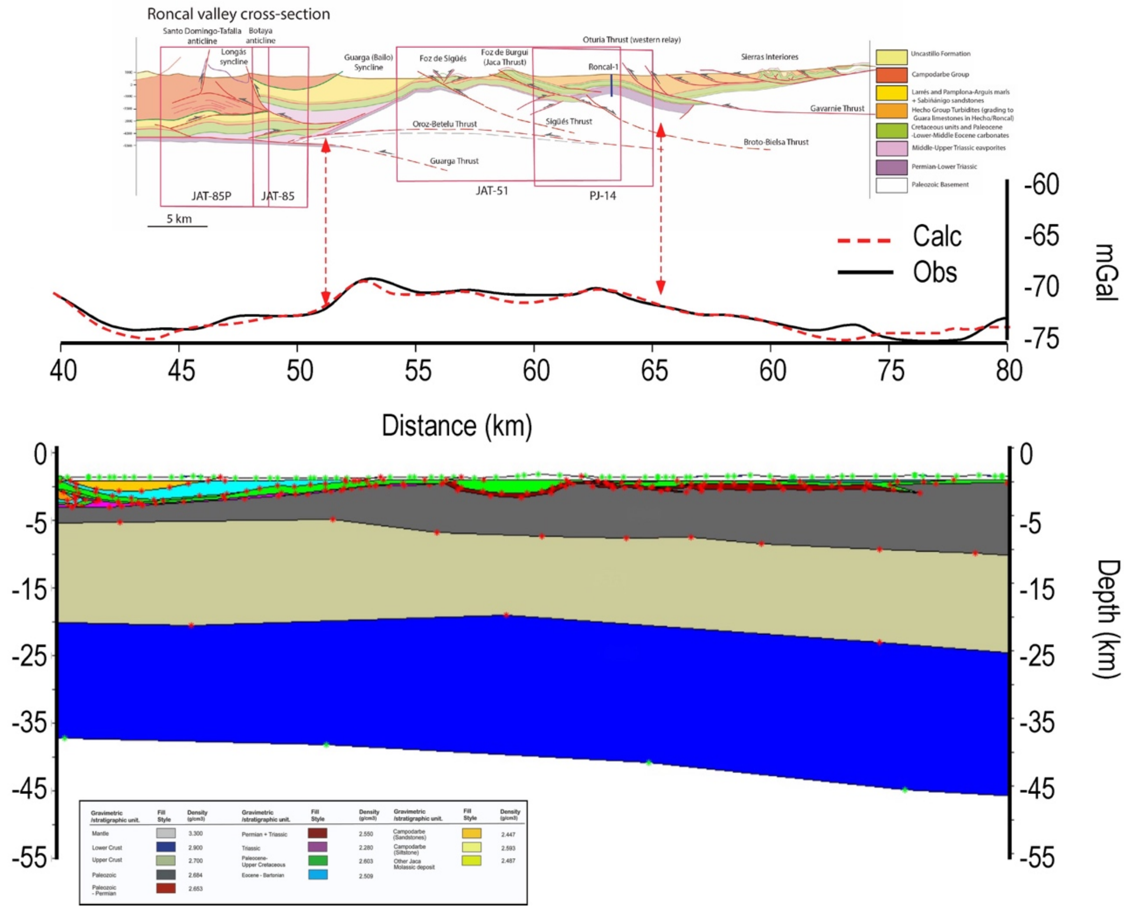

Fig. 31b. 2.5D Forward modeling of the Roncal section in Gravmag

5.2 3D forward and inverse modeling

The modeling in GMSYS-3D requires four different inputs, that must be loaded as a grid:

- the Digital Elevation Model
- the modelled stratigraphic horizons from seismic and balanced sections: Basement top, Permian top, Keuper top (only in the Southern part), the top of the flysch (*), the top of the Bartonian marls, the outcropping top of the Campodarbe Fm (to the South)
- the Bouguer or its residual anomalies (that can be obtained from different methods, the key is to find a suitable residual anomaly for the study area). The use of the Bouguer or the residual anomaly as observable in the calculations will depend on the depth of the model.
- the processed density data (table 2) that can be input as constant value, grid or voxet. In our study case density grids could not be derived due to scarce information and problem access to FDL logs from oil wells.
- (*) for simplicity, the top of the flysch also includes the Upper Cretaceous and Paleocene due to the very similar density values. Moreover, this simplification helps avoiding many structural complexities between the Internal Sierras and Turbiditic units not showing any petrophysical contrast.

Auxiliary, we have also taken into account a map of "density of information" of the basement (main target horizon). This map considers the spatial location of seismic reflectors (map view only) as well as the outcropping surface of the Paleozoic rocks. With this information we have generated a new map showing the distances to closer neighbors as an approach of the uncertainty of the 3D reconstruction (see Fig. 25); as larger this value is, larger the uncertainty will be.

First we evaluate the power spectrum of the Bouguer anomaly to estimate the depth of the main causative bodies. The slope of the different segments of the power spectrum is related to the depth of the structures that originate the gravity anomalies. The power spectrum of the Bouguer anomaly of the area (outlined in red) show a depth estimate of c. 5 km (Fig. 32). It is a surprisingly shallow level and have to be taken with caution. This area is small (42 x 50 km) thus, the size acts as a filter for the long wavelengths that we see on the map but the contribution to the anomalies from deep seated bodies is still present. The radially averaged power spectrum of the Bouguer anomaly (large blue area) indicates causative bodies located at c. 15 km. It is clear then that the size of study area controls the depth of the causative bodies and even the size of the accompanying area (blue) could have not recorded longer (cortical) wavelengths, but the contribution of the lower crustal bodies is evident. Because of this relevant depth signature (which could be larger), we had already decided to first perform the 2D gravimetric modelling at a cortical level (Fig 31). This also allow us stablishing an initial assumption on the significant gravimetric signature caused by the subduction of the Iberian plate underneath the European one. This is well supported by recent gravimetric interpretations of the deepest crustal levels at a Pyrenean scale (Pedrera et al., 2017 and García-Senz et al., 2020) and, accordingly, we have incorporated the Moho geometry in our model (in fact an interpolated surface equivalent to the base of the Upper Crust (UC) which is consistent with previous interpretations (Casas and Pardo, 2004; García-Senz et al., 2020).

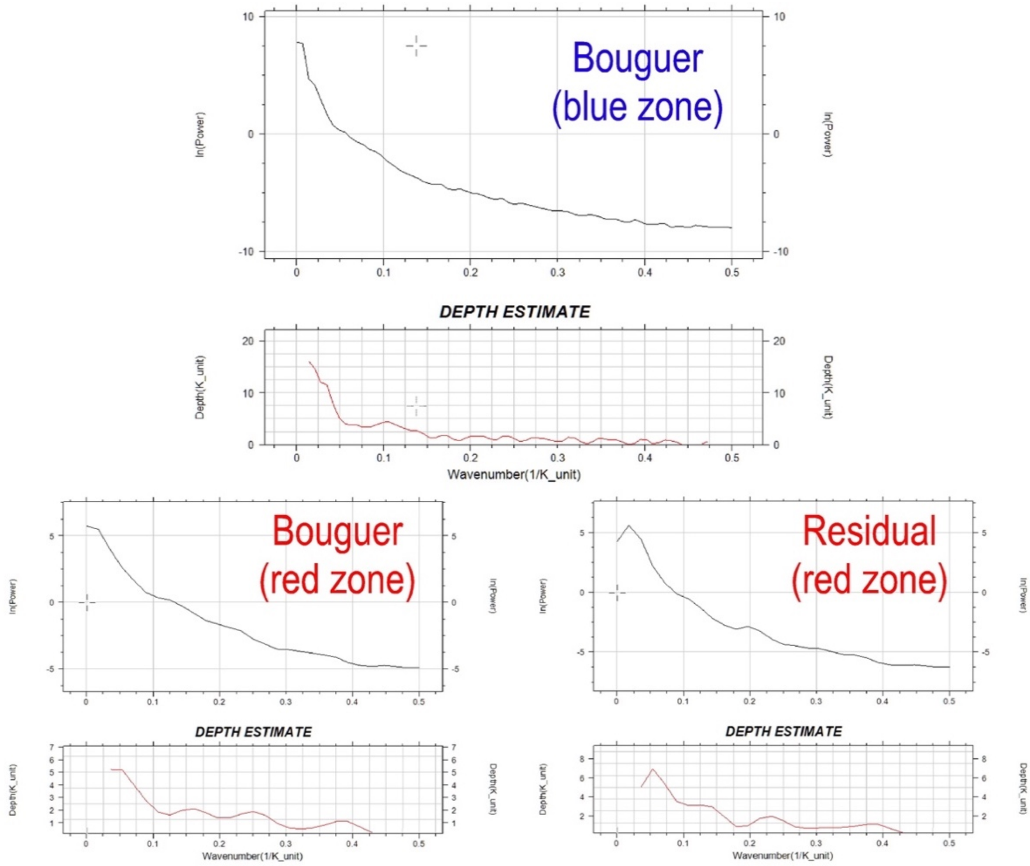

Figure 32: Radially averaged power spectrum of the Bouguer anomaly of the accompanying zone (upper), the one from the BA in the red inner zone (bottom left) and the one form the residual after applying a low band pass filer of 25 km (bottom right).

5.2.1 3D Forward modelling FM

Once we have identified as potential causative the horizons at deeper crustal level, we first run the forward modeling (including almost until the Upper Crust/Lower Crust boundary) to characterize the misfits and to establish hypothesis about its possible origin.

The main assumption behind all these modeling procedures is that the model geometry is likely inaccurate (upper levels) because of the limited seismic information and that the density distribution is rather well constrained (relatively good coverage at surface but not at depth) with the limitation that we will use constant densities in the model whereas the histograms show variations that are difficult to take into account because the distribution of the sampling stations precludes generating a grid of the density distribution for each layer. In any case, the final goal is reconstructing the basement top surface (topography), to compare with the original one and to identify possible mistakes in the initial and (conceptual) misunderstandings of the geometry.

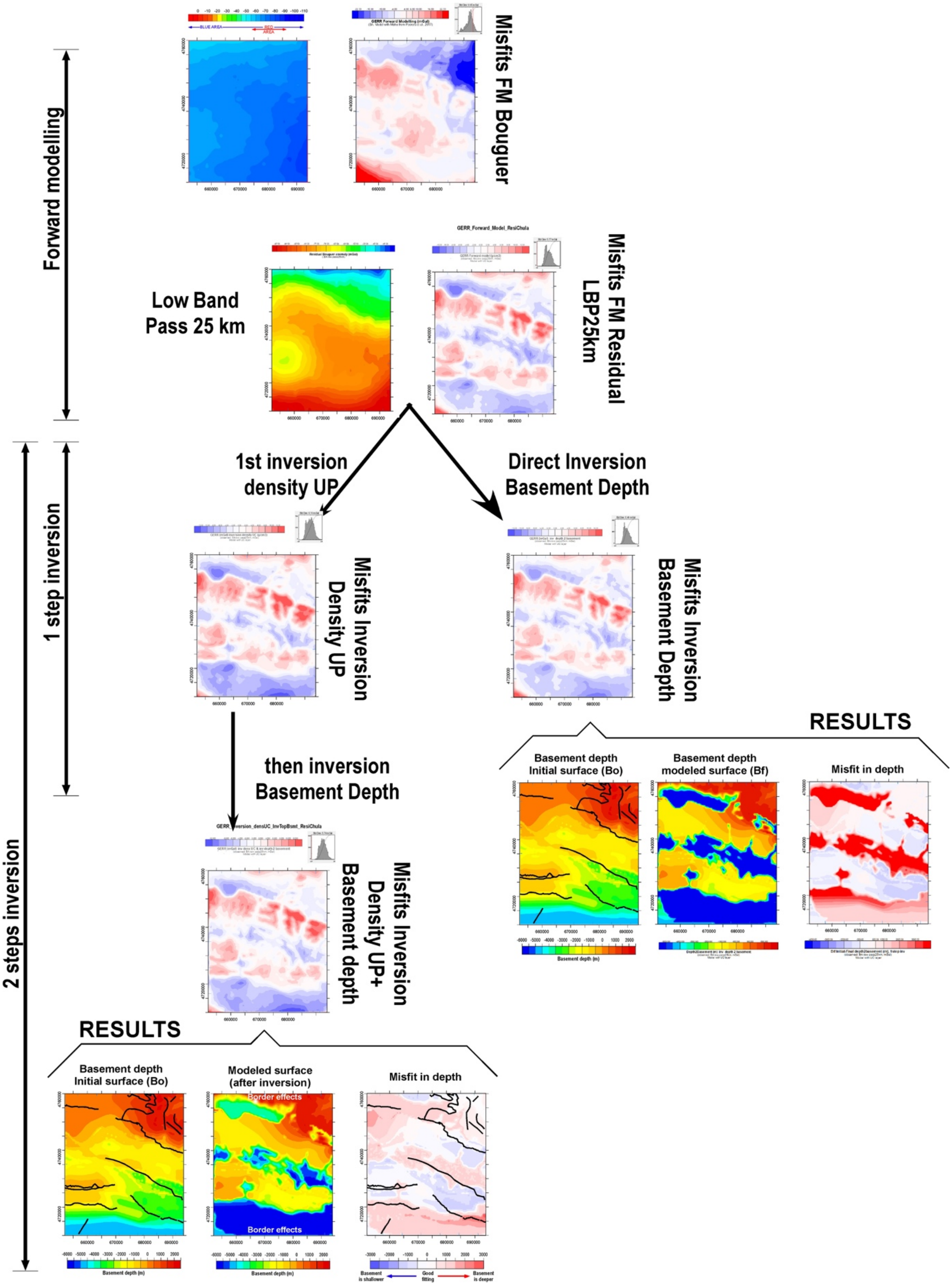

Figure 33: Sequential workflow of modelling procedures, number of steps and results shown in this discussion section.

The sequential workflow has been created step by step based on the results of the forward modelling of the Bouguer and Residual gravity anomaly as well as on the identified uncertainties associated to the densities of the Upper Crustal Layer below the basement, the flysch facies and Permian red beds.

The first step is analyzing the results from the forward modelling of the Bouguer anomaly. The model incorporates the top of the UC, estimated from the 2D models and the Moho boundary (Pedrera et al. 2017). The density of the UC, taken from the 2D models, has been initially set at 2.7 g/cm^3 and it has been assumed a density contrast between the lower crust and the upper mantle of 0.4 g/cm^3.

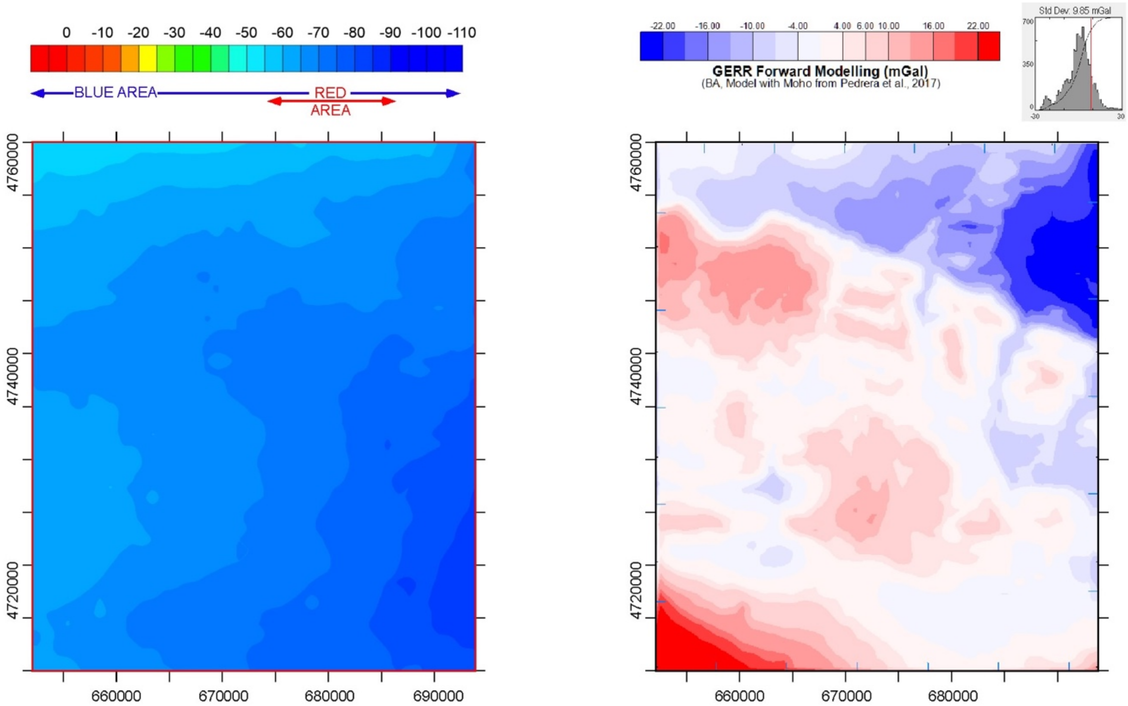

Figure 34: Forward modelling of the Bouguer anomaly (left) and its misfits (Observed-calculated gravity) in the right.

The initial evaluation of the forward modelling displays a strong NW-SE gradient in the misfits, likely indicating the effect of the very upper crustal levels not well constraint at depth. Besides, the range of the misfits is relatively large (-30 to 30 mGal), and the standard deviation reaches almost 10 mGal (Fig. 34). This result is no good enough and therefore, we have carried out the regional-residual separation (Fig. 33). After trying different techniques (upward continuation, polynomial separation, isostatic residual, etc.), the one that can be better correlated with the geology is a low band pass filter of 25 km which is able to remove the regional (very likely crustal in origin) gradient.

Accordingly, we repeat the forward modeling with this residual (Fig. 35). The evaluation of the power spectrum of the filtered Bouguer anomaly (Fig. 32) gives a depth estimate of 6- 7 km which can be interpreted as density variations in the upper levels of the upper crust where our model is located.

The results of the forward modelling of this residual show the vanishing of the S-N gradient that appeared in the misfits after the forward modelling using the Bouguer anomaly as observable. Besides, the range of variation has lowered to -20 to 20 mGal. Positive anomalies of the misfits (Obs-Cal >0) mean that the is a lack of density in the initial model (denser bodies and/or bodies at shallower depths are underestimated), on the other hand, negative anomalies of the misfits (Obs-Cal < 0) indicate the other way around; there is an excess of density (lighter and/or deeper bodies are underestimated or denser bodies and/or at shallower depths are overestimated). The misfits clearly display a Pyrenean anisotropy; N120E according with the main structural trend in the region, especially in its eastern part. A tentative interpretation of the two clear steps (bands of positive misfits) delineated in figure 35 is the feasible relationship with the underlying frontal portion of the Gavarnie hangingwall, that duplicates basement rocks in the NE corner of the model. The second step to the South correlates well with the Leyre-Illón basement uplift, partially well constrained by seismic reflectors.

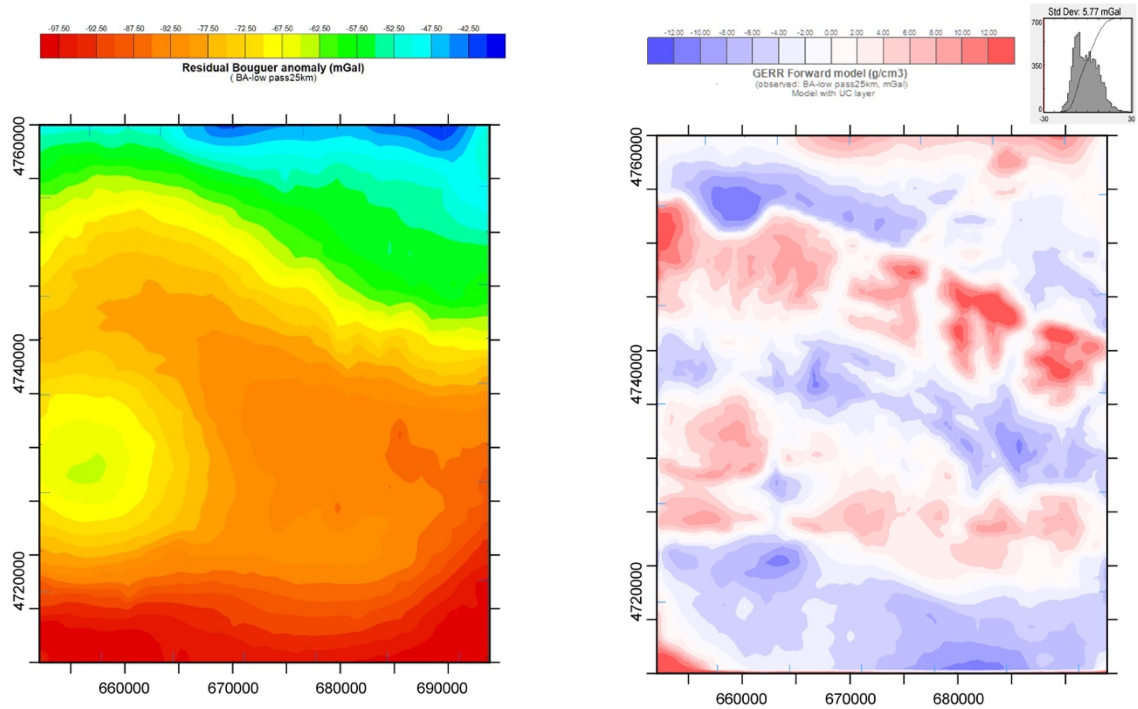

Figure 35: Forward modelling of the Residual anomaly (Low band pass 25 km (left) and its misfits in the right

Although the solution is not optimal, is by far the best we found after numerous trials. Consequently, we use this residual Bouguer anomaly as the observable for the inversion process. It is worth noticing that we have tried several inversion modelling strategies (only part of them are shown in figure 33) aiming to reduce the misfits.

5.2.2 3D inversion

First we calculated the inversion of the top basement geometry. This can be considered as the more simplistic and objective solution (with fewer assumptions behind). An important geometrical constraint was the outcropping surface of the Paleozoic rocks in the NE corner of the project (Axial Zone). The resultant geometry of the misfits follows, the trend of the main structures delineated both at surface and at depth (in the initial 3D model). However, it proposes a generalized deepening of the basement topography in many parts of the model, some of them reaching differences above 6000 m from the initial model that cannot be assumed (Fig. 36).

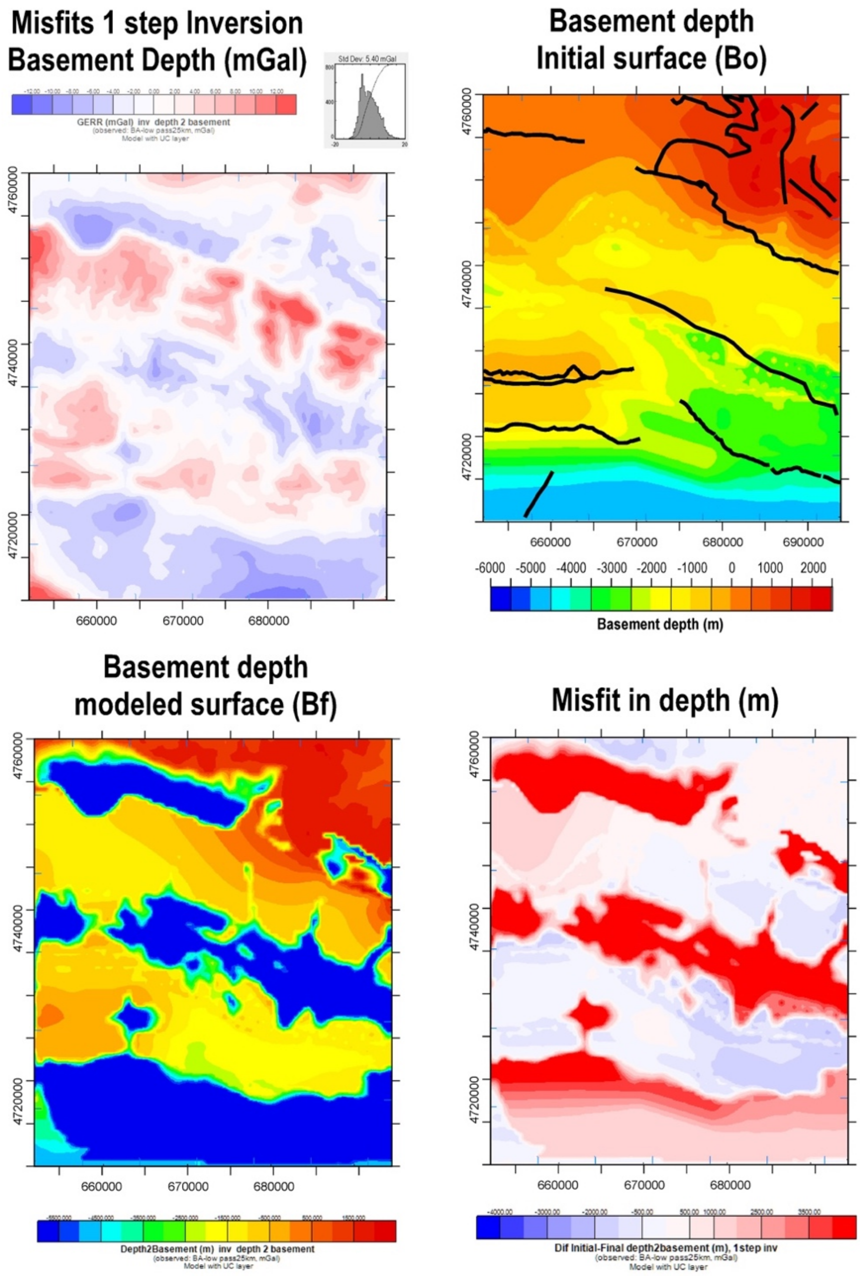

Figure 36: One step inversion of the basement topography Gravimetric misfits. Initial and modeled (calculated) basement topography as well as their differences.

Aiming to plan the subsequent modelling strategy (sequence of steps, inversion of depth [main target] or density), involving more than one inversion step, we have investigated some possible sources of the misfits, being the most relevant, the heterogeneous density distribution at different modeled volumes since the initial model had constant densities which, obviously, is not realistic.

This is the case of the thick flysch facies with known E-W lateral sedimentological changes conditioned by the paleogeography of the turbiditic basin (Mutti et al., 1988) but also displaying a S-N increasing of density caused but the burial history (Pueyo-Anchuela, 2012; Izquierdo-Llavall et al., 2013). Besides, the density of the Permian rocks is another uncertain variable in our model. The average out of our own values (only outcrop data) is 2.653 g/cm^3. This value is a bit below the mean of the older Paleozoic rocks (Carboniferous and Devonian); 2.693 g/cm^3. The used Permian value, as the rest of petrophysical data, assumes the homogeneity of the density for this formation. However, this assumption may easily fail for a number of reasons; 1) gamma-gamma logging from oil exploration wells were not accessible for us, thus we lack any control on the evolution of density at depth. 2) Robust surficial data from lithological equivalent facies (Permian and Buntsanstein rocks from the Iberian Range; Pueyo et al., 2016), yield much lower values (below 2.4 g/cm$^{3)}$ for this detrital (red beds) formation. 3) Surficial outcrops are limited to the very northern part of the model (Axial Zone). Other stratigraphic formations, like the turbidites, have a wider outcropping N-S exposure which indeed represents a section of the buried sequence (northern are deeper and southern are shallower). 4) Permian occurrence at depth is strongly controlled by the development of normal faults (compartmented basins) as we have seen in some seismic sections and in outcrop exposures of the Western Pyrenees (Cantarelli et al., 2013 and cited references). Consequently, the density evolution at depth is totally unconstrained and may hypothetically display a large range distribution (depending on the variable S-N thermal history (Izquierdo-Llavall et al., 2013).

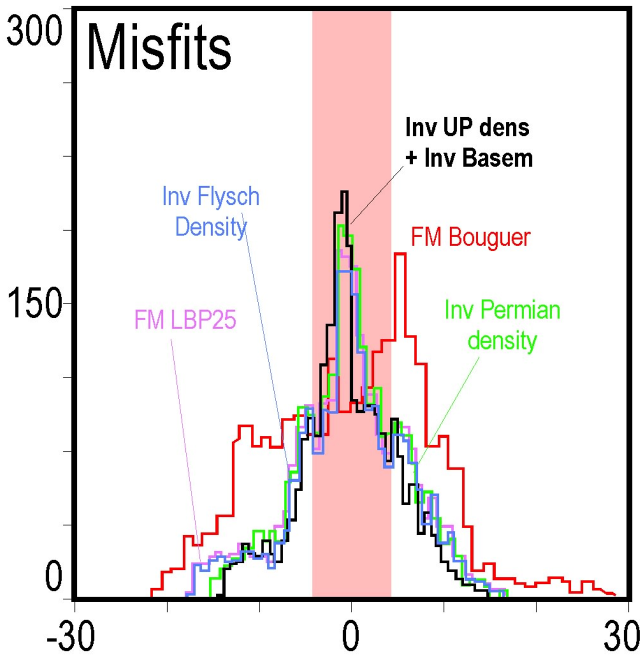

Figure 37: Comparison of misfits derived from different modelling strategies. The pink are shows the range of the acceptable region.

Therefore, assuming that the misfits can be related to both, lateral density variations of some layers but also variations of the basement topography that are unaccounted for in the initial model, we have performed two inversion sequences: Inversion of the Flysch density and then, the basement topography as well we the inversion of the Permian density and then, the basement topography. Surprisingly, none of the derived results from the inversion of these layers improved the misfits (both range or anisotropy) (Fig. 37). In any case, improving the density gridding is one of key steps for near future research. It seems clear by looking at the densities table and the rock formations histograms (Fig. 27) that using a constant density for each layer is one of the origin of the misfits, maybe not the largest one. In this regard, the model could be improved by creating a grid based on the distribution of the samples, especially for those formation displaying an ample surficial distribution and a good control on density vales (Eocene flysch). This would be a better approximation than using a constant density as we did.

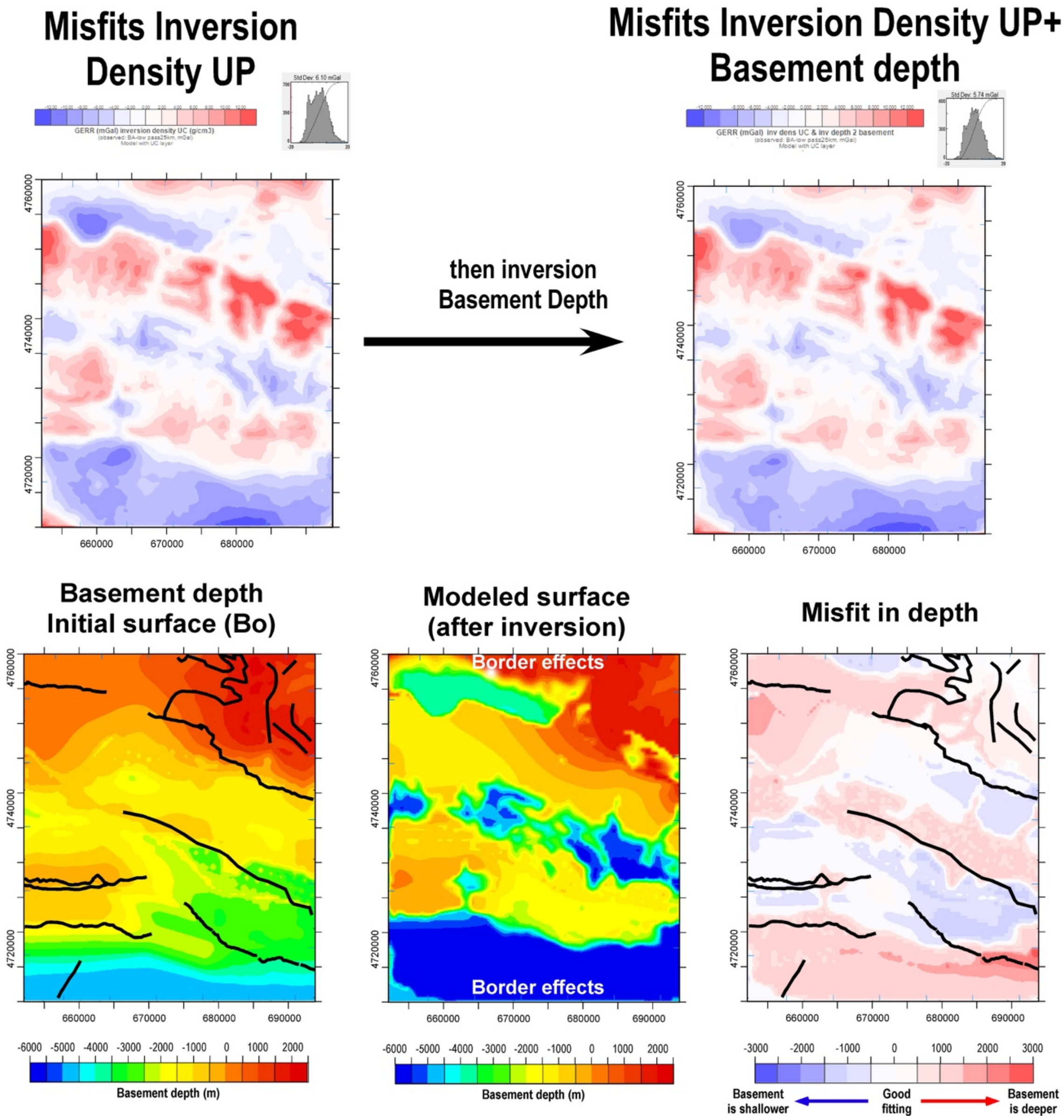

Figure 38: Two steps inversion of the basement topography. Gravimetric misfits. Initial and modeled (calculated) basement topography as well as their differences.

Following recent experiences carried out in the frame of this project, particularly in the cross border harmonization of the Northern Polish-German border, we have applied another two steps inversion (Ayala et al., 2021b). First we invert the density of the lowermost layer of the model, the only one without any single density data. This layer (lower basement rocks above the boundary between the upper and lower crust) follows the geometry of the subducting plate (northward dipping very shallow) from depths at 8 km to the South to depths at 17 km to the North and parallels the geometry modelized by Pedrera et al. (2017) where all major thrust sheets rooted towards the North (as previous interpretations by Casas and Pardo, 2004). After this inversion, we have sequentially performed a second step to infer the geometry of the basement.

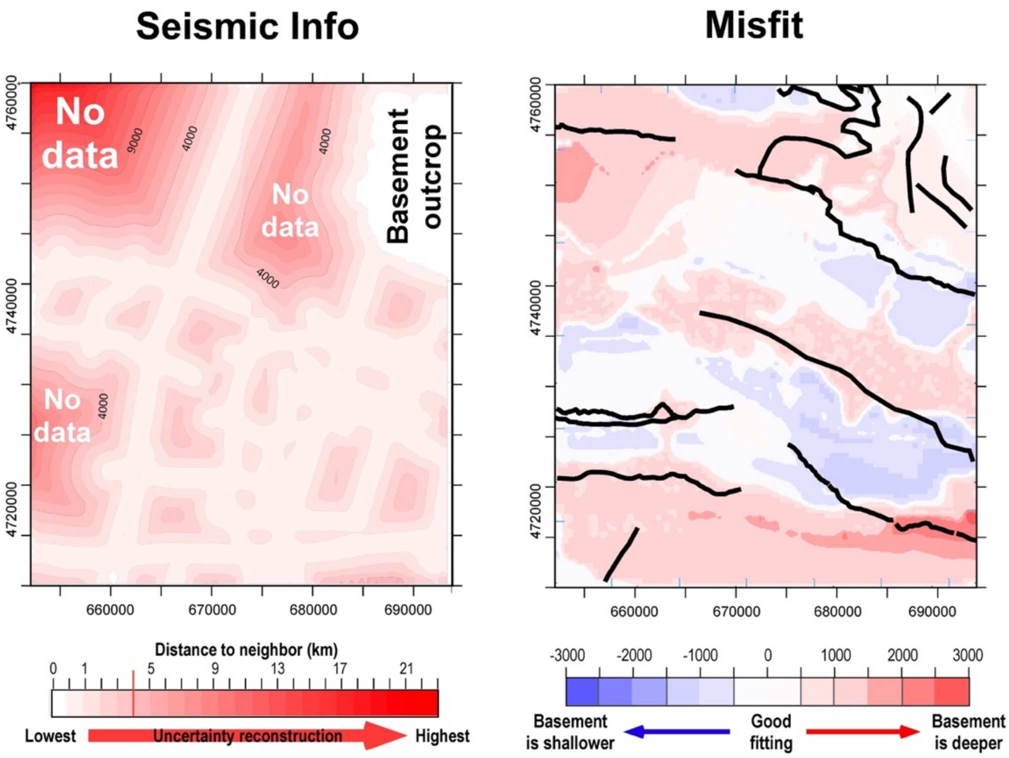

Figure 39: Qualitative estimation of the 3D model uncertainty related to the seismic information positioning and basement topography differences (initial-calculated).

These results are more reasonable (absolute misfit range and its distribution; Figs. 37, 38 and 39) and are also more comparable with the initial geometry of the model. Apart from some border effects to the very South and North, the contour lines mimics well-known (from seismics) subsurface trends and, more importantly, the differences between the initial and calculated topography are smaller. In fact, there are large portions of the model were these differences are neglectable. If we also considered the uncertainties inherent to the time-to-depth conversion (very little constrained in our case), large portions of the model are validated. The Leyre-Illón basement high is one of them, more precise results from further inversion steps at at larger scale (blue model area) could be very useful to accurate its continuation to the the East and to decipher its relationships with eastern basement thrust in the Tena section. The NW corner of the model also merits some attention. This region has a total lack of seismic information (by far the worst of the model) and thus the poorest control in the initial model. However, the inversion of the geometry of the basement yields comparable trends to outcropping structures and thus, validates our strategy. As a general rule, the differences are mostly positive (Fig, 39), meaning that there is a dominant underestimation of the basement depth (red areas). However, in contrast to the one-step inversion results, in some areas the initial basement topography was also over estimated (blue color) in the initial model. This happens, for example, in the footwall of the Jaca thrust sheet (central east part). Another observation is the underestimation of the Guarga thrust top surface (to the South of the model), which could over pass up to 2 km. Finally, an estimation of the matching between the initial and modeled geometry can be establish by analyzing the misfit distribution in detail (Fig, 40). Most of the misfits (88%) in absolute value fall below 1000 m, certainly a significant mismatch in depth estimation. However, this value had to be considered with caution since there is a potential significant uncertainty derived from the time-to-depth conversion used to generate the initial model. Therefore, the degree of validation of the model can be considered satisfactory.

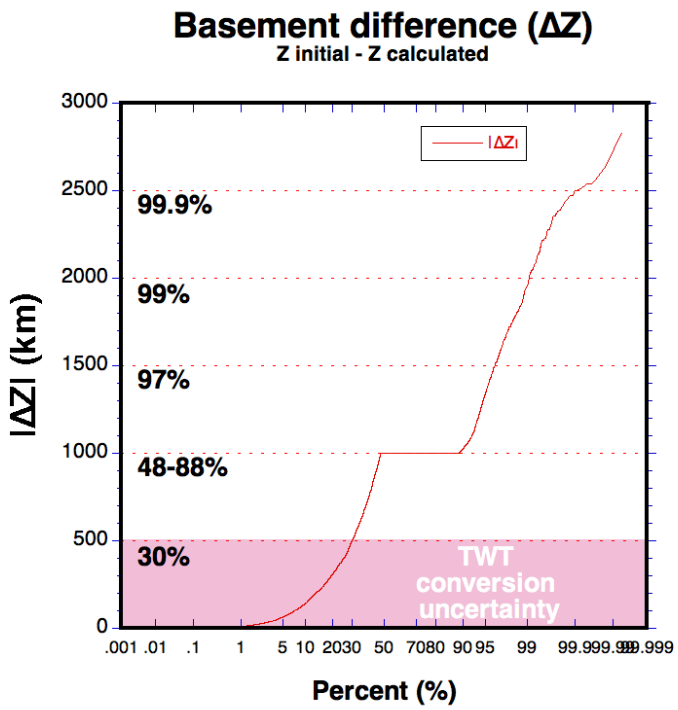

Figure 40: Degree of validation of the modelling procedure

The main goal of this WP was to help in the reconstruction of the basement topography by means of a joint gravimetric, structural and petrophysical integrated modelling. The results obtained during the project life (new basement topography) are consistent and promising; they have helped us to located reconstruction inconsistencies in the initial model, part of them located in areas of very poor seismic coverage (and likely more affected by conceptual uncertainty) and they are also validating good portions of the initial model topography. Additional refinements could be performed in the near future: 1) Building density grids for well-outcropping formations, (e.g. turbidites), 2) Controlling of density at depth, if FDL logs from the oil industry are finally accessible, 3) Improving minor inconsistencies in the initial topography (especially if additional seismic sections are accessible). In conclusion, we firmly believe the approach is promising and may help validating reconstructions in areas of limited seismic exploration.

6 CONCLUSIONS AND LESSONS TO BE LEARNT

6.1 Conclusions

We have built a new 3D model of the SW Pyrenees integrating geological, geophysical (seismic reflection and gravimetry) and petrophysical information. The initial 3D model encompasses the joint interpretation of the well-exposed and mapped geology together with 142 seismic sections (> 2000 km of coverage), and the tracking of ca. 2000 seismic reflectors, as well as, the integration of the lithological record and sonic logs from 4 key boreholes that allow the time-to-depth conversion of the model. Besides, we also generated three new balanced cross sections to support the structural interpretation. Despite all this work, some areas of the project (especially, the N-NW and the SW sectors) has a high uncertainty due to the lack of seismic sections (or because of access problems to the information).

At the same time, we have focused on the acquisition of more than 3,200 new gravimetric stations during the project life to generate an even sampling net (ca. 1 station/km2) with a total of more than 8,500 stations (being the difference, data from previous projects and databases). Besides, almost 900 density determinations from 329 localities in the target area were acquired, compiled from previous works and harmonized together to attain a robust petrophysical local database. The main goal of this part of the work was using the gravimetric modelling to harmonized the subsurface geology characterized by a deficient seismic coverage.

Subsequently, the integration of all aforementioned information was subjected to forward modeling (2D and 3D) and the 3D inversion of the gravimetric signal together with the geological and petrophysical information. Although further improvements could be done, this modelling procedure (methodologically aligned to D6.4, for further details) has allowed us to validate and to better constrain the geometry of the basement rocks (with the highest density contrast). The method was particularly useful in the areas with poorer seismic coverage. The refinement of the initial 3D model (from seismic data) under the light of the results of this project will represent a first keystone to evaluate the potentiality of, for example, deep geothermal energy reservoirs in the region in the near future.

From a methodological point of view, our approach may represent a widespread solution to harmonize 3D models in a cost-efficient way and to aid in the decision making process in areas with scarce information (or without access to it) that will need to be evaluated for their potential as deep geothermal reservoirs, as Hidrogen or Carbon Dioxide storages, etc. in the frame of the Energy Transition (Green Agenda).

6.2 Problems found and lessons to be learnt

Identified problems and lessons to be learnt in future harmonization projects:

Problems found

1) Access to previous oil and gas information. Despite this valuable information was financed in the past by European Governments, in our case, only part of the information was open-access. IGME offers the navigation (digital files) of all seismic sections but only can provide high resolution scans (300 and 600ppp TIFF files) of part of them (below 50% in the GeoERA target area) a veru few digital (*.SGY files). Similarly happens with the borehole information; not a single FDL was accessible for the modeling of the petrophysical information. Moreover, the information used in this project was dispersed in several databases (IGME, Technical Archive of Hydrocarbons, Regional government, etc.).

2) Gravimetric data acquisition was more long-lasting than expected. This was partially due to the forecasted acquisition of gravimetric data in rough terrains. About 14% of the new gravimetric data (more than 400 stations) were acquired in highly mountainous regions of the Western Pyrenees (hiking up to 2700m, cumulated height above 1500m/day) to guarantee a homogeneous data distribution in the model. Therefore, this portion of the dataset implied a higher investment of time (x4) and budget effort (x3) comparing to regular acquisition. Additionally, a number of reasons have hindered the normal development of this working package: a gravimeter crash in summer 2019, early snow during the 2019 autumn, the COVID pandemic (with severe mobility restrictions and accommodation difficulties during 2020-21), in addition to other personal problems (*force majeure*) of part of the IGME staff, seriously affected the data acquisition agenda (more than one-year delay). All these reasons, not totally balanced by the four-month extension of the project deadline, were difficult to consider in the risk-mitigation plan and have precluded an optimal attainment of the project, although we still believe the efforts and results of the project have satisfactorily met the proposed objectives and the project expectations.

3) From a scientific point of view, the standard derivation of residual anomaly maps (Bouguer minus the regional anomaly) was not straight forward in both case studies (the Pyrenean and the German/Poland cross border harmonization one). In the Western Pyrenees this is caused by the non-coaxial geometry of both, the lower crust subduction geometry and the Variscan basement rocks. Similarly happens in the German-Polish border regions with a strong signal from the underneath Variscan rocks. In the Pyrenees we decided to perform a 2D forward modeling including the Moho geometry (based on receiver functions data, deep seismic reflectors and magnetoteluric exploration) additionally, a standard residual anomaly map was derived for the core of the modeling area (much smaller) since it is less affected by non-coaxial geometries.

Lessons to be learnt

1) The public access to the oil exploration information, most of them financed by the European Governments in the past, should be regulated under FAIR principles (Findability, Accessibility, Interoperability, and Reuse of digital assets). Some European countries have already legislated in this sense, but many not. Apart from removing the existent access barrier, these principles would guarantee an easy findability of all critical subsurface information.

2) The joint gravimetric, structural and petrophysical modeling is an excellent tool for harmonizing 3D models, especially where scarce, uneven or non-accessible subsurface information (2D&3D seismics) is available and enough (and robust) density contrast exists. However, the required acquisition or harmonization times must be evaluated and programmed in a realistic agenda. Beyond the exceptional handicaps found in this project, harmonization may take time and can very sensitive to data sharing regulations in case of cross border study cases

3) Estimation of the uncertainty in workflows using structural, geophysical and petrophysical data is known to a certain extent, but its propagation is almost unknown. Future efforts should be done to evaluate the final uncertainty in the subsurface reconstruction.

7 ACKNOWLEDGEMENTS

This project was financed by the European Commission under the ERANET Cofound action 'Establishing the European Geological Surveys Research Area to deliver a Geological Service for Europe' (GeoERA; Grant No.: 731166). The Carolina Fundation is also acknowledged for a PhD fellowship (Rosibeth Toro). Access to databases from the Spanish Geographical Institute (IGN) and ENRESA are also thanked. Previous Spanish National Science Foundation projects (UKRIA4D [PID2019-104693GB-I00], DR3AM [CGL2014-54118-C2-2-R]; Pmag3DRest [CGL2009-14214-BTE]) provided very valuable information used in this project. We are also in debt with Pierre Labaume (U. Montpellier) and Josep Antón Muñoz (U. Barcelona) for delivering us additional subsurface information.

8. REFERENCES

Almela, A., Ríos, JM. (1951) Estudio geológico de la zona surpirenaica aragonesa y de sus sierras marginales. I Congreso Internacional de Estudios Pirenaicos, San Sebastian 2 (1): 327–360

Anastasio, D. J., 1992. Structural evolution of the External Sierra, Southern Pyrenees, Spain. In: Structural Geology of Fold and Thrust Belts (Ed. S. Mitra & G.W. Fisher) Johns Hopkins Univ. Press. 239-251.

Anastasio, D. J., Teletzke, A. L., Kodama, K. P., Parés, J. M., & Gunderson, K. L. (2020). Geologic evolution of the Peña flexure, Southwestern Pyrenees mountain front, Spain. Journal of Structural Geology, 131, 103969.

Arenas, C. and Pardo, G. (1996). Late Oligocene-Early Miocene syntectonic fluvial sedimentation in the Aragonese Pyrenean domain of the Ebro Basin: facies models and structural controls. Cuadernos de Geología Ibérica, 21, 277-296

Ayala, C., Bohoyo, F., Maestro, A., Reguera, M. I., Torne, M., Rubio, F., ... & García-Lobón, J. L. (2016). Updated Bouguer anomalies of the Iberian Peninsula: a new perspective to interpret the regional geology. Journal of Maps, 12(5), 1089-1092.

Ayala, C., Rey-Moral, C., Rubio, F. M., Pueyo, E. L., Casas, A. M., Clariana, P., ... & Martí, Y. J. (2020). Nuevos datos gravimétricos en los Pirineos Centrales (NE de España). Geogaceta, 67, 103-107.

Ayala, C.; Rey-Moral, C.; Rubio, F.M.; Soto, R.; Clariana, P.; Martín-León, J.; Bellmunt, F.; Macau, A.; Gabàs, A.; Casas, A.M.; Martí, J.; Pueyo, E.L.; Benjumea, B. (2021 in press). New gravity data on the Central Pyrenees, a step forward to help a better understanding of the Pyrenean structures. Journal of Maps

Ayala, C.; Pueyo, E.L., Jahnke, C.; Szynkaruk, E.; Obst, K. (2021). Deliverable 6.3- Harmonization procedure in the Polish-German border region using gravimetric data. GEOERA 3DGEO-EU, 3D Geomodelling for Europe, project number GeoE.171.005. Report, 45 p

Barnolas, A., & Teixell, A. (1994). Platform sedimentation and collapse in a carbonate-dominated margin of a foreland basin (Jaca basin, Eocene, southern Pyrenees). Geology, 22(12), 1107-1110.

Barnolas, A., Gil-Peña, I., Alfageme, S., Ternet, Y., Baudin, T., & Laumonier, B. (2008). Mapa geológico de los Pirineos a escala 1:400 000. IGME/BRGM ISBN: 978-2- 7159-2168-9.

Barnolas, A., Teixell, A., Samsó, J.M. y Zamorano, M. (1992). Estructura y evolución sedimentaria del sector central de la cuenca surpirenaica. III Congreso Geológico de España, VIII Congreso Latinoamericano de Geología, Salamanca, Excursiones, 74-114

Beaumont, C., S. Ellis, and A. Pfiffner (1999). Dynamics of sediment subduction accretion at convergent margins: Short-term modes, long-term deformation, and tectonic implications. Journal of Geophysical Research 104, 17, 573-17, 601.

Blakely, R.J., 1995 (2005), Potential Theory in Gravity & Magnetic Applications: Cambridge University Press, pp.441. doi:10.1017/CBO9780511549816

Bosch, G. V., Teixell, A., Jolivet, M., Labaume, P., Stockli, D., Domènech, M., & Monié, P. (2016). Timing of Eocene–Miocene thrust activity in the Western Axial Zone and Chaînons Béarnais (west-central Pyrenees) revealed by multi-method thermochronology. Comptes Rendus Geoscience, 348(3-4), 246-256.

Calvín, P., Santolaria, P., Casas, A. M., & Pueyo, E. L. (2018). Detachment fold vs. ramp anticline: a gravity survey in the southern Pyrenean front (External Sierras). Geological Journal, 53(1), 178-190.

Cámara, P; Klimowitz, J., 1985. Interpretación geodinámica de la vertiente centro-occidental surpirenaica (Cuencas de Jaca-Tremp). Estudios Geol., 41: 391-404.

Cámara, P., & Flinch, J. F. (2017). The southern Pyrenees: a salt-based fold-and-thrust belt. In Permo-Triassic Salt Provinces of Europe, North Africa and the Atlantic Margins (pp. 395-415). Elsevier.

Campanyà, J., Ledo, J., Queralt, P., Marcuello, A., Liesa, M., & Muñoz, J. A. (2012). New geoelectrical characterisation of a continental collision zone in the West-Central Pyrenees: Constraints from long period and broadband magnetotellurics. Earth and Planetary Science Letters, 333, 112-121.

Cantarelli, V., Aldega, L., Corrado, S., Invernizzi, C., & Casas-Sainz, A. (2013). Thermal history of the Aragón-Béarn basin (Late Paleozoic, western Pyrenees, Spain); insights into basin tectonic evolution. Italian Journal of Geosciences, 132(3), 443-462.

Carbayo, A.; del Valle de Lerchundi, J. León, L.; Villalobos, L. (2008a). Mapa geológico de la Hoja nº 116 (Garralda). Mapa Geológico de España E. 1:50.000. Segunda Serie (MAGNA). Instituto Geológico y Minero de España (IGME).

Carbayo, A.; León, L.; Puigdefàbregas, C. (2008b). Mapa geológico de la Hoja nº 117 (Ochagavía). Mapa Geológico de España E. 1:50.000. Segunda Serie (MAGNA). Instituto Geológico y Minero de España (IGME)

Carola, E., Tavani, S., Ferrer, O., Granado, P., Quintà, A., Butillé, M., & Muñoz, J. A. (2013). Along-strike extrusion at the transition between thin-and thick-skinned domains in the Pyrenean Orogen (northern Spain). Geological Society, London, Special Publications, 377(1), 119-140.

Casas, A. M., 2005. Sismicidad inducida por el embalse de Itoiz. Informe Inédito Universidad de Zaragoza 41 pp.

Casas, A. M.; Pardo, G., 2004. Estructura pirenaica y evolución de las cuencas sedimentarias en la transversal Huesca-Oloron. In: Itinerarios geológicos por Aragón (Edited by Colombo, F.; Liesa, C. L.; Meléndez, G.; Pocovi, A.; Sancho, C.; Soria A. R.), Geo Guías (Sociedad Geológica de España), 1, 63-96 (ISBN: 84-930160-2-0).

Choukroune, P., & Séguret, M. (1973). Carte structurale des Pyrénées 1/500.000. Elf-Univ. de Sci. Et Tech. du Languedoc, Lab. de Geol. Struct., Montpellier, France.

Choukroune, P., and ECORS Team (1989). The ECORS deep seismic profile reflection data and the overall structure of an orogenic belt. Tectonics 8, 23-39.

Colmenero, J., Fernández, L.P., Moreno, C., Bahamonde, J.R., Barba, P., Heredia, N. and González, P. (2002). Carboniferous. In: Gibbons, W and Moreno, M.T. (eds.) The Geology of Spain. Geological Society, London

Daignières, M., Séguret, M., Specht, M., & ECORS Team. (1994). The Arzacq-western Pyrenees ECORS deep seismic profile. In Hydrocarbon and petroleum geology of France (pp. 199-208). Springer, Berlin, Heidelberg.

de Lis Mancilla, F., & Diaz, J. (2015). High resolution Moho topography map beneath Iberia and Northern Morocco from receiver function analysis. Tectonophysics, 663, 203-211.

de Rojas, B.J.; Latorre, F. (2006). Mapa geológico de la Hoja nº 175 (Sigüés). Mapa Geológico de España E. 1:50.000. Segunda Serie (MAGNA). Instituto Geológico y Minero de España (IGME)

Del Río, P., Casas, A., Villalaín, J. J., Mochales, T., Soto, R., Oliva-Urcia, B. (2013). Interpretation of gravimetric and magnetic anomalies in the Cameros Basin (North Spain): combination of deep and shallow sources. Studia Geophysica et Geodaetica, 57(3), 442-459.

del Valle de Lersundi, J.; Puigdefábregas, C.; Sánchez Carpintero, I. (2008). Mapa geológico de la Hoja nº 143 (Navascués). Mapa Geológico de España E. 1:50.000. Segunda Serie (MAGNA). Instituto Geológico y Minero de España (IGME)

Dreyer, T., Corregidor, J., Arbues, P., & Puigdefabregas, C. (1999). Architecture of the tectonically influenced Sobrarbe deltaic complex in the Ainsa Basin, northern Spain. Sedimentary Geology, 127(3-4), 127-169.

Farrán, M. L. (2008). IMAGE2SEGY: Una aplicación informática para la conversión de imágenes de perfiles sísmicos a ficheros en formato SEG Y. Geo-Temas, 10, 1215-1218.

Fournier, E. (1905). Études géologiques sur la partie occidentale de la chaîne des Pyrénées entre la vallée d'Aspe et le celle de la Nive, Bull. Soc. Geol. Fr., 5, 699–723.

García Lobón, J.L., Reguera García, M.I., Martín León, J., Rey Moral, C. y Berrezueta Alvarado, E.R. (2011). Plan de selección y caracterización de áreas y estructuras favorables para el almacenamiento geológico de CO2 en España. Resumen ejecutivo. Fondo documental del IGME. Documento nº 64.055 (72 pp).

García Sansegundo, J. (2014). La estructura geológica del entorno del embalse de Itoiz (Navarra, España): un caso de sismicidad inducida por un embalse. Rev. Géol. pyrén., 2014, 1, 1, 7 p.

García-Sansegundo, J. (1996). Hercynian structure of the Axial Zone of the Pyrenees: The Aran Valley cross-section (Spain-France). Journal of Structural Geology 18, 1315-1325.

García-Senz, J. (2002). Cuencas extensivas del Cretácico Inferior en los Pirineos Centrales, formación y subsecuente inversión. PhD Thesis, Univ. de Barcelona, Barcelona, Spain.

García-Senz, J., Pedrera, A., Ayala, C., Ruiz-Constán, A., Robador, A., & Rodríguez-Fernández, L. R. (2020). Inversion of the north Iberian hyperextended margin: the role of exhumed mantle indentation during continental collision. Geological Society, London, Special Publications, 490(1), 177-198.

Gleizes, G., Leblanc, D., Santana, V., Olivier, P., & Bouchez, J. L. (1998). Sigmoidal structures featuring dextral shear during emplacement of the Hercynian granite complex of Cauterets–Panticosa (Pyrenees). Journal of Structural Geology, 20(9-10), 1229-1245.

Granda-Sanz, A. and Granda-París, T. (2014). Reconocimiento por métodos geofísicos en el P.I. Goyo. Gravimetría y Sondeos EM de Dominio de Tiempos (SEDT). Primera y Segunda fases. Technical report. 143 pp.

Hammer, S. (1939). Terrain corrections for gravimeter stations. Geophysics, 4, 184–194.

Hernández Samaniego A.; Simó Marja, A.; Gabaldón, V. (2006). Mapa geológico de la Hoja nº 174 (Sangüesa). Mapa Geológico de España E. 1:50.000. Segunda Serie (MAGNA). Instituto Geológico y Minero de España (IGME)

Hinze, W.J., Aiken, C., Brozena, J., Coakley, B., Dater, D., Flanagan, G., Forsberg, R., Hildenbrand, T., Randy-Keller, G., Kellogg, J., Kucks, R., Li, X., Mainville, A., Morin, R., Pilkington, M., Plouff, D., Ravat, D., Roman, D., Urrutia-Fucugauchi, J.,Véronneau, M., Webring, M. and Winester, D. (2005). New standards for reducing gravity data: The North American gravity database. Geophysics, 70, 125-132.

Izquierdo-Lavall, E.; 2014. Variaciones longitudinales en la estructura de la zona axial pirenaica. Aaportaciones de la fábrica magnética, el paleomagnetismo, la paleotermometría y la modelización analógica. Unpublished PhD Universidad de Zaragoza, 354pp

Izquierdo-Llavall, E., Román-Berdiel, T., Casas, A. M., Oliva-Urcia, B., Gil-Pena, I., Soto, R., & Jabaloy, A. (2012). Magnetic and structural study of the Eaux-Chaudes intrusion: understanding the Variscan deformation in the Western Axial Zone (Pyrenees). International Journal of Earth Sciences, 101(7), 1817-1834.

Izquierdo-Llavall, E., Aldega, L., Cantarelli, V., Corrado, S., Gil-Peña, I., Invernizzi, C., & Casas, A. M. (2013). On the origin of cleavage in the Central Pyrenees: structural and paleo-thermal study. Tectonophysics, 608, 303-318.

Izquierdo-Llaval, E., Casas-Sainz, A., Oliva-Urcia, B., Burmester, R., Pueyo, E.L. and Housen, B. (2015). Multi-episodic remagnetization related to deformation in the Pyrenean Internal Sierras, Geophys. J. Int., 201, 891-914.

Izquierdo-Llavall, E., Ayala, C., Pueyo, E. L., Casas-Sainz, A. M., Oliva-Urcia, B., Rubio, F., ... & García-Crespo, J. (2019). Basement-cover relationships and their along-strike changes in the linking zone (Iberian range, Spain): A combined structural and gravimetric study. Tectonics, 38(8), 2934-2960.

Labaume, P., & Teixell, A. (2018). 3D structure of subsurface thrusts in the eastern Jaca Basin, southern Pyrenees. Geologica Acta, 16(4), 477-498.

Labaume, P., Séguret, M., & Seyve, C. (1985). Evolution of a turbiditic foreland basin and analogy with an accretionary prism: Example of the Eocene south-Pyrenean basin. Tectonics, 4(7), 661-685.

Labaume, P., Meresse, F., Jolivet, M., & Teixell, A. (2016). Exhumation sequence of the basement thrust units in the west-central Pyrenees. Constraints from apatite fission track analysis. Geogaceta, 60, 11-14.

Labaume, P., Meresse, F., Jolivet, M., Teixell, A., & Lahfid, A. (2016). Tectonothermal history of an exhumed thrust-sheet-top basin: An example from the south Pyrenean thrust belt. Tectonics, 35(5), 1280-1313.

Lamarca Irisarri, Daniel (2012). El Yacimiento Geotérmico del Serrablo. MSc Univ. Zaragoza, 74 pp (https://zaguan.unizar.es/record/8248/files/TAZ-TFM-2012-335.pdf)

Lanaja, J. M., 1987. Contribución de la exploración petrolífera al conocimiento de la Geología de España. http://info.igme.es/geologiasubsuelo/GeologiaSubsuelo/Documents.aspx. Instituto Geológico y Minero de España Ed., .465 pp., 17 mapas.

Larrasoaña, J. C., 2000. Estudio magneto-tectónico de la zona de transición entre el Pirieno central y occidental; implicaciones estruucturales y geodinámicas. Tesis doctoral Universidad de Zaragoza, 287 pp.

Larrasoaña, J. C., Parés, J. M., Millán, H., Del Valle, J., & Pueyo, E. L. (2003). Paleomagnetic, structural, and stratigraphic constraints on transverse fault kinematics during basin inversion: The Pamplona Fault (Pyrenees, north Spain). Tectonics, 22(6).

Le Pichon, X., and J. C. Sibuet (1971). Western extension of boundary between European and Iberian plates during the Pyrenean orogeny. Earth Planetary Sciences Letters 12, 83-88.

Mattauer, M., (1968). Les traits structuraux essentiels de la chaîne pyrénéenne. Rev. Géogr. Phys. et Géol. Dyn. 2è sér. 10 (1), 3-12.

McElroy, R., 1990. Thrust kinematics and syntectonic sedimentation: the Pyrenean frontal ramp, Huesca, Spain. Unpublished PhD thesis, University of Cambridge. 175 pp.

Meresse, F. (2010). Dynamique d'un prisme orogénique intracontinental: évolution thermochronologique (traces de fission sur apatite) et tectonique de la Zone Axiale et des piémonts des Pyrénées centro-occidentales (Doctoral dissertation, Université de Montpellier 2), 280 pp.

Mezcua J., Gil A., Benarroch, R., 1996. Estudio gravimétrico de la Península Ibérica y Baleares, Inst. Geogr. Nac., Madrid, Spain, 2 maps.

Millán, H., 1996. Estructura y cinemática del frente de cabalgamiento surpirenaico en las Sierras Exteriores Aragonesas. Tesis Doctoral Universidad de Zaragoza. 330 pp.

Millán Garrido, H., 2006. Estructura y cinemática del frente de cabalgamiento surpirenaico en las Sierras Exteriores aragonesas. Colección de Estudios Altoaragoneses, 53. Instituto de Estudios Altoaragoneses ISBN 84-8127-165-9. Huesca, 398 pp.

Millán, H., Aurell, M., & Meléndez, A. (1994). Synchronous detachment folds and coeval sedimentation in the Prepyrenean External Sierras (Spain): a case study for a tectonic origin of sequences and systems tracts. Sedimentology, 41(5), 1001-1024.

Millán, H., Pocoví, A., Casas, A. (1995). El frente de cabalgamiento surpirenaico en el extremo occidental de las Sierras Exteriores. Revista Sociedad Geológica España, 8(1–2), 73–90

Millán-Garrido, H., Pueyo, E., Aurell, M., Luzón, A., Oliva-Urcia, B., Martínez-Peña, M.B., Pocoví Juan, A. (2000). Actividad tectónica registrada en los depósitos terciarios del frente meridional del Pirineo central. Revista Sociedad Geológica España, 13(2), 279–300

Millán-Garrido, H., Oliva-Urcia, B., & Pocoví-Juan, A. (2006). La transversal de Gavarnie-Guara. Estructura y edad de los mantos de Gavarnie, Guara-Gèdre y Guarga (Pirineo centro-occidental). Geogaceta, 40, 35-38.

Mochales, T; Pueyo, E. L.; Casas, A. M.; Soriano, A. (2007). Magnetic prospection as an efficient tool for doline detection. A case study in the central Ebro Basin (Northern Spain). In: Natural and anthropogenic hazards in karst areas (Edited by: Parise, M.; Klimchouk, A.; Gunn, J.). Geological Society of London Special Publication 279, 73-84

Mochales, T., Casas, A. M., Pueyo, E. L., & Barnolas, A. (2012). Rotational velocity for oblique structures (Boltaña anticline, Southern Pyrenees). Journal of Structural Geology, 35, 2-16.

Montes, M. J. (2002). Estratigrafía del Eoceno-Oligoceno de la cuenca de Jaca (sinclinorio del Guarga). PhD dissertation Universitat de Barcelona, Barcelona.

Montes Santiago, M. J. (2009). Estratigrafía del Eoceno-Oligoceno de la cuenca de Jaca (sinclinorio del Guarga). Colección de estudios altoaragoneses, vol 59, 355 pp. Instituto de Estudios Altoaragoneses. ISBN: 8481272027

Moritz, H. (1980). Geodetic Reference System 1980. Bulletin Géodésique, 54, 395-405.

Muñoz, J.A., (1992). Evolution of a continental collision belt: ECORS-Pyrenees crustal balanced cross section. In: McClay, K.R. (Ed.), Thrust Tectonics. Chapman and Hall, London, 235-246.

Muñoz, J. A. (2019). Alpine Orogeny: deformation and structure in the northern Iberian margin (Pyrenees sl). In The geology of iberia: A geodynamic approach (pp. 433-451). Springer, Cham.

Muñoz, J. A., Beamud, E., Fernández, O., Arbués, P., Dinarès-Turell, J., & Poblet, J. (2013). The Ainsa Fold and thrust oblique zone of the central Pyrenees: Kinematics of a curved contractional system from paleomagnetic and structural data. Tectonics, 32(5), 1142-1175.

Mutti, E. & Sgavetti, M. (1987). Sequence stratigraphy of the Upper Cretaceous Aren strata in the Orcau-Aren region, south-central Pyrenees, Spain: Distinction between eustatically and tectonically controlled depositional sequences. Annali de I' Università di Ferrara. Sezione Science della Terra, 1, 22p.

Mutti E., Seguret M. and Sgavetti M., 1988. Sedimentation and deformation in the Tertiary sequences of the Southern Pyrenees. AAPG Mediteranean Basins Conference, Nice. Field Trip Guidebook, 7, 1-169.

Nabighian, M.N., Ander, M.E., Grauch, V.J.S., Hansen, R.O., LaFehr, T.R., Li, Y., Pearson, W.C., Peirce, J.W., Phillips, J.D. and Ruder, M.E. (2005). Historical development of the gravity method in exploration. Geophysics, 70, 63ND-89ND.

Nichols, G. J., 1984. Thrust tectonics and alluvial sedimentation, Aragón, Spain. Unpublished Ph. D. Thesis, Univ. of Cambridge. 243pp.

Nichols, G. J., 1987. The Structure and Stratigraphy of the Western External Sierras of the Pyrenees, Northern Spain. Geological Journal, 22: 245-259.

Oliva-Urcia, B., 2000 Estructura y cinemática del frente surpirenaico en el sector central de la cuenca de Jaca-Pamplona. Tesis de Licenciatura Universidad de Zaragoza, 100 pp.

Oliva-Urcia, B.; 2004. Geometría y cinemática rotacional en las Sierras Interiores y Zona Axial (sector de Bielsa) a partir del análisis estructural y paleomagnético. Unpublished PhD University of Zaragoza, 290 pp.

Oliva-Urcia, B., Larrasoaña, J. C., Pueyo, E. L., Gil, A., Mata, P., Parés, J. M., ... & Pueyo, O. (2009). Disentangling magnetic subfabrics and their link to deformation processes in cleaved sedimentary rocks from the Internal Sierras (west central Pyrenees, Spain). Journal of Structural Geology, 31(2), 163-176

Oliva-Urcia, B., Casas-Sainz, A. M., Pueyo Morer, E. L., & Pocovi Juan, A. (2012). Structural and paleomagnetic evidence for non-rotational kinematics of the South Pyrenean Frontal Thrust at the western termination of the External Sierras (southwestern central Pyrenees). Geologica Acta, 10(2), 125-144.

Oliva-Urcia, B., Beamud, E., Arenas, C., Pueyo, E. L., Garcés, M., Soto, R., ... & Pérez-Rivarés, F. J. (2019). Dating the northern deposits of the Ebro foreland basin; implications for the kinematics of the SW Pyrenean front. Tectonophysics, 765, 11-34.

Payros, A., Pujalte, V., & Orue-Etxebarria, X. (1999). The South Pyrenean Eocene carbonate megabreccias revisited: new interpretation based on evidence from the Pamplona Basin. Sedimentary Geology, 125(3-4), 165-194.

Pedley, R.C., 1991. GRAVMAG User Manual: Interactive 2.5D Gravity and Magnetic Modelling Program. British Geological Survey, Keyworth, Notingham .

Pedreira, D., Pulgar, J. A., Gallart, J., & Díaz, J. (2003). Seismic evidence of Alpine crustal thickening and wedging from the western Pyrenees to the Cantabrian Mountains (north Iberia). Journal of Geophysical Research: Solid Earth, 108(B4).

Pedreira, D., Afonso, J. C., Pulgar, J. A., Gallastegui, J., Carballo, A., Fernandez, M., ... & García-Moreno, O. (2015). Geophysical-petrological modeling of the lithosphere beneath the Cantabrian Mountains and the North-Iberian margin: geodynamic implications. Lithos, 230, 46-68.

Pedrera, A., García-Senz, J., Ayala, C., Ruiz-Constán, A., Rodríguez-Fernández, L. R., Robador, A., & González Menéndez, L. (2017). Reconstruction of the exhumed mantle across the North Iberian Margin by crustal-scale 3-D gravity inversion and geological cross section. Tectonics, 36(12), 3155-3177.

Poblet, J., (1991). Estructura herciniana i alpina del Vessant sud de la zona Axial del Pirineu Central. Unpublished PhD Thesis, Univ. of Barcelona, 604 pp.

Poblet, J., & Hardy, S. (1995). Reverse modelling of detachment folds; application to the Pico del Aguila anticline in the South Central Pyrenees (Spain). Journal of Structural Geology, 17(12), 1707-1724.

Pueyo Anchuela, 2003. Estructura y cinemática del frente de cabalgamiento surpirenaico en el sector occidental de la Cuenca de Jaca-Pamplona, sierra de Alaiz. Tesis de Licenciatura Universidad de Zaragoza.

Pueyo Anchuela, Ó. (2012) Estudio de fábricas magnéticas y su relación con la deformación en el sector centro-occidental del Pirineo central (Aragón y Navarra). Serie Tesis de la Universidad de Zaragoza, 2012, nº 68. 391 páginas

Pueyo-Anchuela, Ó., Pueyo, E. L., Juan, A. P., & Imaz, A. G. (2012). Vertical axis rotations in fold and thrust belts: comparison of AMS and paleomagnetic data in the Western External Sierras (Southern Pyrenees). Tectonophysics, 532, 119-133.

Pueyo, E. L. (2000). Rotaciones paleomagnéticas en sistemas de pliegues y cabalgamientos. Tipos, causas, significado y aplicaciones (ejemplos del Pirineo Aragonés). Unpublished PhD thesis, Universidad de Zaragoza, 296.

Pueyo, E. L., Millán, H., & Pocovı, A. (2002). Rotation velocity of a thrust: a paleomagnetic study in the External Sierras (Southern Pyrenees). Sedimentary Geology, 146(1-2), 191-208.

Pueyo, E. L., Pocoví, A., Millán, H., Sussman, A. J., & Weil, A. B. (2004). Map-view models for correcting and calculating shortening estimates in rotated thrust fronts using paleomagnetic data. Orogenic Curvature: Integrating Paleomagnetic and Structural Analyses, 383, 55-71.

Pueyo, E.L.; García-Lobón, J.L.; Klimowitz, J.P.; Alcolea, M.; Bastante, R.; Escalante, S.; Hermida, E.; Morante, M.; Ruíz, G.; Pardos, M.; Juez, F.J. + ALGECO2-PE team, (2010). Selección y caracterización de áreas y estructuras favorables para el almacenamiento geológico de

CO2 en España, v. II-1 Cadena Pirenaica y Cuenca del Ebro—Geología (Atlas DIN A2, 200 p.): Instituto Geológico y Minero de España.

Pueyo, E. L., Calvin, P., Casas, A. M., Oliva-Urcia, B., Klimowitz, J., García-Lobón, J. L., ... & ALGECO, T. (2012). A research plan for a large potential CO2 reservoir in the Southern Pyrenees. Geo-Temas, 13, 1970-1973.

Pueyo, E. L., Izquierdo-Llavall, E., Rodríguez-Pintó, A., Rey-Moral, C., Oliva-Urcia, B., Casas, A. M., ... & García-Lobón, J. L. (2016). Petrophysical properties in the Iberian Range and surrounding areas (NE Spain): 1-density. Journal of Maps, 12(5), 836-844.

Puigdefábregas, C. (1975). La sedimentación molásica en la cuenca de Jaca. Monografías del Instituto de Estudios Pirenaicos. 104, 188p.

Puigdefábregas, C. and Soler, M. (1973). Estructura de las Sierras Exteriores Pirenaicas en el corte del río Gállego (Prov. Huesca). Pirineos, 109, 5-15.

Puigdefàbregas, C.; Rojas Tapia, B.; Sánchez Carpintero, I.; del Valle de Lersundi, J. (2008). Mapa geológico de la Hoja nº 142 (Aoiz). Mapa Geológico de España E. 1:50.000. Segunda Serie (MAGNA). Instituto Geológico y Minero de España (IGME)

Ramón, M. J., Pueyo, E. L., Briz, J. L., Pocoví, A., & Ciria, J. C. (2012). Flexural unfolding of horizons using paleomagnetic vectors. Journal of Structural Geology, 35, 28-39.

Robador, A., Ramajo, J., Muñoz, A., Pérez, A., Luzón, A., Arenas, C. González, A. (2011); Mapa Geológico Digital continuo E. 1: 50.000, Zona Cuenca del Ebro (Zona-2700). In GEODE. Mapa Geológico Digital continuo de España.

Robador, A., Samsó, J.M., Ramajo, J., Barnolas, A., Clariana, P., Martín, S. Gil, I (2019) (2; Mapa Geológico Digital continuo E. 1:50.000, Zona Pirineos Vasco-Cantábrica (Zona-1600). in GEODE. Mapa Geológico Digital continuo de España.

Rodríguez, L., Cuevas, J., & Tubía, J. M. (2014). Structural evolution of the sierras interiores (Aragón and Tena Valleys, South Pyrenean Zone): tectonic implications. The Journal of Geology, 122(1), 99-111.

Rodríguez Méndez, L. (2011). Análisis de la estructura varisca y alpina en la transversal Sallent-Biescas (Pirineos centrales, Huesca). Servicio Editorial de la Universidad del País Vasco/Euskal Herriko Unibertsitatearen Argitalpen Zerbitzua.

Rodríguez-Méndez, L., Cuevas, J. and Tubia, J.M. (2019). The Western-Central área of Aragonese-Catalan Pyrenees. In: Cecilio Quesada and José Tomás Oliveira (eds.). The Geology of Iberia: A Geodynamic Approach, Vol. 3: The Alpine Cycle, 40-41.

Santolaria, P., Casas-Sainz, A. M., Soto, R., Pinto, V., & Casas, A. (2014). The Naval diapir (Southern Pyrenees): Geometry of a salt wall associated with thrusting at an oblique ramp. Tectonophysics, 637, 30-44.

Santolaria, P., Ayala, C., Pueyo, E. L., Rubio, F. M., Soto, R., Calvín, P., ... & Casas-Sainz, A. M. (2020). Structural and geophysical characterization of the western termination of the South Pyrenean triangle zone. Tectonics, 39(8), e2019TC005891.

Schellart, W. 2002. Alpine deformation at the western termination of the Axial Zone, Southern Pyrenees. In: Reconstruction of the evolution of the Alpine-Himalayan orogeny (Eds.: Rosenbaum, G. and Lister, G. S.). Journal of the Virtual Explorer, 8, 35-55.

Seguret, M. 1970. Étude téctonique des napes et séries décolles de la partie centrale du versant sud des Pyrenees. (Doctoral dissertation, Universidad de Montpellier).

Sherman, G. E., Sutton, T., Blazek, R., & Luthman, L. (2004). Quantum GIS User Guide.

Soto, R., Casas-Sainz, A. M., & Pueyo, E. L. (2006). Along-strike variation of orogenic wedges associated with vertical axis rotations. Journal of Geophysical Research: Solid Earth, 111(B10).

Soto, R., F. Storti, and A. M. Casas-Sainz (2006). Impact of backstop thickness lateral variations on the tectonic architecture of orogens: Insights from sandbox analogue modeling and application to the Pyrenees. Tectonics, 25, TC2005, doi:10.1029/2004TC001693.

Souquet, P. (1967). Le Crétacé supérieur sudpyrénéen en Catalogne, Aragon et Navarre, PhD thesis, Univ. De Toulouse, France

Souriau, A., Rigo, A., Sylvander, M., Benahmed, S., & Grimaud, F. (2014). Seismicity in central-western Pyrenees (France): A consequence of the subsidence of dense exhumed bodies. Tectonophysics, 621, 123-131.

Teixell, A. (1992). Estructura Alpina en la transversal de la terminación occidental de la zona Axial Pirenaica (Doctoral dissertation, Departamento de Geología Dinámica, Geofísica y Paleontología. Facultad de Geología, Universitat de Barcelona).

Teixell, A. (1996). The Ansó transect of the southern Pyrenees: basement and cover thrust geometries. Journal of the Geological Society, 153(2), 301-310.

Teixell, A. (1998). Crustal structure and orogenic material budget in the west central Pyrenees. Tectonics 17, 395- 406.

Teixel. A.; Barnolas, A. (1994). Mapa geológico de la Hoja nº 176 (Jaca). Mapa Geológico de España E. 1:50.000. Segunda Serie (MAGNA). Instituto Geológico y Minero de España (IGME)

Teixell, A., Montes, M. J., Arenas, C., & Garrido, E. A. (1989). Mapa Geológico De España a Escala 1: 50000. Hoja 118 (Zuriza).

Teixell, A., Arboleya, M. L., (1996). Tectónica de cabalgamientos y sedimentación sinorogénica en el Pirineo centro-occidental. VIII Reuniónde la Comisión de Tectónica de ls SGE. Edited by: Universidad de Barcelona, 90 pp. ISBN 84-600-9350-6

Teixel. A.; García San Segundo, J; Barnolas, A. (1994). Mapa geológico de la Hoja nº 118 (Zuriza). Mapa Geológico de España E. 1:50.000. Segunda Serie (MAGNA). Instituto Geológico y Minero de España (IGME)

Teixel. A.; García San Segundo, J; Zamorano, M.; Barnolas, A. (1994). Mapa geológico de la Hoja nº 144 (Ansó). Mapa Geológico de España E. 1:50.000. Segunda Serie (MAGNA). Instituto Geológico y Minero de España (IGME)

Teixell, A., Labaume, P., & Lagabrielle, Y. (2016). The crustal evolution of the west-central Pyrenees revisited: Inferences from a new kinematic scenario. Comptes Rendus Geoscience, 348(3-4), 257-267.

Teixell, A., Labaume, P., Ayarza, P., Espurt, N., de Saint Blanquat, M., & Lagabrielle, Y. (2018). Crustal structure and evolution of the Pyrenean-Cantabrian belt: A review and new interpretations from recent concepts and data. Tectonophysics, 724, 146-170.

Ternet, Y., Baudin, T., Laumonier, B., Barnolas, A., Gil-Peña, I. and Martín-Alfageme, S. (2008). Mapa geológico de los Pirineos a escala 1:400000. BRGM-IGME.

Toro, R.; Izquierdo-Llavall, E.; Casas, A.M.; Ayala, C.; Rubio, F.M.; Martín-León, J.; Santolaria, P.; Navas, J.; Pueyo, E.L. (2021). Deliverable 6.2. 3D model of the Southwestern Pyrenees, digital files. GEOERA 3DGEO-EU, 3D Geomodeling for Europe, project number GeoE.171.005. Report and Digital files, 12 p.

Turner, J. P., 1996. Switches in subduction direction and the lateral termination of mountain belts: Pyrenees-Cantabrian transition, Spain. Journal of the Geological Society, London, Vol. 153, 1996, pp. 563-571

Turner, J. P.; Hancock, P. L., 1990. Thrust systems of the southwest Pyrenees and their control over basin subsidence. Geological Magazine, 127: 383-392.

Vaquero, P.A., Sainz-Maza, S. 2011. Reseña de Punto Destacado de Gravimetría Absoluta, Red Española de Gravimetría Absoluta. IGN: Madrid; 2

Vera, J. A., et al. (2004), Rasgos geofísicos esenciales y estructura de la litosfera. In Geología de España, edited by J. A. Vera, pp. 7-12, Sociedad Geológica de España, Instituto Geológico y Minero de España, Madrid.